Na-ijlende gevolgen steenkolenwinning Zuid-Limburg

Final report
on the results of the working group
5.2.7 - small earthquakes

by

Projectgroup
"Na-ijlende gevolgen van de steenkolenwinning in Zuid-Limburg"
(projectgroup GS-ZL)

on behalf of

Ministerie van Economische Zaken - The Netherlands

Amsterdam, 31.08.2016
(Rev. a: 02. December 2016)

This report consists of 85 pages and 4 appendices

Na-ijlende gevolgen steenkolenwinning Zuid-Limburg

WG 5.2.7 - small earthquakes -
Final report

The report is edited by

Witteveen+Bos
Van Twickelostraat 2
7411 SC Deventer
The Netherlands
Telephone: +31 0570 69 79 11
E-mail: info@witteveenbos.com

Authors: Dr. Ir. Siefko Slob CEng
Dr. Carolina Sigaran-Loria
Ir. Els Weijermans
Ir. Stef Carelsen

Internal reviewers: Dr. Bernard Dost (KNMI)
Prof. Dr. K. Schetelig (IHS)

External reviewer: Dr. Ralf Fritschen (DMT)

Contents

Figures

Tables

Appendix

1 Introduction

1.1 General remarks

The working group 5.2.7 has studied possible correlations between the hard coal extraction and the thereby effected mass shifting, the ground or mine water lowering during the exploitation period and the groundwater rise after abandoning the mines and occasional small earthquakes in the area of interest. The main issue was the investigation of any correlations between the earthquake swarms in the years 1985 - 1986 and 2000 - 2002 and the groundwater rise or the delay between end of mining processes and the earthquake events.

The report in hand presents a hypothesis in view of an analysis and identification of the causes and mechanisms of the earthquake swarms by corresponding spatial and temporal correlations as well as an estimation of the mass shifts by extraction and groundwater rise. The earthquakes can be tectonic or man-made, induced tremors. This general approach does not offer actually a definite answer, but it aims at a clarifying of the questions by the recommended monitoring and a corresponding analysis of further earthquakes, possibly occurring in the future.

A clear physical relation between the various phenomena and parameters cannot be actually presented.

This document has significantly been improved by the comments and suggestions of Dr. Ralf Fritschen from DMT. His assistance and effort is greatly appreciated.

1.2 Background

In the Netherlands, earthquakes can be subdivided into tectonic and induced. Induced earthquakes in the Netherlands are usually related to subsidence due to conventional gas extraction in Groningen. This subsidence is due to pore pressure decrease in the reservoir and this creates local stress changes, which can trigger movements along faults in or near the reservoir. Tectonic earthquakes in the Netherlands are related to natural movements along the Peelrandbreuk in South Limburg (see Fig. 1). An example is the M 5,8 earthquake in Roermond on 13.04.1992, which was the strongest earthquake ever recorded in the Netherlands.

In Germany induced earthquakes are recorded related to on-going coal mining activities (see Fig. 2). In the Ruhr area for instance, about 1.400 seismic events with magnitudes smaller than M_L 3,3 are detected every year (BISCHOFF et al., 2010). There is a strong correlation in time and space between the seismic events and mining activity. For example, the hypocentre locations follow the progressive motion of the longwall. Significantly less earthquakes occur at the weekend when there are no works going on (BISCHOFF et. al., 2005). Induced seismicity in mining can also be related to large open pit mining in rock or underground blasting activities. Other experiences with mining-related seismicity are described in chap. 1.4.

Rise in groundwater level can also trigger (small) earthquakes. These earthquakes will be generated by faults being under shear stress due to regional tectonics or due to past mining activities. An increase of water pressure along the stressed faults will reduce the normal stress and thus the friction along the fault and this could induce fault movement, resulting in an earthquake. Another mechanism may be the increase in mass due to the rising groundwater. This

increase in mass could be an additional driving force of fault movement and thus the development of seismicity.

Two earthquake swarms have occurred at the Southern edge of the former coal mining area, around the village of Voerendaal. The first swarm occurred in 1985 and the second swarm at the end of 2000 until the beginning of 2001. These two swarms could be related to the rising mine water.

1.3 Scope

The scope of the investigations of minor earthquakes ("Onderzoek naar lichte aardbevingen") was specified in the research plan that accompanied the tender (SODM, 2014b). The scope is given in Section 5.2.7 of the research plan. This Section is translated from Dutch and repeated below:

It is currently unclear to what extent rising mine water can trigger minor earthquakes. Before this can be defined as an after-effect of the coal mining, it is at first required to study whether a possible relationship exists between rising mine water and earthquakes in South Limburg. For this research the following steps are suggested:

- Collecting data on earthquakes occurring in the last century in the South Limburg mining area
- Analysing earthquake data on "normal" and anomalous occurrence
- Comparing these earthquake data with data on the rise of mine water
- Assessment whether rising mine water in South Limburg has triggered earthquakes
- Assessment whether rising mine water in South Limburg can still trigger earthquakes in the future

- Review of the physical causes of the assumed correlations, such as mass shifting and change of the main stress conditions around the fault zone
- Review of the findings by recognized experts

The end result of this study is a peer-reviewed position to what extent rising mine water in South Limburg can trigger (small) earthquakes.

Based on the results of this study it will be decided to what extent these small earthquakes should be included in a risk analysis or hazard map. It is recommended that any risk due to possible triggered quakes is compared with the existing risk due to natural tectonic earthquakes in South Limburg. The existing seismic hazard map for the Netherlands is provided in Appendix 3. This seismic hazard map relates to one of the main performance levels (in terms of return period or probability of exceedance) used in Eurocode 8, which is the seismic design norm for Europe (NEN-EN 1998-1:2005).

A seismic monitoring system is already in place in South Limburg. The monitoring system could be expanded, if this is deemed necessary. It may be possible to link to studies initiated in connection with the gas-related tremors in Groningen. Attention for strengthening weak structural elements such as chimneys seems advisable in view of natural (tectonic) earthquakes. For prevention at the (possible) source only a restart of the mine water pumping seems to be an option to stop the mine water rise. This option is further elaborated in working group 5.4.1.

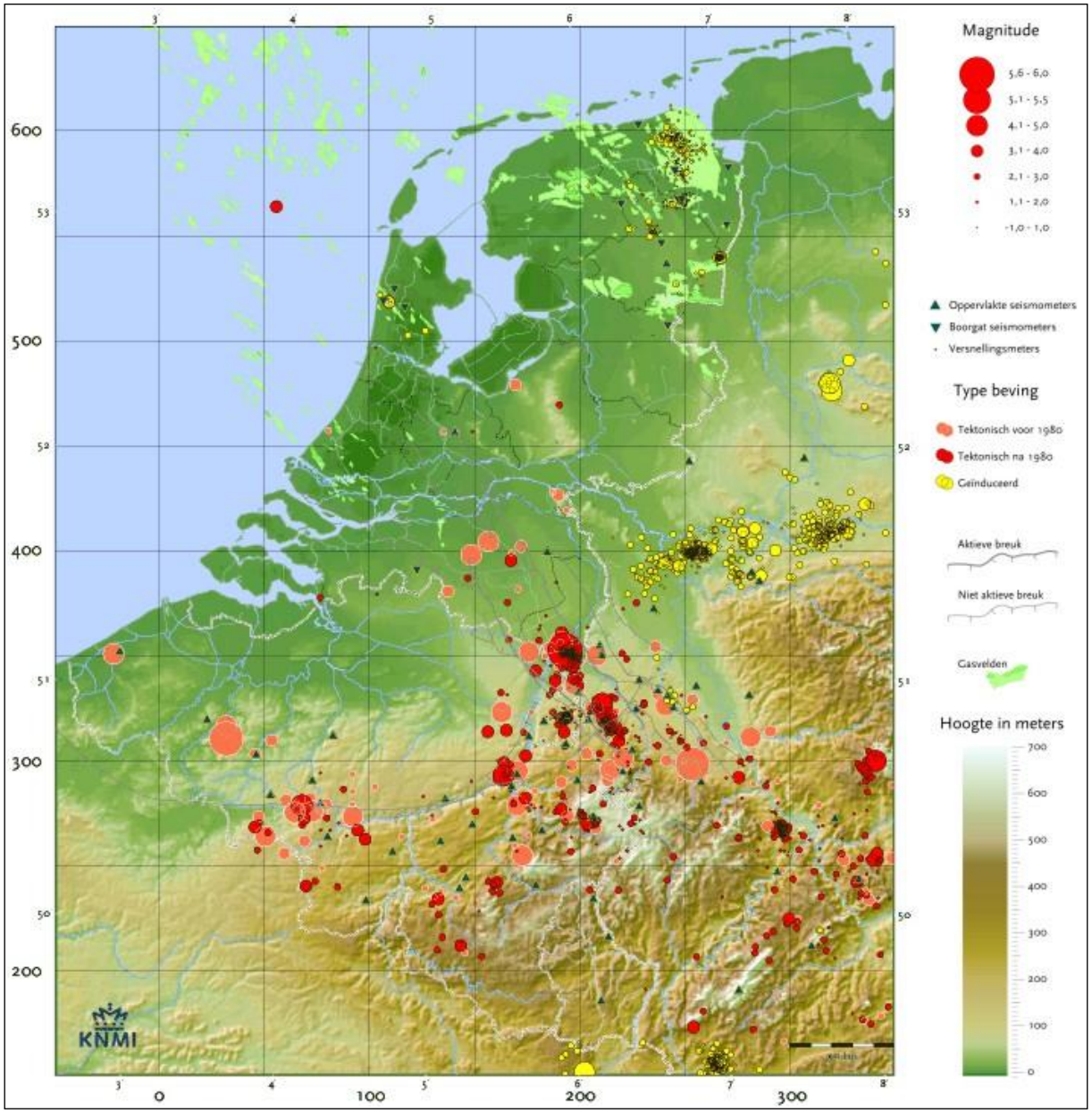

Fig. 1: Overview of tectonic (red) and induced earthquakes (yellow) in the Netherlands and surrounding areas (KNMI, 2013). The light red dots are tectonic earthquakes recorded before 1980 and the dark red dots are tectonic earthquakes recorded after 1980. The yellow marked induced earthquakes in the North of the Netherlands are due to natural gas extraction. The yellow marked earthquakes in Germany in the Ruhr area are due to coal mining.

1.4 Experiences in other mining areas

South Limburg is not the only former mining region where mines have been flooded. Experiences with flooding-induced seismicity in other mining areas are summarised in this chapter.

In the former coal mine region Campine in Belgium mines have been flooded, but water levels have not been monitored. No earthquakes have been measured (ROSNER, 2015) and it is therefore concluded that no experience with flooding-induced seismicity exists in Belgium.

In Germany, parts of the Ruhr and Saar mining areas are being flooded. In the Ruhr region no flooding-induced seismicity has been observed so far (FRITSCHEN, 2015). During active mining, mining-induced seismicity occurred in the Saar region of which the earthquake of February 2008 with M 4,0 is an important example (see also Fig. 2). Active mining in the Saar area came to an end in June 2012. Since May 2013 mines have been flooded and on 15.09.2014 the strongest flooding-induced seismic event so far has been measured in the Saar region with M 2,7 (SAARLAND, 2014). According to SAARLAND (2014) the seismic monitoring network has registered 156 events in 2013 and 205 events in 2014 in areas where mining-induced seismicity occurred in the past. Here it was also described that increasing water pressure changes the stress state at faults, leading to failure. However, according to FRITSCHEN (2015) nothing has been officially published on this so far.

An example of flooding-induced seismicity in France is in the Gardanne coal mining region in the Provence. Seismicity measurements started in 2008 (MATRULLO et al., 2015) and seismic events were measured in November 2012 and in December 2014 (M > 2,5). Apart from these larger events that were felt by the inhabitants of the area, numerous smaller events have been registered as well.

At this moment studies are also carried out to relate seismicity to rising mine water, geology and local tectonics. This is an example where the number of seimic events has increased with the rate of mine water rise.

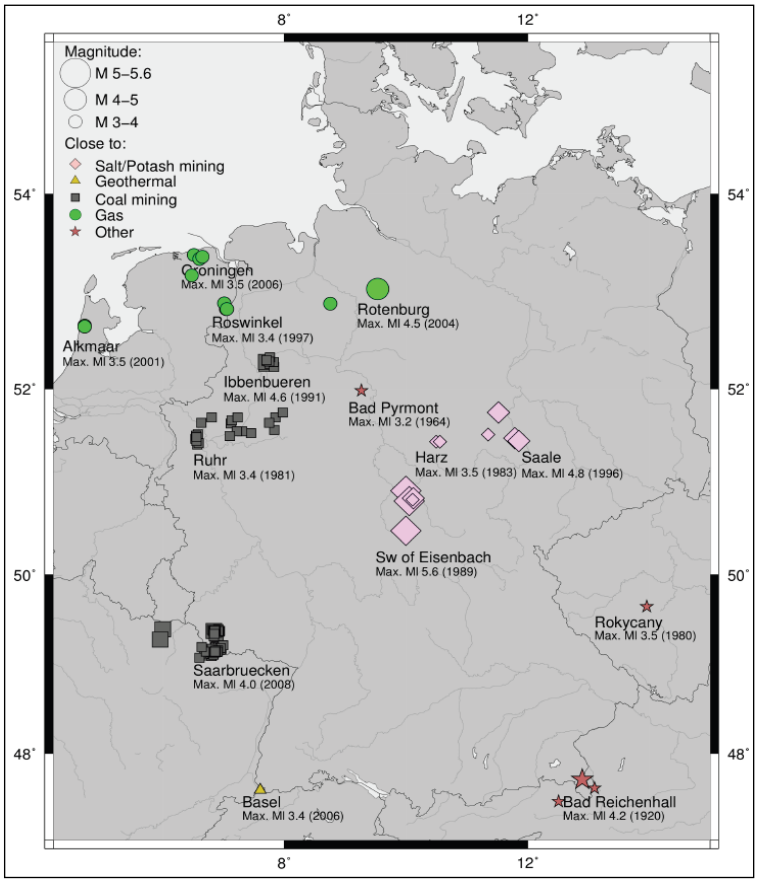

Fig. 2: Overview of induced earthquakes in Germany and surrounding areas with M > 3 from 1899 to 2010 (DAHM et al., 2010)

GOLDBACH (2009) describes experiences with flooding-induced seismicity in South African gold mines. Here mining-induced seismicity was measured in the active part of the mine and flooding-induced seismicity in the abandoned part of the mine. Reference is made to the theory of increasing pore pressure leading to failure along faults due to changing stress conditions. By comparing mine water level increase with seismicity, it was found that the majority of events took place

about 14 months after the start of flooding. Initially, the mine water level rose at a relatively high rate. After 1 year this rate decreased and also fewer seismic events were measured.

1.5 Hypothesis

In view of the background, scope and previous experiences in other mining areas, the following hypothesis has been defined:

Rising mine water triggers small earthquakes in a seismically active area. The two earthquake swarms around Voerendaal could be evidence for this. There are two possible mechanisms behind the induced seismicity:

1. The increase of groundwater level results in an increase in pore (water) pressure along a fault. This results in a decrease of shear resistance along an active fault, causing fault movement. This fault movement can be experienced as a (small) earthquake. This mechanism is illustrated in Fig. 3 and is further elaborated in chap. 4.
2. The increase in groundwater level results in an increase or shift of mass within a certain structural block. This mass increase or mass shift may be a driving mechanism behind a fault movement, in addition to (natural) tectonic activity. The possible release of seismic energy may be a result of the increase in potential energy. This mechanism is illustrated in Fig. 4 and is further elaborated in chap. 5.

The decrease in shear strength does not necessarily result in fault movement, because there should be a driving force. The main driving force for fault movement is the existing tectonic stress regime (see chap. 2), which is

extensional (horizontal), causing normal fault movement. In addition to the tectonic stress the mass shift (vertical) could be an additional driving force.

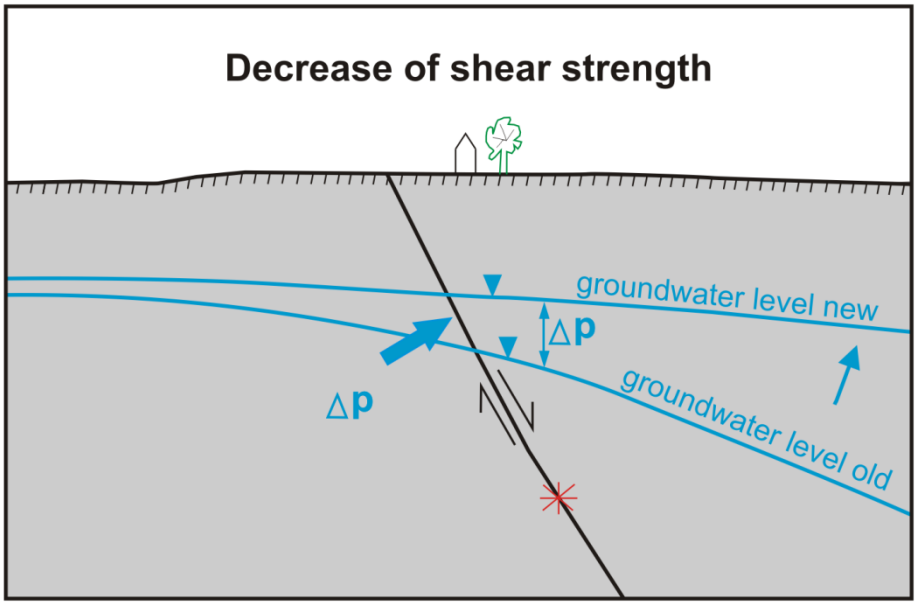

Fig. 3: Illustration of decrease of shear resistance as triggering mechanism

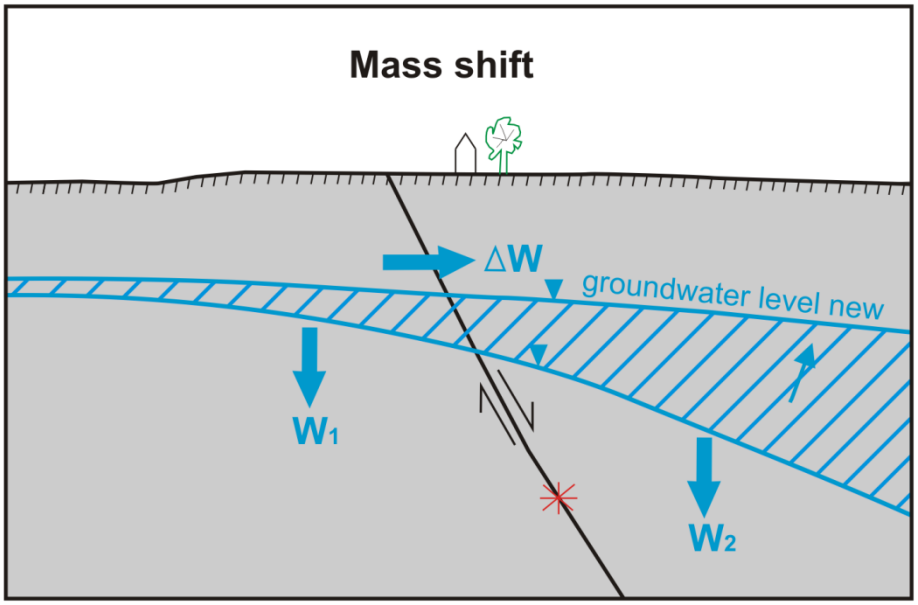

Fig. 4: Illustration of mass shift as triggering mechanism

1.6 Methodology

In order to accept or reject the hypothesis specified in chap. 1.5, the following methodology will be followed, which consists of the following steps:

A. Description of geological and seismic setting - chap. 2

The first step is to describe the general geological and seismic setting. This is done through literature review and assembly of existing data. The seismic data is in the form of earthquake catalogues and GIS. The geological data is in the form of GIS maps showing the top of the Carboniferous and the location of active faults in the area. Additional information, such as the outline of mined areas and location of old mine shaft are also assembled. The data is visualised in the form of maps and cross sections. The aim of the visualisation of the data is to see whether there are apparent relations between the general seismicity, the Voerendaal swarms, the geology and the active faults.

B. Multivariate analysis - chap. 3

The next step is to show the development of groundwater over time and to relate this with the development of seismicity and ground ground heave over time. The objective is to determine whether trends and correlations can be seen. The development of the seismicity can be extracted from the earthquake catalogue. The development of the ground ground heave over time is determined by working group 5.2.1. The final expected (stationary) groundwater level is determined by working group 5.2.5.

C. Analysis of stress-state conditions to evaluate slip potential - chap. 4

The third step is to determine the in-situ stress conditions at different depths of the active faults in the area. The fault characteristics are determined in terms of

dip angle, friction angle and cohesion. With a Mohr-Coulomb analysis the critical stress state of the fault in relation to the in-situ stress conditions is calculated. Subsequently, it can be determined what increase in pore pressure could result in slip and this can be related to the actual measured increase in pore pressure due to mine water rise.

D. Analysis of energy balance - chap. 5

The final step is to calculate the total energy balance of the system and to what extent a mass shift due to rising mine water could be the driving force behind seismic activity. This is done through calculation of increase in mass (potential energy) due to mine water rise, taking into account the size of the relevant mining basin, the porosity in the Carboniferous rocks and the porosity in the overburden material. Then the release of energy due to seismic events is calculated. Possible partitioning effects and the loss of potential energy due to ground ground heave is also incorporated in the analysis.

E. Conclusion - chap. 6

The findings of the analysis are checked against the original hypothesis. First, an evaluation is done whether the hypothesis is a valid one. Secondly, if possible, the hypothesis is rejected or accepted. The findings are viewed in terms of impact on the existing natural seismic hazard in the area.

F. Bow-Tie-Analysis - chap. 7

In this study the Bow-Tie-Analysis is used as the method to analyse the risks per after-effect, to create possible impact maps, define mitigation and prevention measures.

Bow-Tie-Analysis is a strong tool to visually clarify the risks and map measures associated with the effects or hazards. The power of a BowtieXP diagram is that it gives an overview of multiple plausible scenarios in a single picture

Fig. 5 shows a schematic representation of a Bow-Tie-Analysis. The knot of the Bow-Tie, i.e., the centre of the diagram, is formed by the incident, or Top Event, which is connected to a certain Hazard. On the left side, the various causes that may trigger the incident are summarised, i.e., the Threats. On the right side, the potential impacts from the Top Event are listed, i.e., the Consequences.

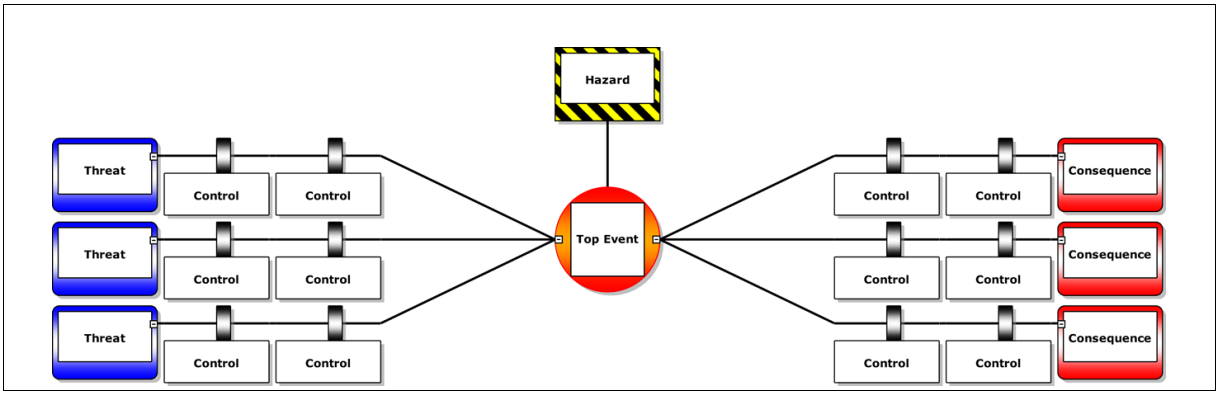

Fig. 5: Schematic representation of a Bow-Tie-Analysis

Subsequently, Controls can be added in between the Threats, Consequences, and the Top Event. These can be either preventive, i.e. prevent the cause from escalating into a Top Event, or mitigating, i.e., reduce the Consequences once the Top Event occurred. Also, monitoring controls can be added to detect a Top Event or to direct preventive and/or mitigating controls.

2 Tectonic setting and seismicity

2.1 Introduction

The former South Limburg coal mining district is located in a seismically active area, the only area in the Netherlands with active tectonism (Fig. 1). The coal mining district is situated at the southwestern edge of the Roer Valley Graben structure, south of the Feldbiß fault. The coal was mined from the Carboniferous rocks, which appear at varied depths ranging from 0 to 800 m. below ground surface in the mining district (DE VENT & ROEST, 2013). The top level of the Carboniferous rocks has a downward trend towards the northwest. The Carboniferous rocks are dissected by various faults, at the edge of the Roer Valley Graben. This Chapter describes first the regional tectonic setting, followed by the local active faults present at or near the coal mining district. Afterwards, the seismic catalogue and identified seismic swarms are described. At the end, the relation between the swarms and local faults is explained including the possible relation between the local seismicity to the overall ground ground heave.

2.2 Tectonic setting

The southern region of the Netherlands and its surroundings experience an extensional tectonism, associated to the active rift system of the Roer Valley. At regional scale, this graben is part of the Rhine Graben Rift System, illustrated in Fig. 5. The extensional stress regime (the red arrows in Fig. 5) results from the interaction between the main tectonic plates (Fig. 6). The spreading at the Mid-Atlantic ridge leads to a strain of the Eurasian plane and forces the Eurasian plate in a southeastern direction (the blue arrow in Fig. 5), while the African plate

compresses northwards (see Fig. 6 and the green arrow in Fig. 5). As result from that compression, extensional structures have developed in a northwest orientation, which created the Rhine Graben Rift, perpendicular to the tension forces. The Rhine Graben System is subdivided regionally into: Upper Rhine Graben, Lower Rhine Graben, Hessian Graben and Belgian Brabant Massif region.

In the Netherlands, the Roer Valley Graben is the main tectonic feature, which represents the northwestern branch of the Rhine Graben System (DE VOS, 2010). It consists mainly of normal faults with a northwest-southeast direction, perpendicular to the extensional stress regime (Fig. 5). The region between the faults subsides by the gravity movement along the geological structures. Along the Roer Valley Graben, the governing active faults are the Feldbiß fault and Peel Boundary fault (Fig. 5 and Fig. 7). These faults are active since late Oligocene (GELUK et al., 1994) and have an estimated slip rate of 0,05 - 0,01 mm/year (GIARDINI et al., 2013) and are dominantly normal with a small strike-slip component in depth (DOST & HAAK, 2007). Most of the seismicity occurs within the graben, but there is also seismicity out of it, mainly near its southern boundary (chap. 2.3).

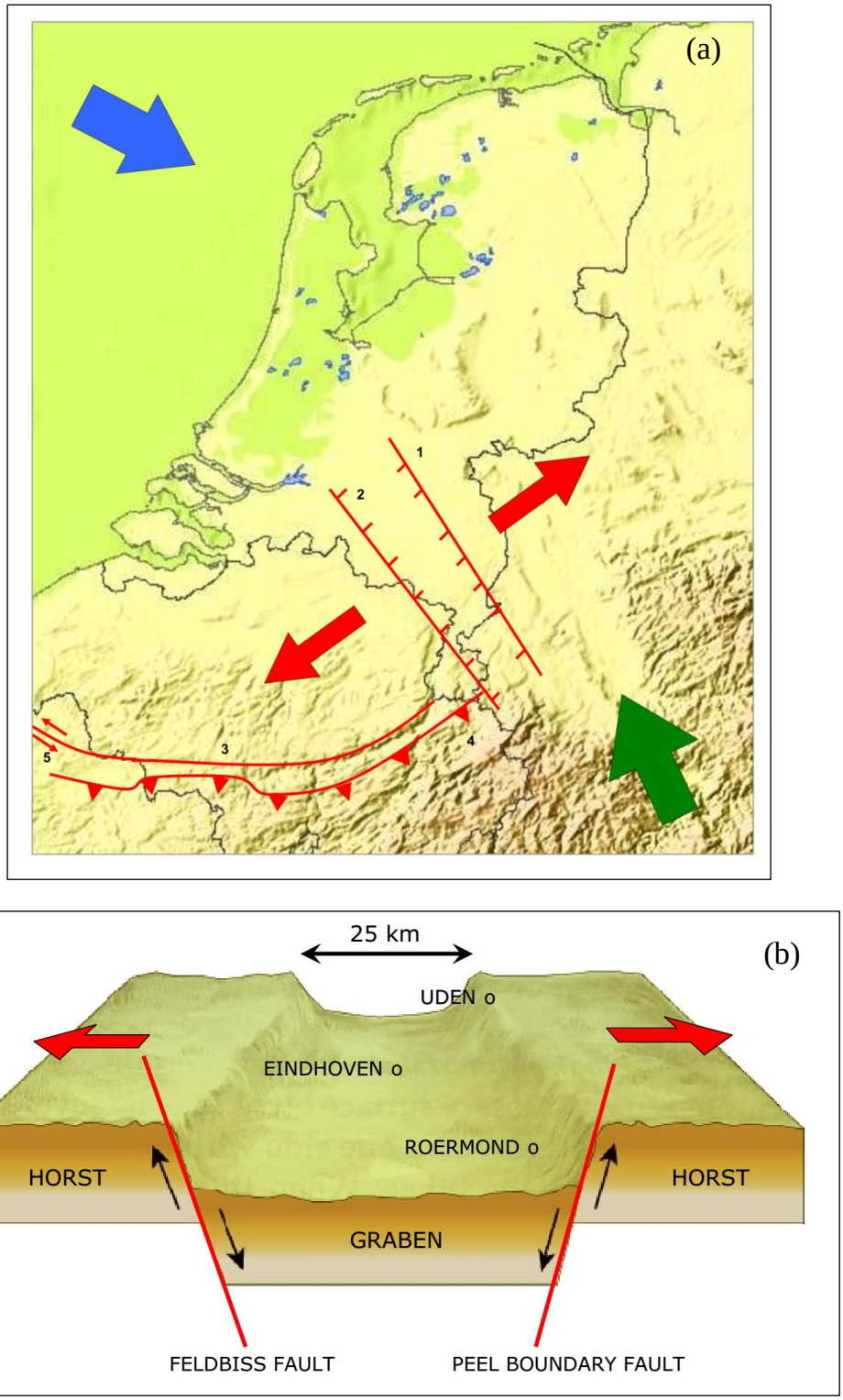

Fig. 6: Schematic representation of the Rhine Graben System: (a) major stress components in blue and green: compression by tectonic plates movement; red: resultant extension, 1: Peel boundary fault, 2: Feldbiß fault; (b) section through Roer Valley Graben (DE VOS, 2010)

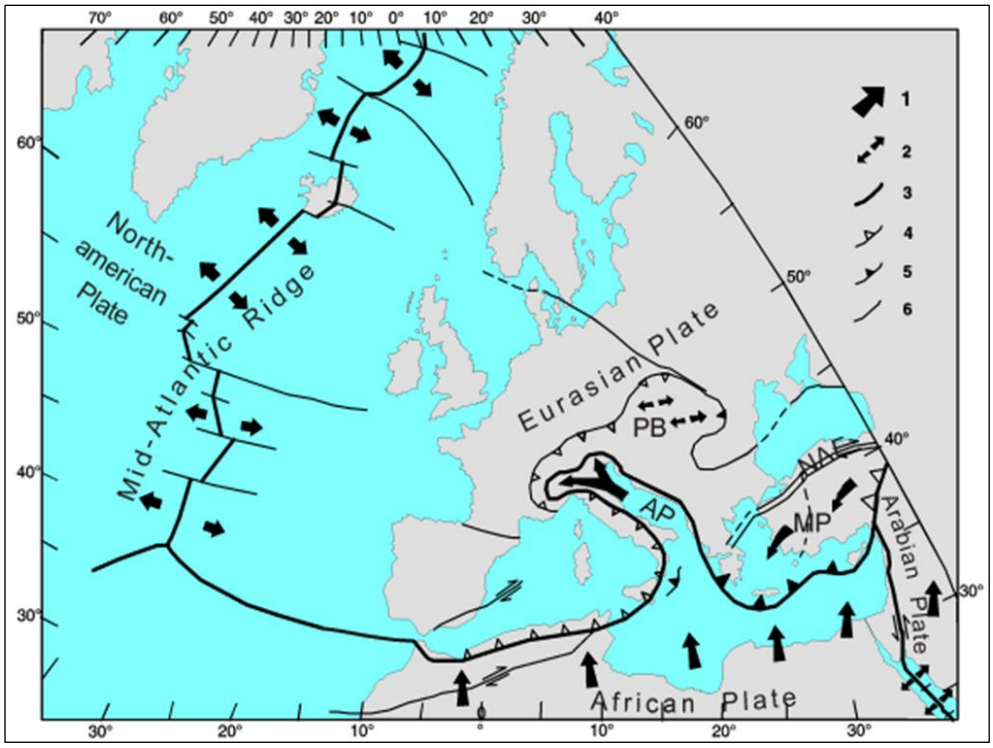

Fig. 7: Tectonic map of Europe. Arrows indicate direction of movement of the plates (After: GRÜNTHAL, 2004.)

2.3 Active faults and top of Carboniferous rocks

For this project, TNO provided an updated map of active faults, as well as the depth distribution of the top surface of the Carboniferous rocks (Fig. 7). The faults are illustrated at two levels: ground surface and top of the Carboniferous (Fig. 7). The faults being present in the area of this study correspond to the southern boundary of the Roer Valley Graben: the north-west-south-east faults Feldbiß, Heerlerheide, Benzenrade and the west-northwest Kunrader fault (Fig. 6). The horizontal offset between the fault lineament levels indicates a steep NE dipping direction. They display important vertical offset in the geological formations (Fig. 8). The source mechanism of these faults is normal (Fig. 9), but CAMELBEECK (1994) reports a strike-slip movement in the Kunrader fault.

Together with the observation of shallow and deeper seismicity (up to 20 km approximately) south of the Feldbiß fault, where source mechanisms vary (Fig. 9), there are different hypotheses summarised by DOST & HAAK (2007) as:

- decoupling of the crust, where the upper crust is more brittle than the lower crust expected to be ductile;
- presence of deeper faults with different orientation. This is plausible given by the fact that older geological formations carry on a different tectonic history (e.g. Brabant Massive, overthrusting of the Hoge Venen (Hautes Fagnes) Massive).

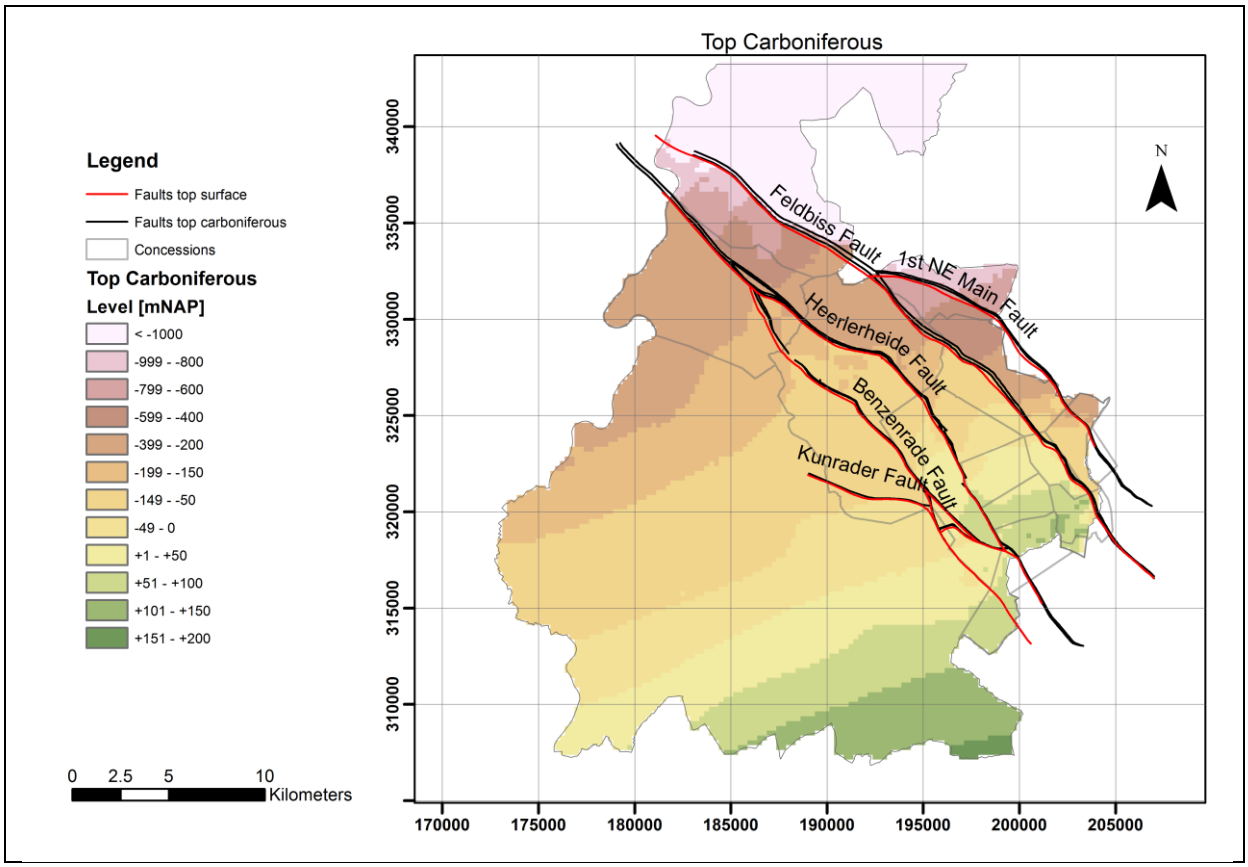

Fig. 8: Active faults and top surface level of the Carboniferous (bed)rock

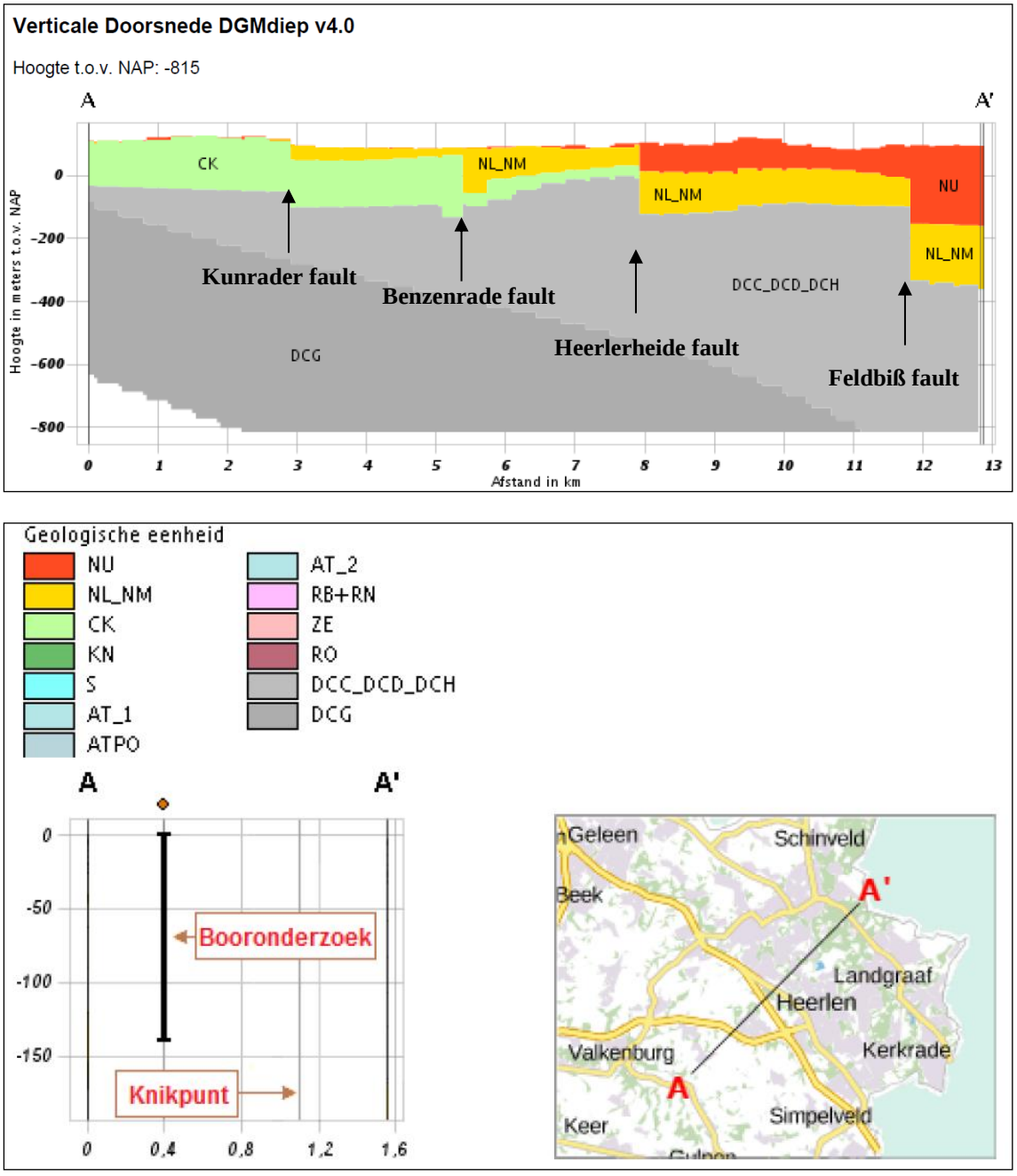

Fig. 9: NE-SW geological cross section retrieved from Dinoloket, DGMdiep v4.0. Grayish formations (DCG, DCC): Carboniferous; green (CK): Cretaceous limestones, orange (NM) Eocene-Miocene Middle North Sea Group; red (NU): Miocene-Quaternary Upper North Sea Group

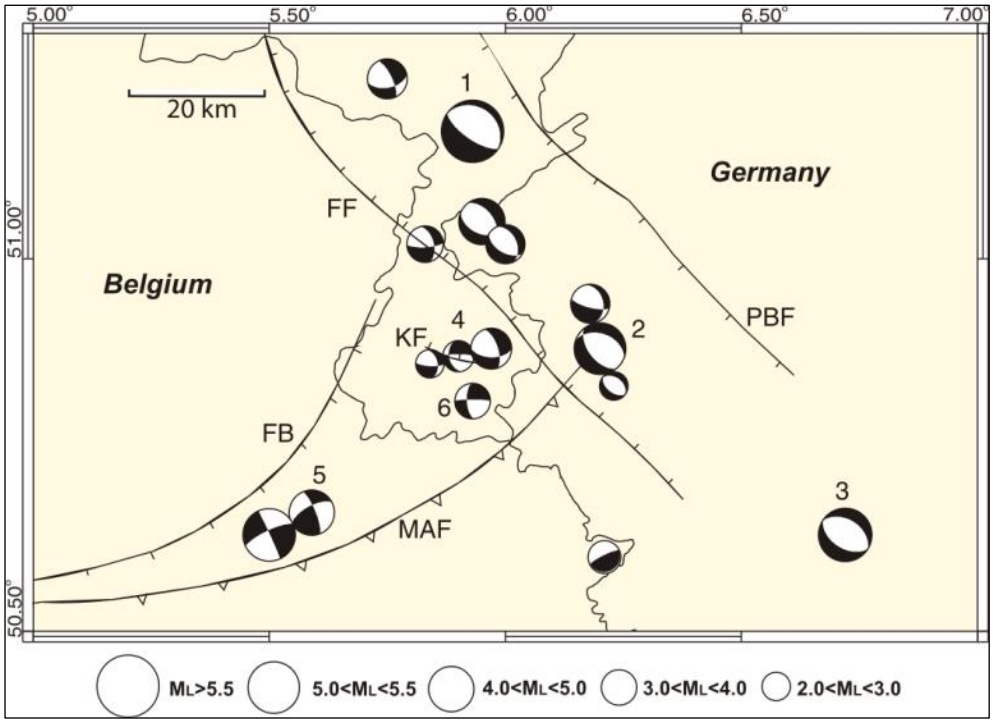

Fig. 10: Rupture mechanisms in and around the Roer Valley Graben. Fault names: KF: Kunrader Fault; FF: Feldbiß fault; PBF: Peel Boundary Fault; FB: Faille Bordière; MAF: Midi-Aachen Thrust Fault (DOST & HAAK, 2007). The circles show for each recorded earthquake the focal mechanism, which refer to the orientation of the fault plane that slipped and the direction of the slip. The focal mechanisms within the Roer Valley Graben and around the Kunrader Fault show mainly normal fault mechanisms.

2.4 Local Seismicity

Until now, the seismicity registered in the southern region from the Netherlands is related to tectonics only. The KNMI seismic catalogue makes a clear distinction between tectonic earthquakes and induced earthquakes (KNMI, 2014a). Induced seismicity occurs in the north of the Netherlands or western part of Germany by gas and mining exploitation (Fig.). In the area of

this study only tectonic seismicity was recorded. This does not mean that induced seismicity due to mining did not occur. It is possible that induced events have been so small that they were not recorded during the active mining period. Fig. 10 illustrates the distribution and magnitudes of the seismicity in the Roer Valley Graben.

The largest tectonic earthquake registered in the area occurred on 13.04.1992 in Roermond (the Netherlands) and a similar one on 14.03.1951 in Euskirchen (Germany), 80 km SE from Roermond. Both earthquakes had a magnitude M_L=5,8 (Fig. 10) and an intensity Mercalli VII, which is destructive (DOST & HAAK, 2007). The Roermond earthquake and most of the seismicity from the region is associated to the Peel fault, the northern boundary of the graben. The Feldbiß fault has events of lower magnitude in comparison to the Peel fault. However, for many events that occurred in the middle of the graben it is unclear to which structure they are associated (DOST & HAAK, 2007). The Kunrade fault, at the southwestern side of the graben, has associated seismic swarms during 1985 - 1986 and 2000 - 2002 (chap. 2.8).

The maximum expected earthquake for the south of the Netherlands is M_L = 6,3 ± 0,2 or M_w = 6,2 ± 0,2 (DOST & HAAK, 2007; KNMI, 2014a).

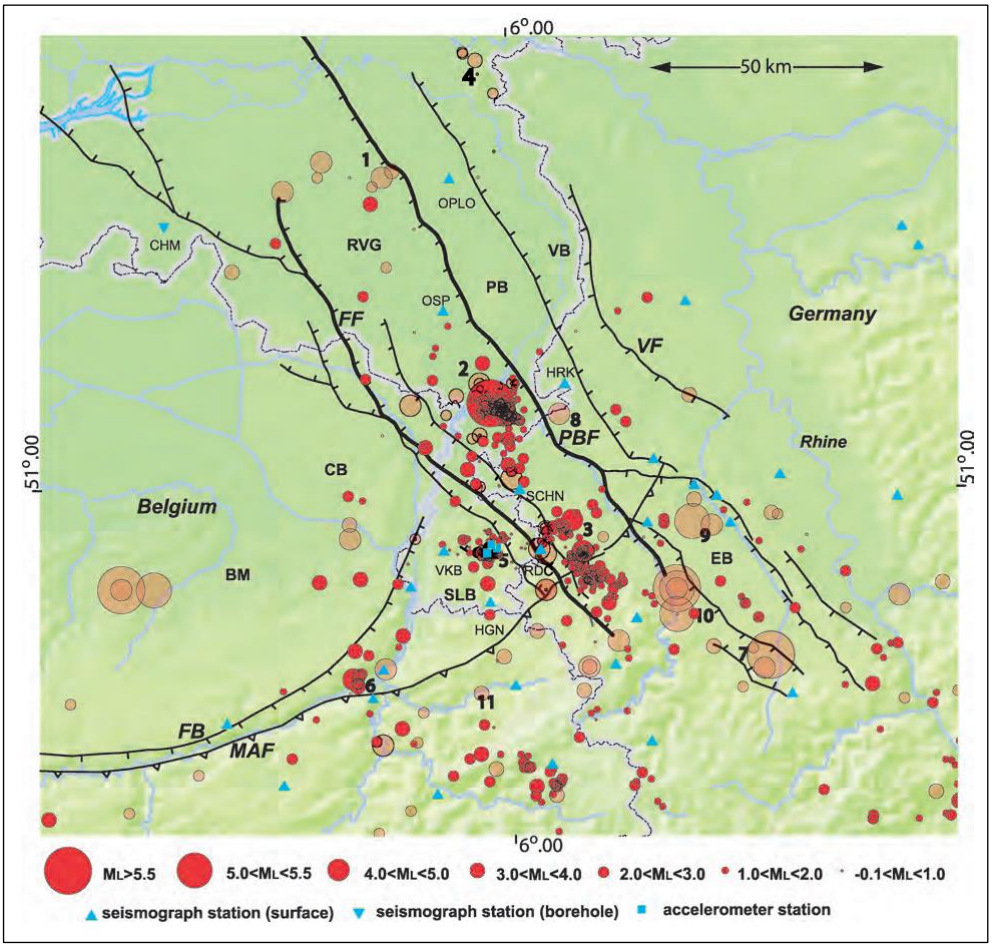

Fig. 11: Natural seismicity in and around the Roer Valley Graben for the period 1700 - 2003. Earthquakes are shown in circles, scaled according to magnitude; events before 1980 in light red, those after 1980 in red. Localities mentioned in text: 2: Roermond; 7: Euskirchen; Tectonic structures: BM: Brabant Massif; RGV; Roer Valley Graben; PB: Peel Block; VB: Venlo Block; CB: Campine Block; EB: Erft Block; SLB: South Limburg Block; PBF: Peel Boundary Fault; FF: Feldbiß fault; VF: Viersen fault; FB: Faille Bordière; MAF: Midi-Aachen thrust fault (DOST & HAAK, 2007)

2.5 Seismic catalogues

In the Netherlands, KNMI maintains the reference seismic catalogues. The neighbouring countries, Belgium and Germany, have counterpart institutes, listed in Tab. 1, that maintain the reference seismic catalogues from each respective country.

Tab. 1: Seismological observatories responsible for the seismic monitoring

Country	Source	Instrumental records
the Netherlands	KNMI (2014a)	Since 1908
Belgium	Royal Observatory of Belgium (ORB, 2014)	Since 1910
Germany	National: BGR, SDAC (2016) and GFZ (2016)	Since 1896
	Earthquake observatorium Bensberg (University of Cologne) (BNS, 2016).	Since 1975
	Federal: Geological Survey NRW Krefeld (GDNRW, 2016)	Since 1980

Different seismic catalogues from one region might differ in magnitude ranges and location interpretation, given by the different instrumentation used in the different countries. Besides, the instrumentation for a given country varies over time, resulting on different degrees on interpretation uncertainties (chap. 2.7). In the Netherlands, KNMI has a continuous record of seismicity since 1908, but until 1970 approximately, only events with magnitudes above 4 to 5 were possible to be registered. Since the 1970s - 1980s a larger instrumentation network enhanced the detection capacity, detailed in chap. 2.7.

For this study, the KNMI catalogue (KNMI, 2014a) is used because KNMI is the organization responsible for the seismic monitoring and reference catalogue for the Netherlands. KNMI is able to use more local data and applies additional corrections based on the local seismo-tectonic knowledge (DOST, 2015). The monitoring network from KNMI in the south of the Netherlands is illustrated in Fig: 11.

Fig. 12: Monitoring network from KNMI in south of the Netherlands (KNMI, 2014a)

There are other relevant European seismic portals and references with seismic catalogues, i.e.: CSEM-EMSC (2014), ISC (2014), EFEHR (2014), REAMER & HINZEN (2004), VANNESTE et al. (2013). An attempt towards a unified catalogue of historical and instrumental earthquakes from central, northern, and north-western Europe (CENEC) is presented by GRÜNTHAL et al. (2009).

2.6 Seismic catalogue for the project area

The seismicity registered within the area of interest for this project was selected and extracted (see blue area in Fig. 12), generating a new project-specific sub-catalogue The project area of interest is delimited as:

1. Minimum and maximum longitude: 5°40'E; 6°00'E;

2. Minimum and maximum latitude: 50°45'N; 51°15'N.

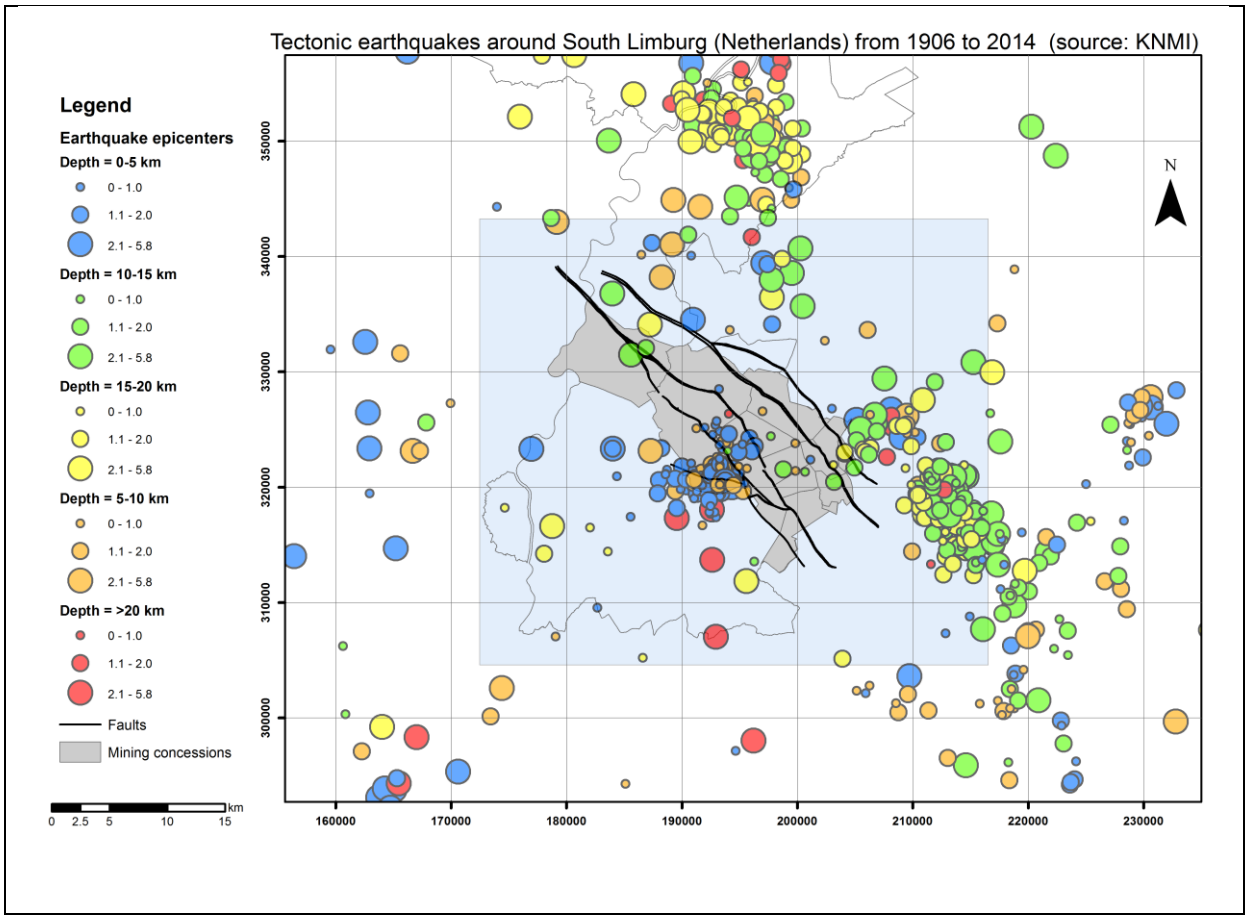

Fig. 13: Seismic catalogue (KNMI). The different colours represent depth ranges (as specified) at which the events occur. The sizes of the epicentres represent magnitude ranges. The area of interest for this study is shown in blue

The seismic catalogue within this area of interest consists of 244 events between 1906 and 2014. From this, 6 earthquakes with focal depths larger than 20 km were removed because their source mechanism differs from the more shallow seismicity, which is focus of the project. Dost, 2015). The final catalogue in the project area consists of 238 events with magnitudes (M_L) ranging between 0,0 and 3,9, at depths within the upper 19 km (Fig. 12).

2.7 Location, depth and detection threshold seismic catalogue

The detection and location interpretations have always a certain amount of error in the seismic catalogue. This error or uncertainty is related to the amount and type of instruments available throughout different time periods. At least 3 independent seismic observations are needed to locate a seismic event (KNMI, 2012). Data from more stations usually give more precise results. Old events were generally recorded with fewer instruments and the instruments at the time were also less precise, therefore the error in the determination of epicentre and depth of old events is larger. The accuracy of the tectonic catalogue from the KNMI in the project area can roughly be divided into two periods (Dost, 2015):

- Before 1985: epicentre: ~5 km, depth ~5 km
- After 1985: epicentre ~1 km, depth: ~1 km

In terms of magnitude, the overall KNMI network in the Netherland has a detection threshold of M_L=1,0 (Fig. 14). This means that earthquakes smaller than this detection threshold are generally not recorded. However, there are parts further from a seismic station where the detection threshold is larger than 1,5, but also areas within the dense grid of stations (as is the case in the project area) where smaller earthquakes can be detected.

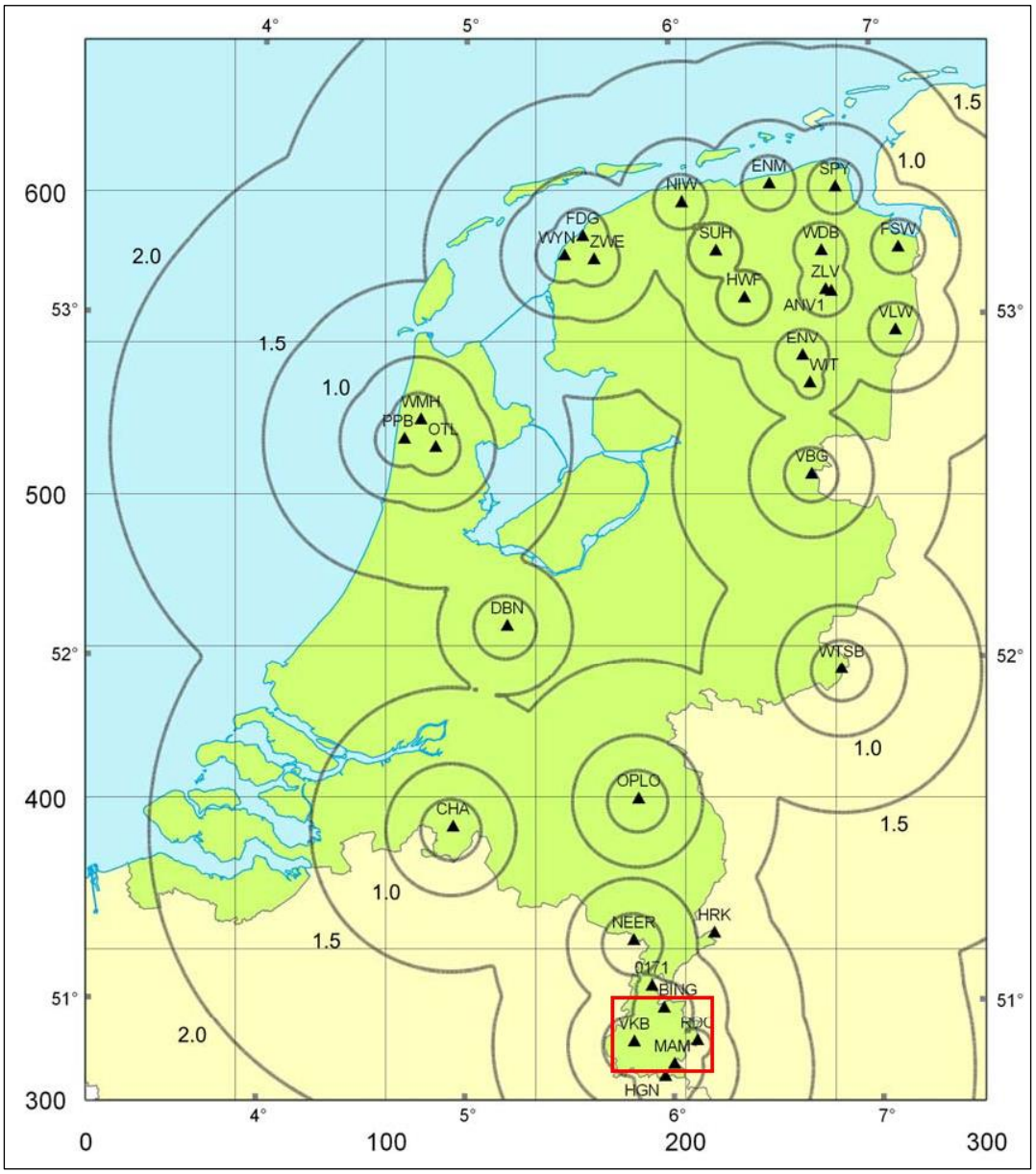

Fig. 14: Detection threshold during 2005 - 2010 (KNMI, 2012). The triangles show the seismic stations. The lines show the iso-magnitude threshold values. The area of interest is shown in the red box. Along the horizontal and vertical axes the coordinates (latitude and longitude are shown in degrees and distance is shown in kilometres)

2.8 Voerendaal-Kunrade swarms

An earthquake swarm is a sequence of seismic events that strike a certain area within a relative short time. The time frame can vary largely from days to months. A seismic sequence or swarm can also occur as fore- or aftershocks of a main event, but there is not always a main event distinguished.

Two earthquake swarms have been recognised in South Limburg: the first between 1985 - 1986 and the second between 2000 and 2002 (see Fig. 18 and Fig. 19):

- 1985 - 1986 swarm: Between 07.12.1985 and 07.01.1986, 9 events were registered in the Voerendaal area. These had magnitudes (M_L) between 1,4 and 3,0, and occurred at depths from 2,3 to 8,1 km (Fig. 18). The biggest event with M_L 3,0 occurred on 07.12.1985. The events from this swarm are interpreted as normal (HOUTGAST, 1991, in DOST & HAAK, 2007) with 270° strike and 80° N dip. However CAMELBEECK (1994) classifies the events as strike-slip. The latter interpretation is referring to the hypothesis regarding (deeper) movements further south in Belgium, which appears to be characterised by strike-slip. According to DOST (2015) the shallow events here are more likely related to normal movement than strike-slip.
- 2000 - 2002 swarm: Between 20.12.2000 and 31.08.2002 145 events were registered and attributed to the Voerendaal swarm. These events reached magnitudes (M_L) up to 3,9 and depths up to 10,4 km. The mean depth is 5 km, and most of the events are shallower than 8 km (Fig. 14). The biggest event with M_L 3,9 occurred on 23.06.2001 and damage was reported as a result of this. It is also apparent that this event occurred at a relatively shallow depth of 2,2 km. Newspaper articles report on about

400 damage cases, mainly damage to chimneys, cracks in walls, interior damage, see Fig. 15. There were no casualties reported. KNMI (2014b) relates these events to the Kunrader fault. A normal-faulting mechanism is better constrained for these events and is considered typical for these events (DOST & HAAK, 2007). KNMI (2014b) considered a possible relation between those events with the former mining activities unlikely due to their deeper location in relation to the depth of the abandoned mines.

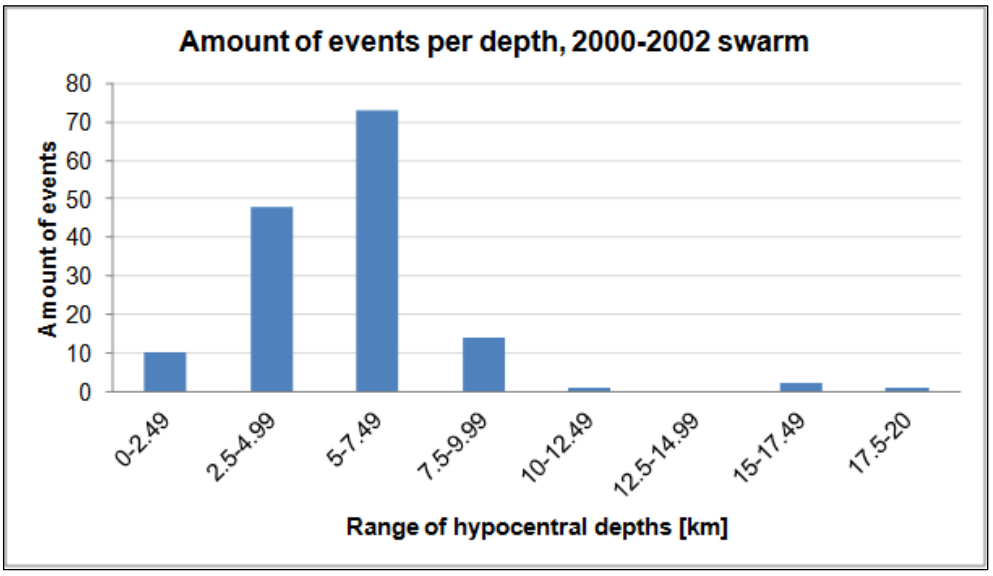

Fig. 15: Amount of events from the 2000 - 2002 swarm per depth

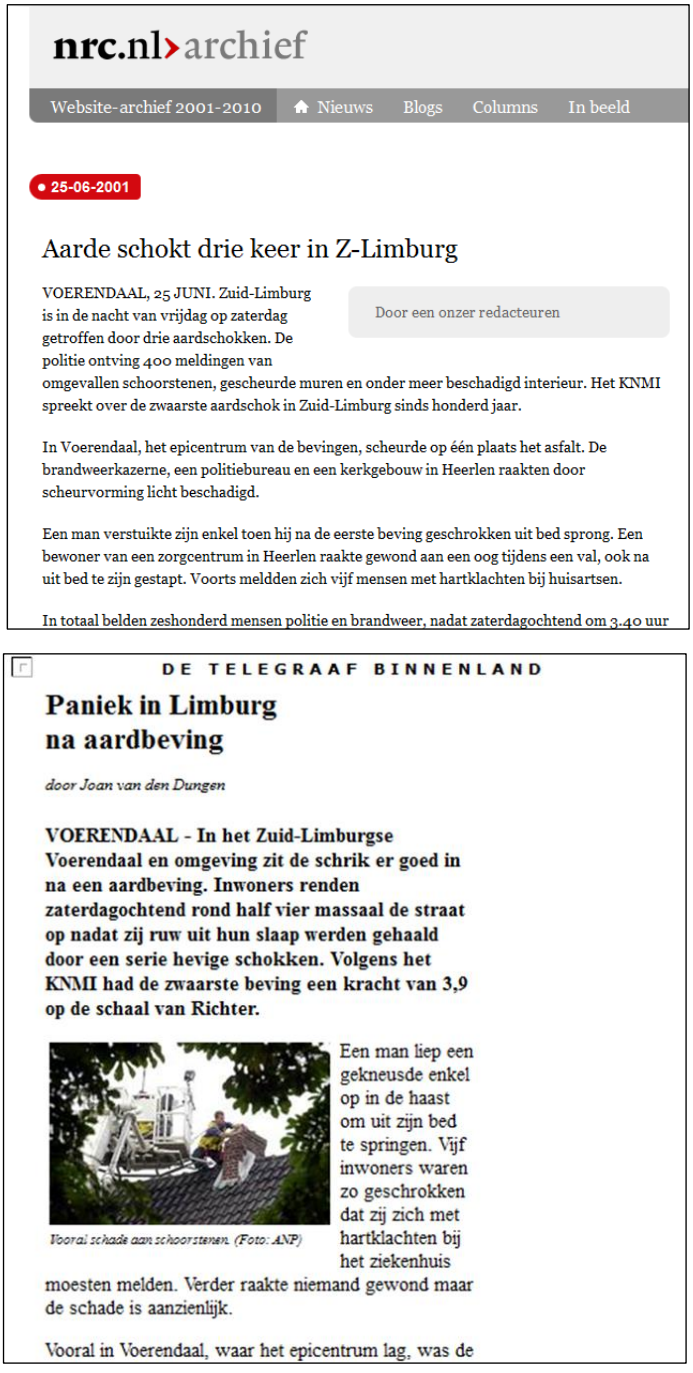

nrc.nl›archief

Website-archief 2001-2010 | Nieuws | Blogs | Columns | In beeld

• 25-06-2001

Aarde schokt drie keer in Z-Limburg

Door een onzer redacteuren

VOERENDAAL, 25 JUNI. Zuid-Limburg is in de nacht van vrijdag op zaterdag getroffen door drie aardschokken. De politie ontving 400 meldingen van omgevallen schoorstenen, gescheurde muren en onder meer beschadigd interieur. Het KNMI spreekt over de zwaarste aardschok in Zuid-Limburg sinds honderd jaar.

In Voerendaal, het epicentrum van de bevingen, scheurde op één plaats het asfalt. De brandweerkazerne, een politiebureau en een kerkgebouw in Heerlen raakten door scheurvorming licht beschadigd.

Een man verstuikte zijn enkel toen hij na de eerste beving geschrokken uit bed sprong. Een bewoner van een zorgcentrum in Heerlen raakte gewond aan een oog tijdens een val, ook na uit bed te zijn gestapt. Voorts meldden zich vijf mensen met hartklachten bij huisartsen.

In totaal belden zeshonderd mensen politie en brandweer, nadat zaterdagochtend om 3.40 uur

DE TELEGRAAF BINNENLAND

Paniek in Limburg na aardbeving

door Joan van den Dungen

VOERENDAAL - In het Zuid-Limburgse Voerendaal en omgeving zit de schrik er goed in na een aardbeving. Inwoners renden zaterdagochtend rond half vier massaal de straat op nadat zij ruw uit hun slaap werden gehaald door een serie hevige schokken. Volgens het KNMI had de zwaarste beving een kracht van 3,9 op de schaal van Richter.

Vooral schade aan schoorstenen. (Foto: ANP)

Een man liep een gekneusde enkel op in de haast om uit zijn bed te springen. Vijf inwoners waren zo geschrokken dat zij zich met hartklachten bij het ziekenhuis moesten melden. Verder raakte niemand gewond maar de schade is aanzienlijk.

Vooral in Voerendaal, waar het epicentrum lag, was de

Fig. 16: Newspaper articles on damage from largest event of the second Voerendaal Swarm (M. 3,9, 23.06.2001)

The two swarms are associated to the E-W Kunrader fault (DOST & HAAK, 2007), which diverts in strike from the general NW-SE trend of

the Roer Valley Graben (see chap. 2.2 and chap. 2.10). The events related to these swarms are listed as a separate catalogue in Appendix 3.

Historically, there is reference to one event in that region on 04.03.1930 (KNMI, 2014b). The larger earthquakes have been felt up to 10 km away from their source, with a Mercalli Intensity IV-V.

These swarms are evaluated in further detail in this report to determine a possible relation with the groundwater rise.

2.9 Ground heave

Radar interferometry (InSAR) has been used to study ground movements in the South Limburg coal district during 1992 - 2009 (DE VENT & ROEST, 2013; CARO CUENCA, 2012). But, in both cases only a relation was established between ground deformation and mining activity and not with seismicity (Fig. 16). CARO CUENCA & HANSSEN (2011) looked at possible relation between the seismic swarms and ground deformation, but they were not conclusive.

A continuation of the ground movement analysis was done within the scope of this project by working group 5.2.1. Also here several cross sections were made across the former mining area. The cross section along the Kunrader fault and Voerendaal is provided in Fig. 17. More details can be found in the report of working group 5.2.1.

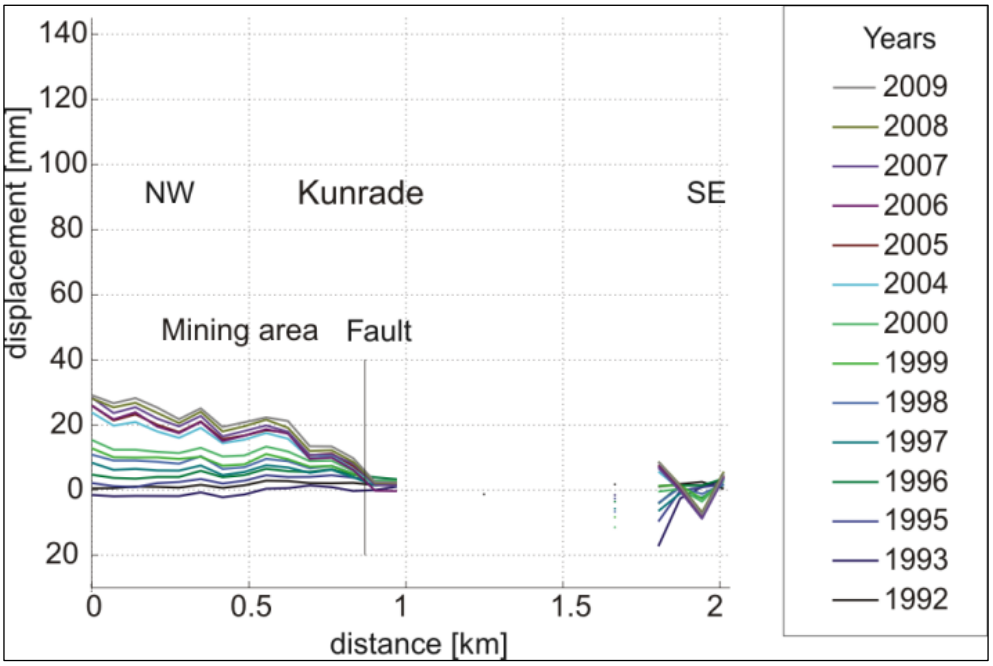

Fig. 17: Mean annual displacement near Kunrader fault (CARO CUENCA, 2012)

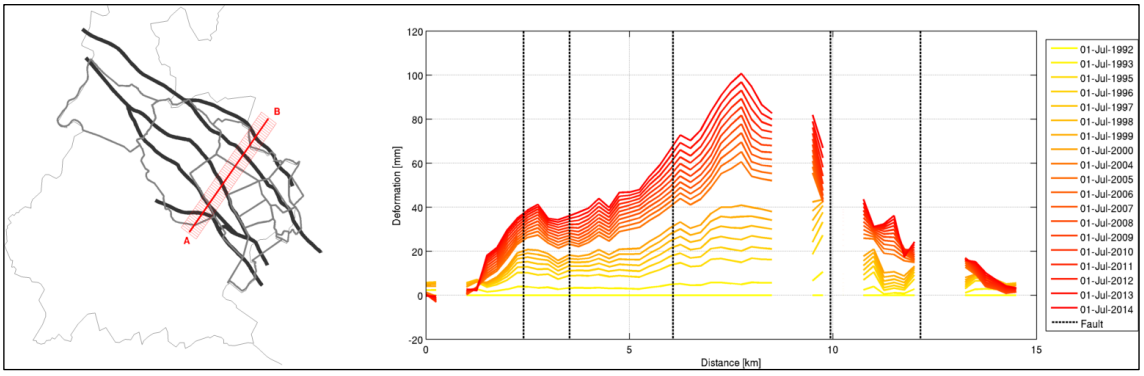

Fig. 18: InSAR profile along Voerendaal. Faults from left to right are: Kunrader, Benzenrader, Heerlerheide, Feldbiß and 1st NO Hoofdbreuk. The largest ground uplift can be observed between the Heerlerheide and Feldbiß faults in the centre of the former coal mining district

2.10 Relation between seismicity and faults

Although DOST & HAAK (2007) and KNMI (2014b) are clear on the relation from the Voerendaal swarms to the Kunrader fault, an additional check is made in this study for confirmation. For this purpose sections have been prepared perpendicular to the general orientation of the active faults and across the area where the Voerendaal-Kunrade swarms occurred (see Fig. 18 and Fig. 19 for the location of the section and see Fig. 20 and Fig. 21 for these sections). In these cross sections the current topographic surface and the top of the Carboniferous rocks have been drawn based on the available GIS data. The orientations of the active faults (Kunrader fault, Benzenrader fault, Heerlerheide fault and Feldbiß fault) have been derived from the fault map (Fig. 7). The fault map depicts the intersection of the faults with the topographic surface and the top of the Carboniferous surface. Thus, the orientation of the fault can be extrapolated downward. It should be noted that the orientation of the fault is highly uncertain, especially at larger depths. At greater depths in general a certain flattening occurs. Considering the total tectonic setting, the NW-SE striking faults in South Limburg may show an angle of dipping at a depth of 5 km in the order of magnitude of 50°. This is due to the fact that the stress field at greater depth becomes more isotropic.

Despite the uncertainty in the location of the epi- and hypocentres and the orientation of the faults, the seismic events from both swarms can be spatially correlated to the Kunrader fault, as already pointed by DOST & HAAK (2007).

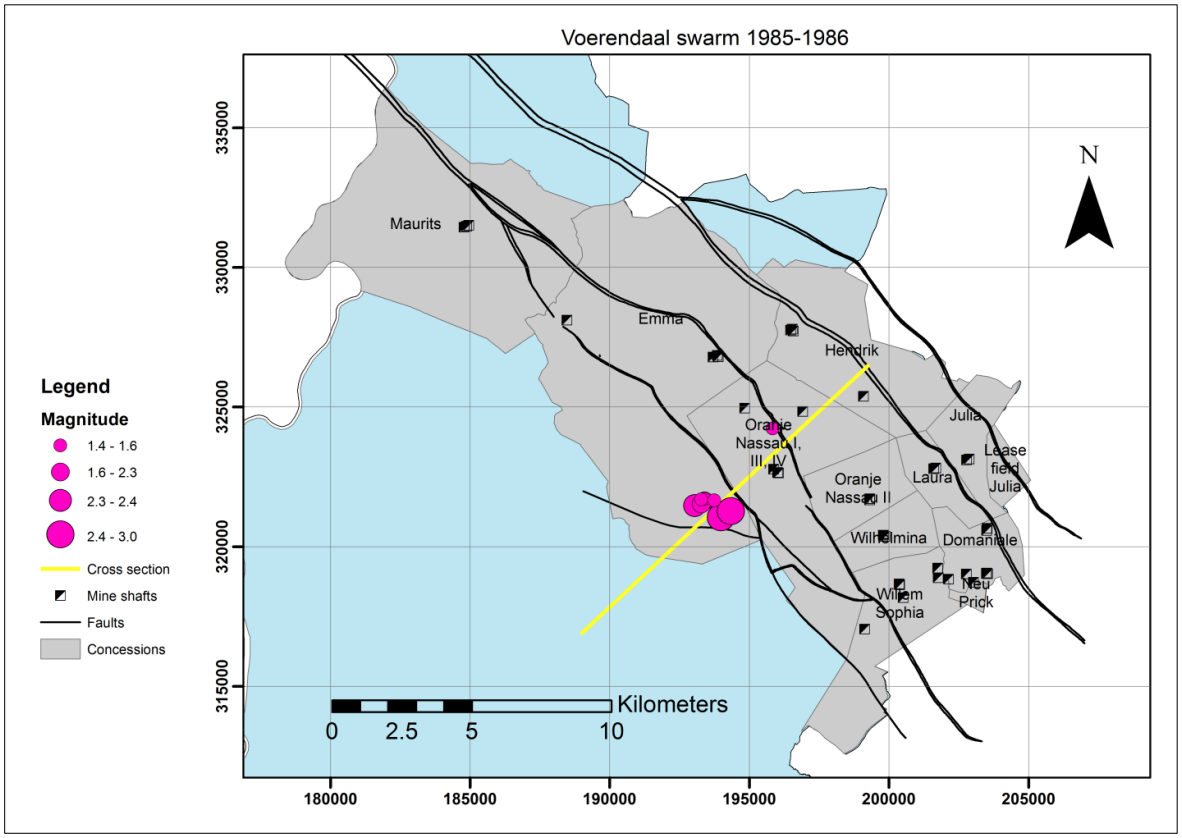

Fig. 19: Location of the 1985 - 1986 epicentres of the Voerendaal swarm with respect to the faults and mining areas. The yellow line depicts the cross section shown in Fig. 20. The shown events correspond with the listed events in Appendix 1

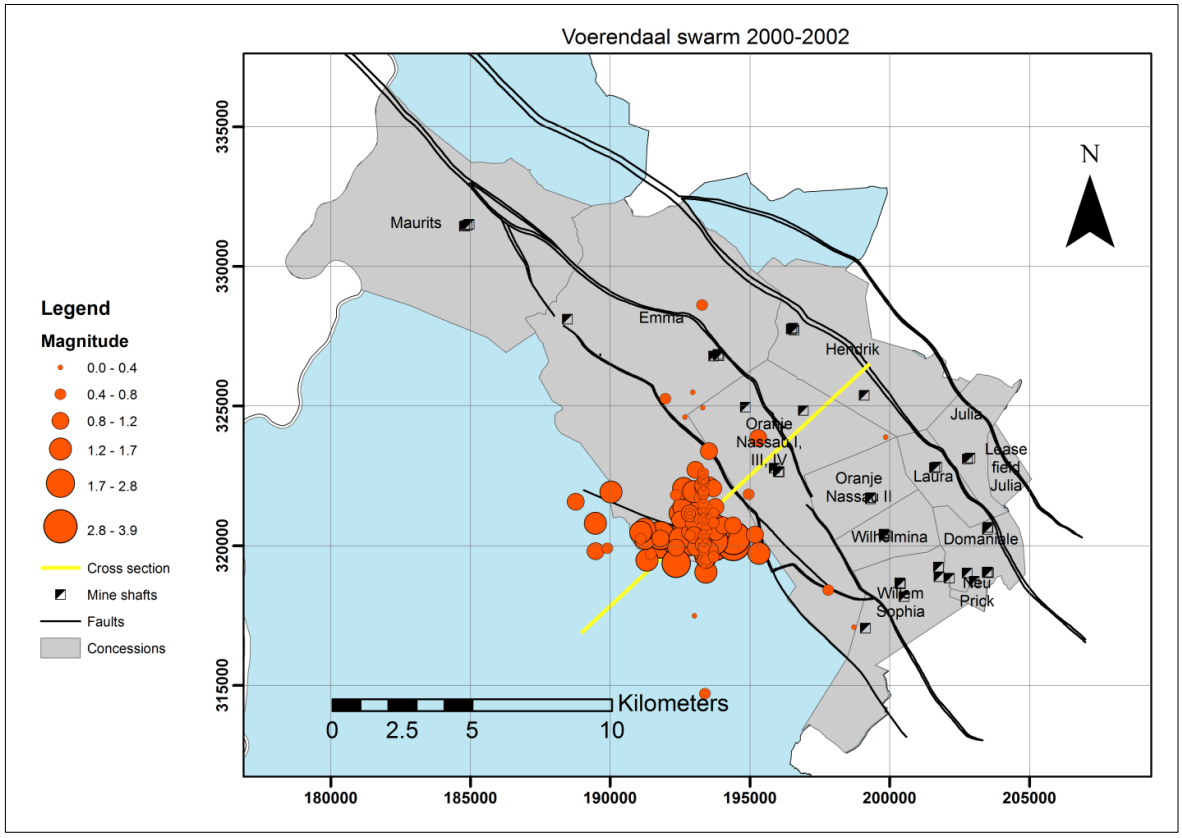

Fig. 20: Location of the 2000 - 2001 epicentres of the Voerendaal swarm with respect to the faults and mining areas. The yellow line depicts the cross section shown in Fig. 21. The shown events correspond to the listed events in Appendix 1

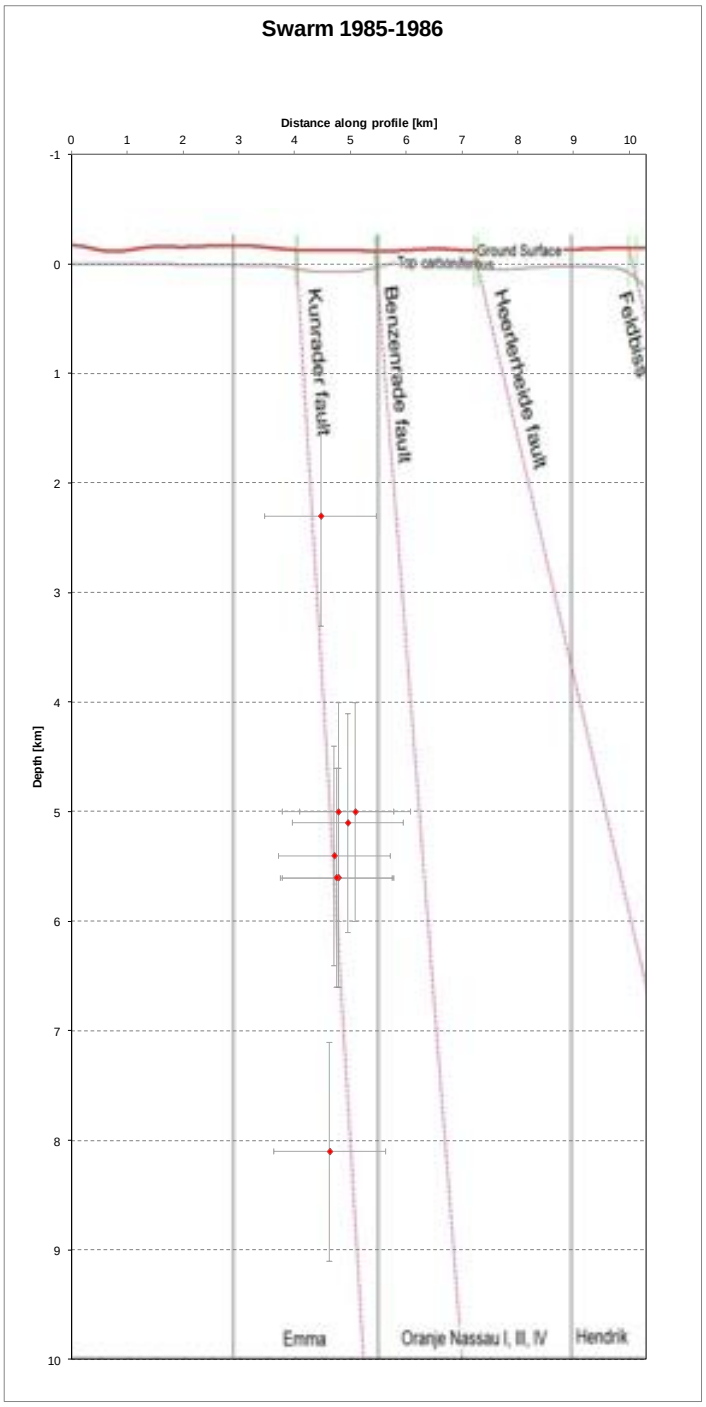

Fig. 21: Cross section along Voerendaal with the 1985 - 1986 events shown as red dots. The vertical scale is 2x the horizontal scale. The horizontal and vertical bars around the red dots (the hypocentres) show the uncertainty in the location

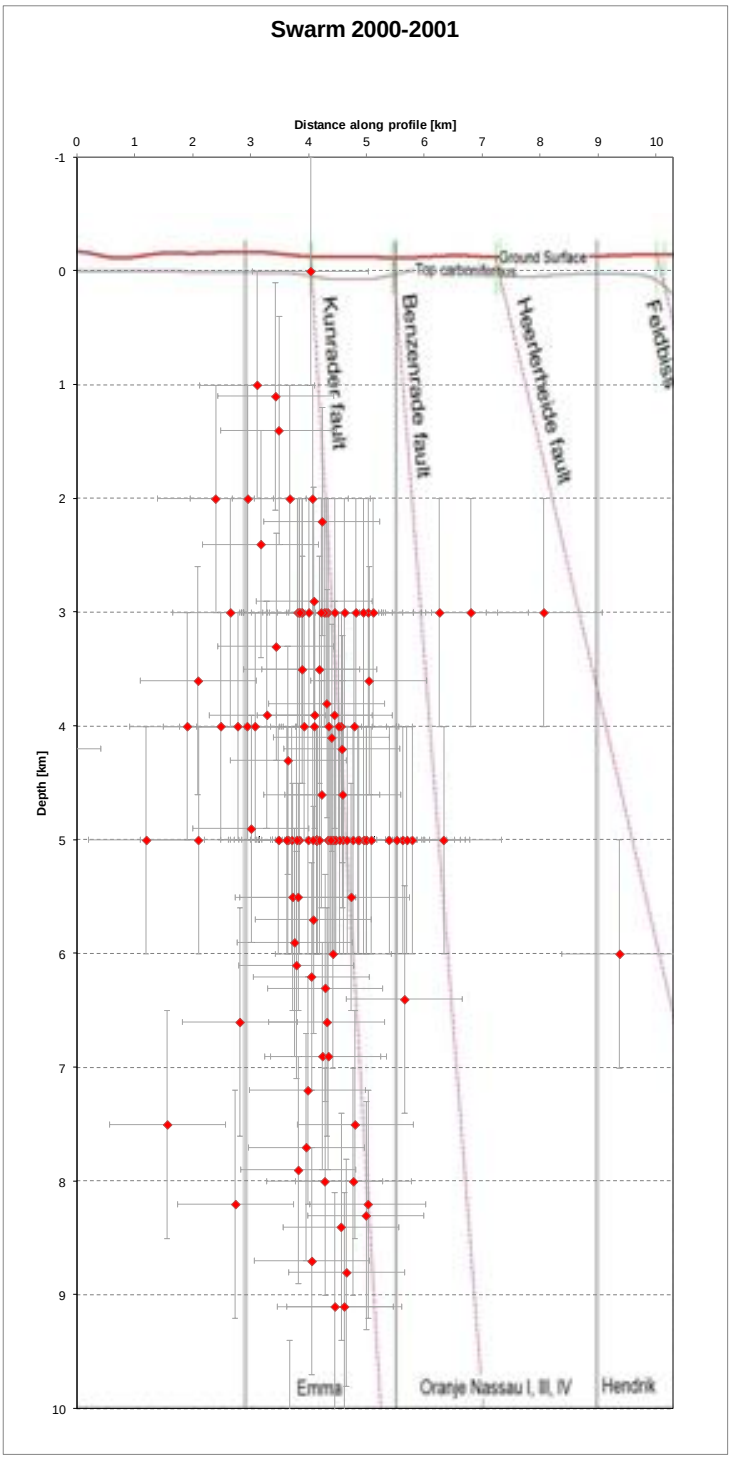

Fig. 22: Cross section along Voerendaal with the 2000 - 2002 events shown as red dots. The vertical scale is 2x the horizontal scale. The horizontal and vertical bars around the red dots (the hypocentres) show the uncertainty in the location

3 Spatial and temporal analysis

3.1 Introduction

Possible relations over time and space between groundwater variation, ground ground heave and seismicity are analysed in this chapter. These relations can be indicators on the identification of possible induced or triggered seismicity by the mining after-effects. The starting points used in this analysis are:

- Seismic catalogue within area of interest covering the project area.
- Seismic sub catalogues for seismic swarms 1985 - 1986, 2000 - 2002.
- Fault map and top of Carboniferous map provided by TNO.
- Ground deformation (subsidence/ground heave) rates provided by TU Delft based on InSAR data and conventional geodetic measurements.
- Groundwater variations provided by IHS and modelled by W+B. Two types of data are used:
    - Local and regional aquifers in and around the abandoned mine;
    - Predicted levels for the stationary situation (infinite time from now).

3.2 Ground heave over time

Working group 5.2.1 has extracted detailed levels of ground surface over time from InSAR data. This is described in the report of working group 5.2.1. With the data the ground deformations (ground heave or subsidence) can be calculated over different time periods. To determine whether there is a possible relation between ground deformation and seismicity both data are plotted in maps. These maps are shown in Fig. 22 to Fig. 23. The selected time frames are based on the availability of InSAR data and the mission types. The first InSAR satellite data

became available in 1992. Between 2000 and 2003 there was no operational InSAR satellite system. After 2010 a different InSAR satellite system came in operation and was used for the analysis. From the three maps there is no clear relation between the seismicity and ground deformation. Only in Fig. 22 and there is a seismic event in the Maurits concession near Geleen at the Heerlerheide fault line, which is right at the northern boundary of an area experiencing ground heave. These two events are:

- Locality Elsloo: 15.05.1996, M_L 2,2, Depth 13,7 km
- Locality Geleen: 02.03.2003, M_L 1,8, Depth 13,6 km

Because of the relatively large depths (>10 km) at which these two events occur, a relation between the ground heave and the seismicity is not likely. The ground heave is a phenomenon that only reflects what is happening in the shallow subsurface.

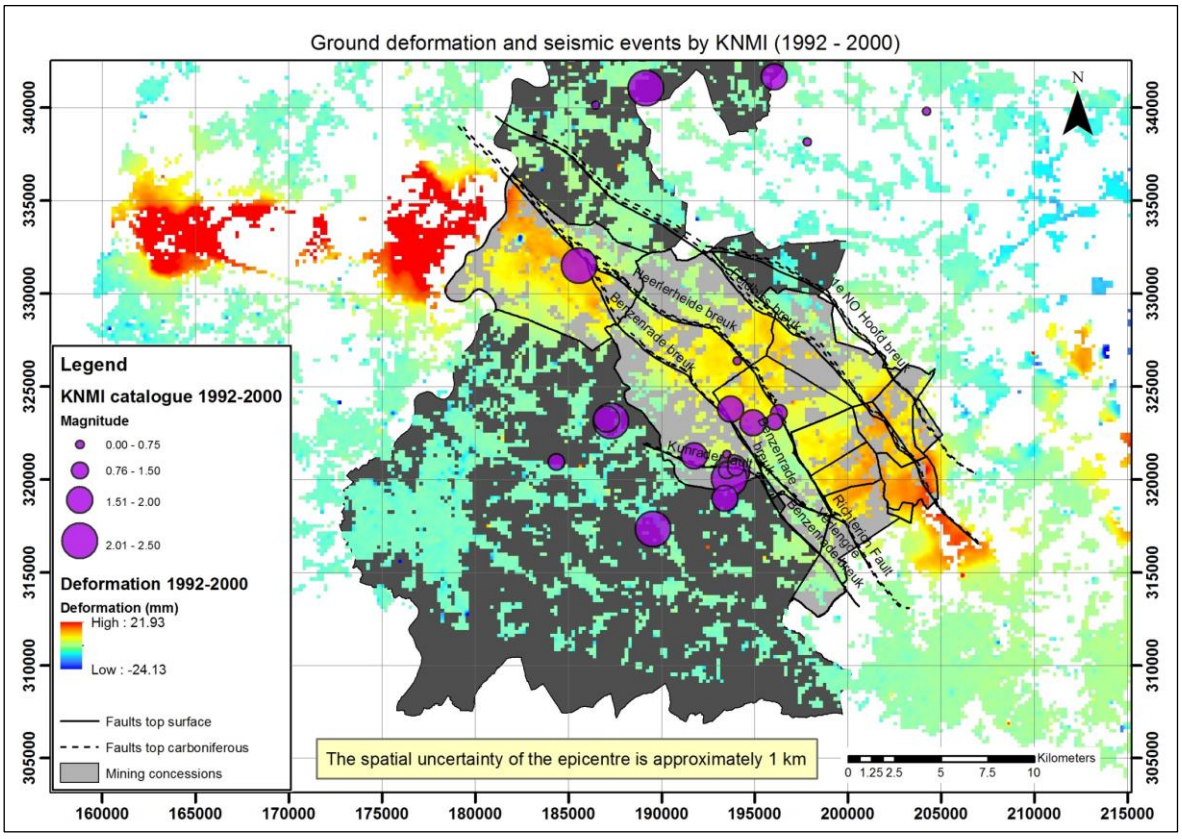

Fig. 23: Ground deformations from InSAR and seismic events 1992 - 2000

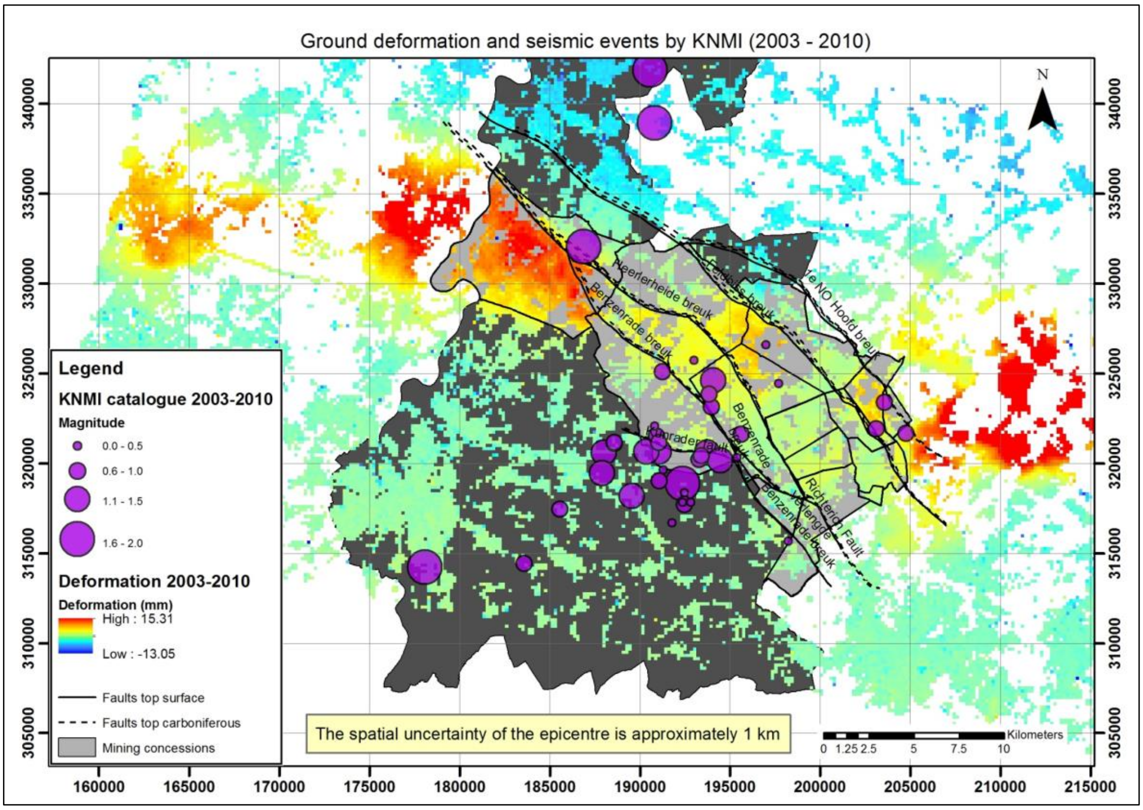

Fig. 24: Ground deformations from InSAR and seismic events 2003 - 2010

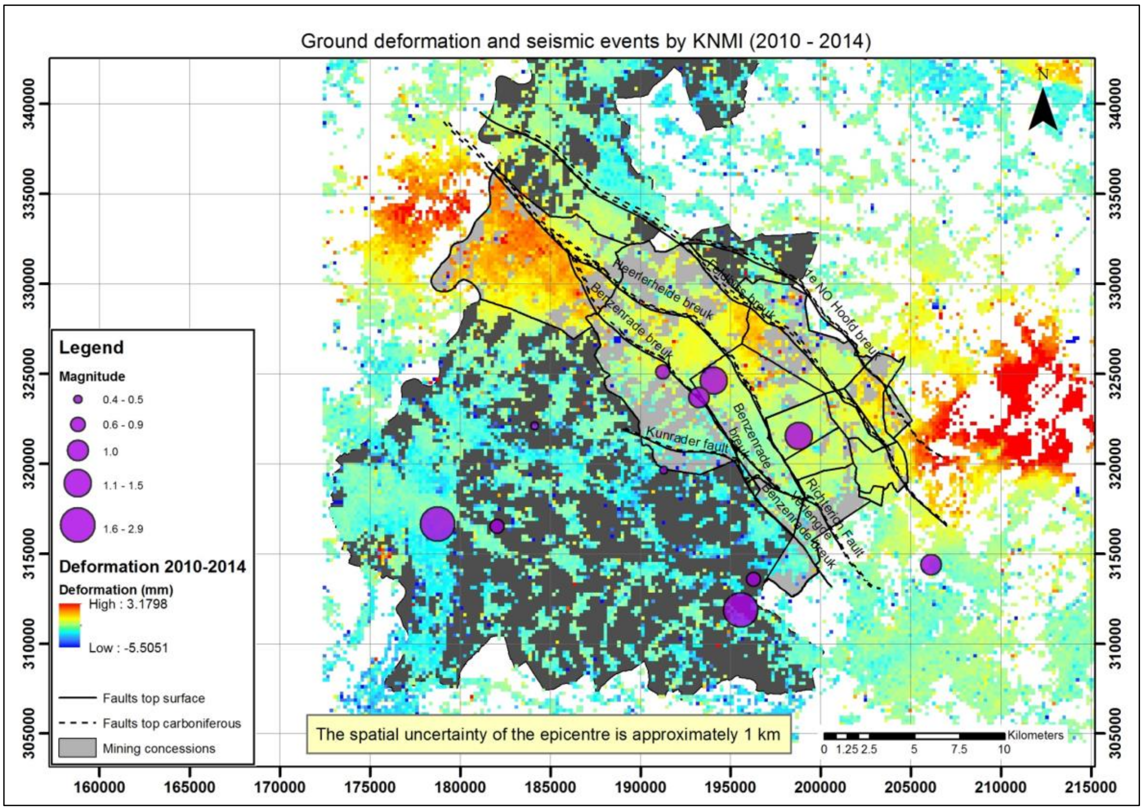

Fig. 25: Ground deformations from InSAR and seismic events 2010 - 2014

3.3 Integration and visualisation of mine water and seismic data

The temporal evolution of the seismicity from the KNMI catalogue is plotted as amount of energy (in joules) released per year with the temporal variation of the mine water measured per basin in Fig. 26. The same yearly seismic energy is plotted again as an accumulated energy with the rise in mine water in Fig. 25. The seismic energy is calculated based on the following equation from Gutenberg and Richter:

$$\log E_s = 11{,}8 + 1{,}5M$$

In which:

- E_s is seismic energy in ergs (1 erg is equal to $1 \cdot 10^{-7}$ joules).
- M is earthquake magnitude

The energy is calculated per seismic event and summed as total energy per year. In Fig. 25, two non-stationary phases appear at two periods, the first in 1982 and the second around 2000. The latter can be associated with the second Voerendaal swarm. The first Voerendaal swarm is not shown very clearly because there were relatively few and small events. There was one large event in 1982 with M_L 3,5 (Sittard, 02.03.1982, Depth 6,6 km), but this event was north of the Feldbiß fault, just outside the mining area (near Sittard). This event influences the accumulated energy curve strongly.

3.4 Temporal relation

The Voerendaal swarms seem to occur after some years of important groundwater rise at the mine basins. The first Voerendaal swarm (1985 - 1986)

appears about 11 to 12 years after the main groundwater rise of 1974 - 1975. The second Voerendaal swarm (2000 - 2002) appears about 5 to 6 years after the main groundwater rise of 1995. A certain time delay is expected, if the fault is not in a critical state and pressure needs time to build up first. This is further discussed in chap. 4.3. However, the large time delay between the first groundwater rise and first Voerendaal swarm makes a possible relation less apparent. The second Voerendaal swarm appears to have a stronger temporal relation with the second groundwater rise. It may be possible that a certain critical threshold value is required to be exceeded for more fault movement (seismicity) to occur. The first Voerendaal swarm could therefore have been a precursor for the more profound second Voerendaal swarm.

3.5 Findings

The seismicity registered by KNMI was compared to the variation in groundwater level over time, as well as to the ground deformations. Spatially, the seismicity was plotted in maps with the ground deformations. The main findings are as follows:

- The two Voerendaal swarms appear to be spatially related to the Kunrader fault
- Temporally, the two seismic swarms appeared 11 - 12 and 5 - 6 years after the important water rise. There is a stronger temporal relation between the second swarm (2000 - 2002) and the groundwater rise of 1994.
- There is no clear relation between ground heave, subsidence and seismicity

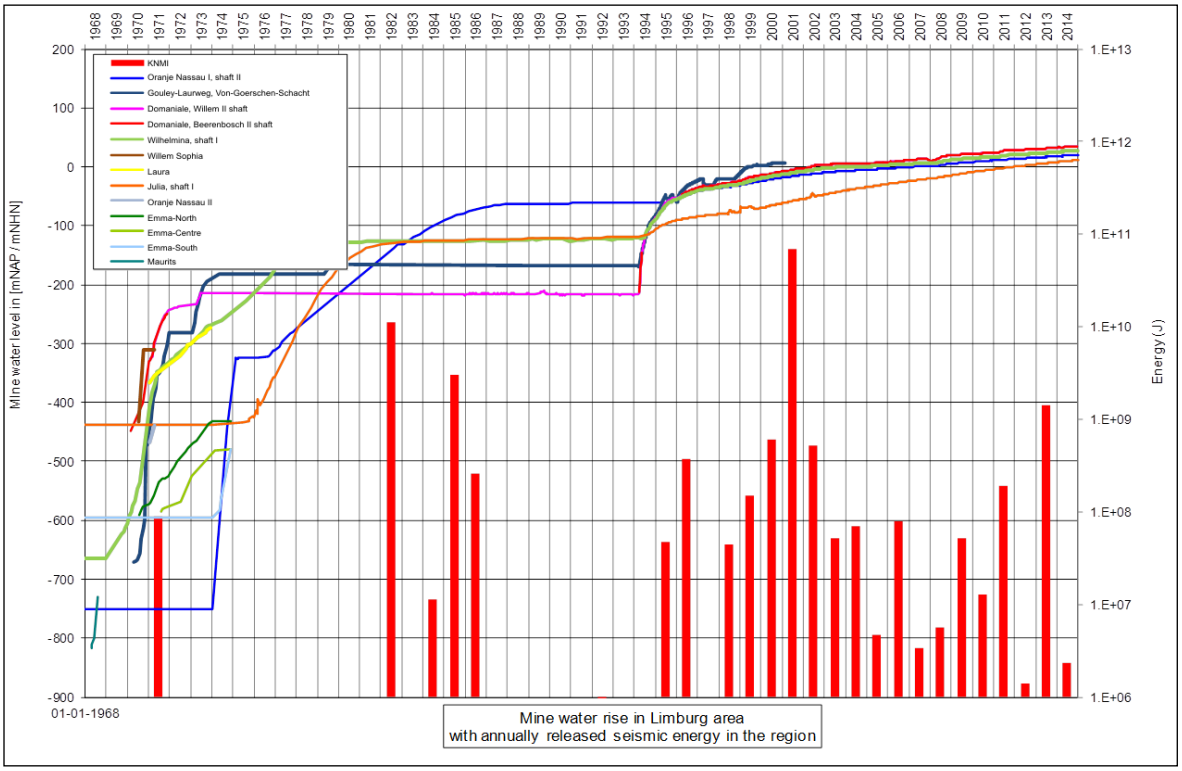

Fig. 26: Mine water rise per basin (ROSNER, 2011) with annual seismic energy (red vertical bars) from KNMI catalogue

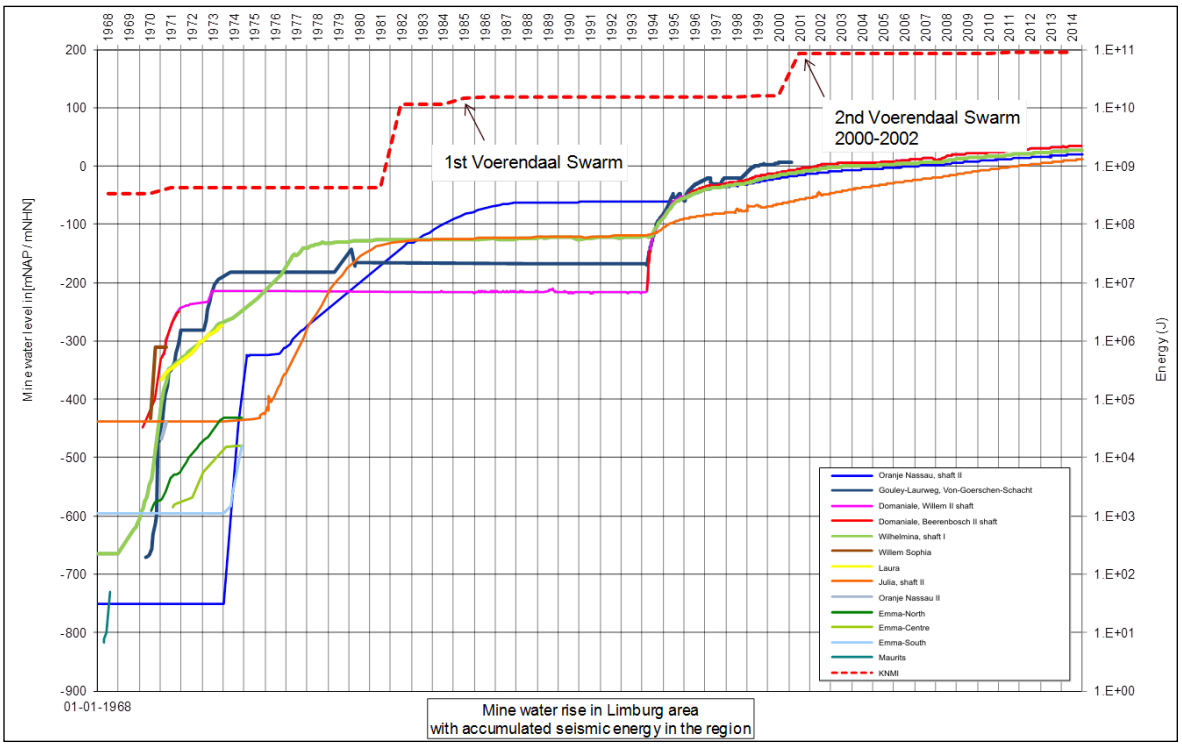

Fig. 27: Mine water rise per basin (ROSNER, 2011) with accumulated yearly seismic energy (red dashed line) from KNMI catalogue

4 Stress analysis

4.1 Introduction

The first approach in the investigation of earthquake mechanisms is to study the stress state of a fault. When shear stress along a fault is larger than the shear resistance, slip occurs along the fault, which can be felt as an earthquake.

The stresses along a fault can be expressed with the Mohr-Coulomb theory. The Mohr-Coulomb criterion describes a linear relationship between normal and shear stresses (or maximum and minimum principal stresses) at failure for all kinds of (brittle) materials. The failure line or failure envelope is defined by the strength parameters cohesion (c) and friction angle (φ) of the material. In this case the failure envelope is defined by the strength parameters along the fault, which is the surface along which failure is assumed to occur.

The friction angle in this case is not the friction angle of the material, but the friction angle of the fault. This friction angle is determined by the roughness and infill material of the fault. One can imagine that a rough surface creates more friction resistance and thus result in a larger friction angle (a steeper angle of the failure envelope in the Mohr-Coulomb relation). If there is much clay infill in the fault, this “lubricates” the fault and thus less friction resistance is expected (a lower angle of the failure envelope).

The shear stress along the fault can thus be represented by the following Mohr-Coulomb relation:

$$\tau = c + (\sigma_n - \sigma_{pp}) \cdot \tan \varphi$$

Where:

- τ = shear stress
- c = cohesion (or intercept of the failure envelope with the τ axis). In this case the cohesion is 0, assuming that the fault plane does not provide bonding between the two adjacent blocks, i.e. the fault is not cemented or filled-in with clay-like material
- φ = friction angle (or slope of the failure envelope)
- σ_n = normal stress along fault (total stress perpendicular to fault plane). The normal stress is composed of the minimum σ_3 and maximum σ_1 total stress vectors at depth and depends on the dip angle of the fault
- σ_{pp} = pore pressure (or total water pressure) at depth

Fig. 27 shows the graphical representation of the stress state along a fault following the Mohr-Coulomb theory. It consists of the following components:

1. The Mohr circle composed by the major and minor principal (total) stresses σ_1 and σ_3;
2. The Coulomb failure envelope determined by the cohesion c and friction angle φ of the fault. The stress state of the fault: a line starting from σ_3 with the inclination equal to the dip of the fault (θ in Fig. 27). This line intersects the Mohr circle at the combination of normal stress (σ_n) and shear stress (σ_s) that represents the stress state of the fault.[1]

When the stress state of the fault is below the fault failure envelope in the Mohr-Coulomb diagram, no slip occurs along the fault ($\sigma_s < \tau$). The stress state changes when water pressure, or pore pressure σ_{pp} are introduced, reducing the effective

[1] Remark: This is only valid if the principal total stress σ_1 is vertical.

stress. The Mohr circle shifts towards the origin of the diagram with the amount of water pressure. This is illustrated in Fig. 28.

The amount of pore pressure that can be added to the system before slip occurs corresponds to a water column of a certain height. This is the water level increase at which slip occurs along the fault. Per metre of water level increase, water pressure increases with 10 kPa and the Mohr circle shifts 10 kPa towards the origin of the diagram.

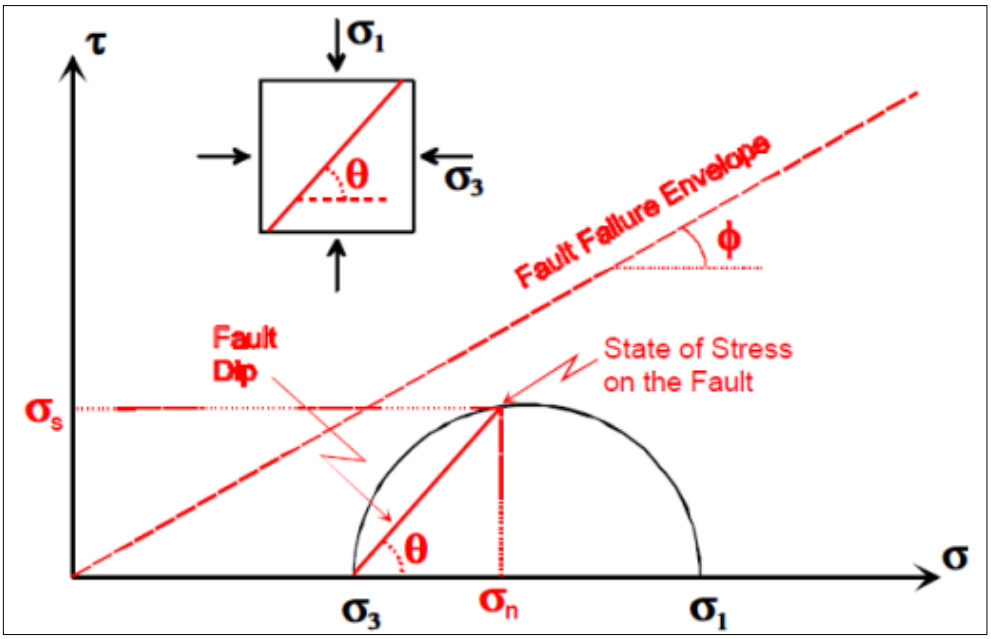

Fig. 28: Representation of stress state: Mohr circle and Coulomb failure envelope (GOLDBACH, 2009). The horizontal axis is the total stress. The vertical axis is the shear stress, in this case the shear stress along the fault. The cohesion along the fault is assumed to be 0 (no intercept with the vertical axis)

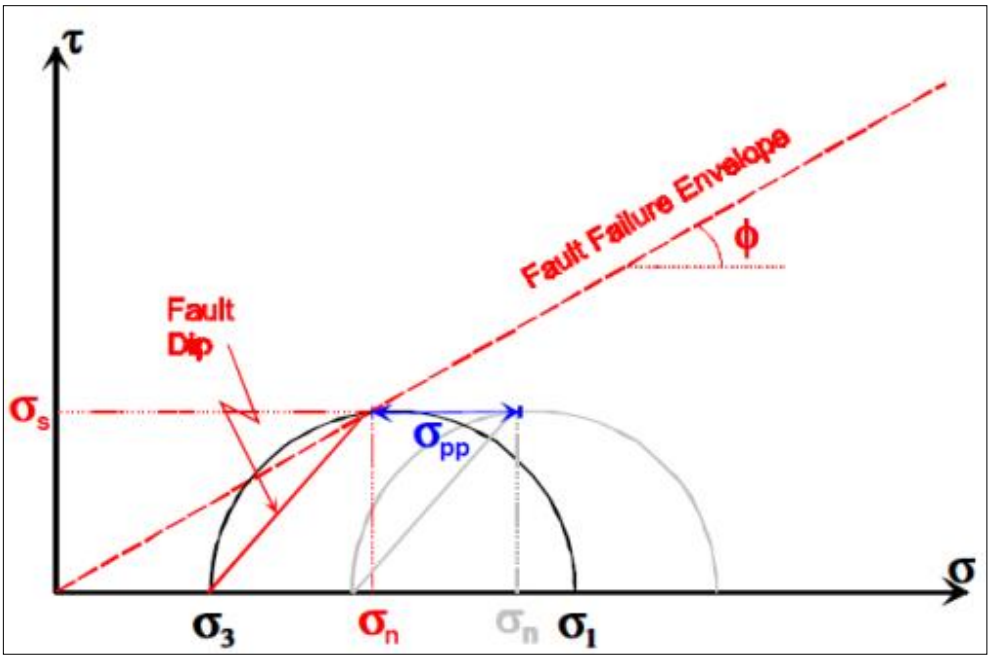

Fig. 29: Introduction of pore pressure in stress state representation (GOLDBACH, 2009)

4.2 Stress regime

In the subsurface of South Limburg the faults of the Roer Valley Rift System (RVRS) are present. This rift system originates from the regional extensional stress regime and is characterised mainly by normal faulting and some strike-slip faulting. In normal faulting the major principal stress σ_1 is oriented vertically, the intermediate principal stress σ_2 is in the (horizontal) orientation of the strike of the fault and the minor principal stress σ_3 is oriented perpendicular to the strike of the fault. The general strike direction of the faults in South Limburg is NW-SE, see Fig. 7 (DE VOS, 2010). This probably means that the orientation of the minor principal stress is NE-SW in general.

It should be noted here that this orientation is presumably correct at the time that the faults were created, which could have been millions of years ago. Since then the stress regime may have changed. Also the very recent underground mining activities may have had a (local) effect on the stress regime and thus also the orientation of the principal stresses. However, for this case it is assumed that the stress regime has not changed significantly.

For strike-slip faults the major principal stress is oriented horizontally in the same direction as the strike of the fault, the intermediate principal stress is oriented vertically and the minor principal stress is oriented in the horizontal direction perpendicular to the strike of the fault.

In WORUM et al. (2004) it has been studied at which ratios between the major and minor principal stress faults in the RVRS are expected to be activated. In this study σ_v is the vertical principal stress, σ_H the major horizontal principal stress and σ_h the minor horizontal principal stress. For normal faulting $\sigma_v > \sigma_H > \sigma_h$ and the ratio of σ_h/σ_v at which slip occurs was determined 0,33 to 0,59. For strike-slip faulting $\sigma_H > \sigma_v > \sigma_h$ and the ratio of σ_h/σ_v at which slip occurs was determined 0,3 to 0,5.

4.3 Groundwater regime

The Voerendaal swarms are associated with the Kunrader fault which is the southern boundary of the basin Emma South which belongs to the Northern main basin. In this main basin water levels are known from shaft II of the Oranje Nassau I mine, which give for the area the most continuous measurement series. These groundwater levels are plotted in Fig. 29.

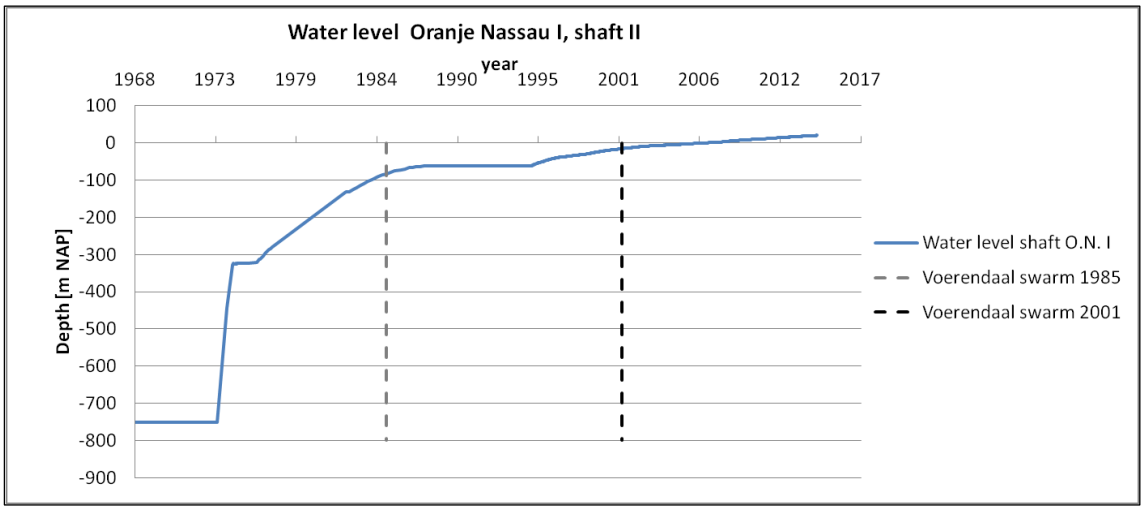

Fig. 30: Water level in shaft II of Oranje Nassau I mine

Since 1974 water level has risen and since 1975 water level measurements are registered on a frequent basis until 1977. Measurements were started again in 1982 and until 1993 around 4 measurements are registered each year. Since 1994 measurement frequency has increased from a monthly to a daily basis. Between 1974 and 1975 the groundwater level rose with a very fast rate of about 350 m/year, between 1976 and 1988 with about 21 m/year and between 1995 and 1996 with about 13 m/year.

From Fig. 29 it can also be seen that between 1988 and 1995 the groundwater level stagnates. During this period the groundwater level was maintained at a constant level to avoid flooding of mines on the German side of the border.

As already concluded in chap. 3.4 the two seismic swarms appear 11 and 6 years after the important water rise. There is a stronger temporal relation between the second swarm (2000 - 2002) and the groundwater rise of 1994. However, the rate of groundwater rise in the period 1974 - 1975 was far more substantial than in the period 1995 - 1996. A faster and more pronounced effect should therefore have been expected after the first rapid increase. It is not directly evident why this did

not happen. It may be because of the lower accuracy (higher detection threshold level) of the seismic monitoring network at the time. There could have been small swarms before the 1985 - 1986 swarm, which were simply not detected. Another reason may be that the groundwater level increase (as measured for instance in the ON I shaft II, shown in Fig. 29) takes a certain amount of time to develop within the entire area. There could thus be a significant time delay for the water pressure build-up in the fault system to take effect. Also, for the first fault movement to take place, a certain critical threshold (water pressure) value could have been required. Because some movement has already taken place relatively shortly before the second swarm, the critical threshold value could have been lower, resulting in faster and more pronounced response.

4.4 Mohr-Coulomb analysis

To determine the vertical stress at a certain depth a geological profile and material properties are required. The geological profile was derived from the borelog of borehole VRD-01 near Voerendaal that is available via NLOG (see Appendix 2). It is summarised in Tab. 2. Material properties are assumptions.

Tab. 2: Geological profile and material properties

Soil/rock	Top [m NAP]	Thickness [m]	Weight γ [kN/m^3]	Poisson's ratio ν [-]
sand/clay	86	32	18	0,25
marl	54	79	21	0,25
sand/clay	-25	75	20	0,25
Carboniferous	-100	700*	25	0,35
End of borehole	-634*	-	-	-

*) Bottom of Carboniferous is not found in borehole, it is assumed to continue untill at least -800 mNAP. This is considered a valid assumption since mining took place down to -750 mNAP in the nearby Oranje Nassau I mine.

With Poisson's ratio being assumed 0,35 for Carboniferous the stress ratio σ_h/σ_v is 0,54. This is in the range of 0,33 - 0,59 that was the result of the slip tendency analysis (WORUM et al., 2004) for normal faults. Fault properties c = 0 kPa, φ = 17 - 30°were taken from (WORUM et al., 2004) as well. This means that with every metre of water level rise, water pressure below the water table increases with 10 kPa. As a consequence, effective stress decreases 10 kPa, which makes the Mohr circle shift 10 kPa towards the failure envelope.

Since the dip of the Kunrader fault is not known exactly, it is not taken into account in the first instance which is intended to get an idea on the stress state and the influence of increasing water level and pressure. This means that the dip of the fault as indicated in Fig. 27 and is not taken into account.

The stress state analysis consists of the following steps:

1. Select depth of investigation;
2. Estimate vertical and horizontal stress at this depth;

3. Plot Mohr circle and failure envelope;
4. Determine maximum water pressure that can be added until Mohr circle reaches failure envelope;
5. Convert water pressure to height of water column;
6. Add height of water column to depth of investigation. This is the water level at which failure envelope is reached at depth of investigation;
7. Determine at what time this water level was measured in shaft II of Oranje Nassau I mine.

These steps have been carried out for several values of depth of investigation. It was found that for φ = 17°, the failure envelope was already reached at all target depths. Therefore calculations have been made for φ = 20° and φ = 30°. Results are presented in Fig. 30.

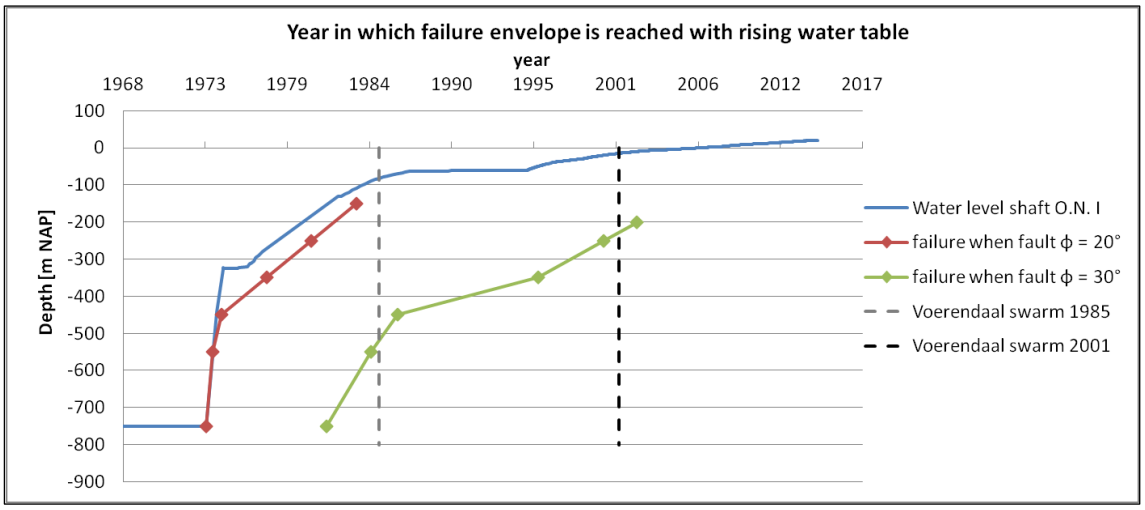

Fig. 31: Stress state analysis in relation to groundwater rise. The dotted lines show the start dates of the two Voerendaal swarms

The diagram in Fig. 30 is explained using the result for φ = 30° (green curve) and depth of investigation of NAP -350 m as an example.

1. Depth of investigation is: NAP -350 m;

2. With subsurface profile from Tab. 2 σ_1 = 10,0 MPa and σ_3 = 5,4 MPa;
3. Water pressure required to achieve failure (slip) at fault: σ_{pp} = 3,0 MPa, see Fig. 31;
4. σ_{pp} = 3,0 MPa corresponds to a water column of 300 m;
5. Depth of investigation + height of water column is NAP -50 m;
6. This groundwater level was reached in 1995, so this point (-350, 1995) is plotted

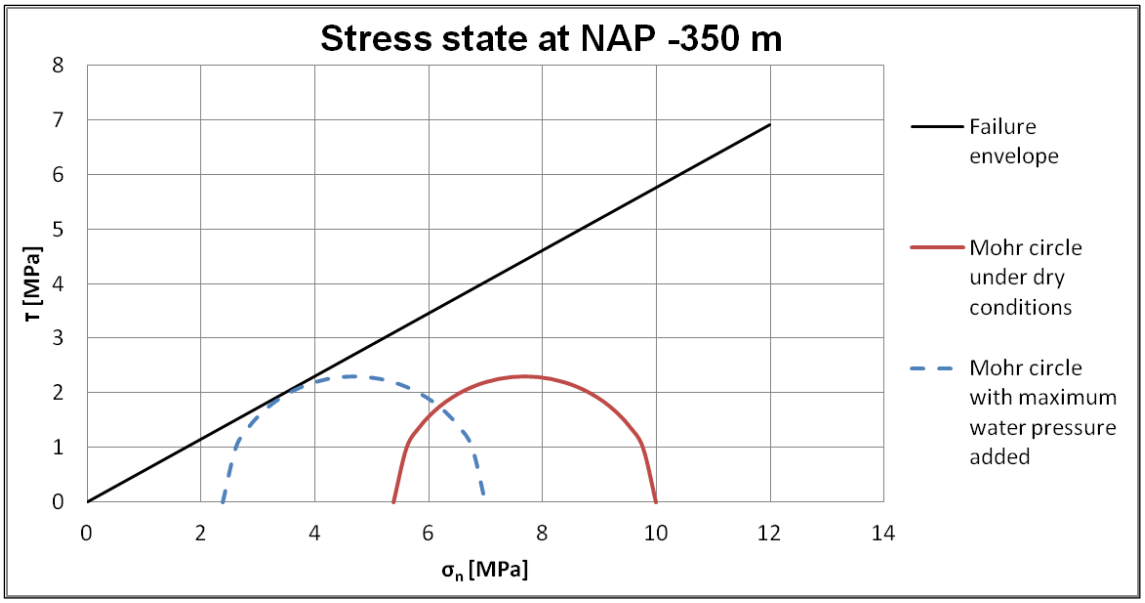

Fig. 32: Stress state at NAP -350 m, as an example

The two curves in Fig. 30 show the critical stress state of a model of the Kunrader fault for two conditions: a lower boundary friction angle of 20 degrees and an upper boundary friction angle of 30 degrees. The analysis shows that it is very sensitive to the parameter friction angle. The curves show that at larger depth the critical stress state is reached very soon and that with increasing groundwater level rise, the higher parts of the fault (at shallower depth) start to become in its critical state. In other words, with progress of groundwater level over time, a larger part of the fault, at shallower depths, becomes in its critical

state and is thus more likely to move. Following this Mohr-Coulomb analysis, the entire fault is already at its critical stress state over the entire depth for friction angles lower than 20 degrees.

A very important assumption in this entire analysis is that the groundwater level increase at relatively shallow depth is translated to increase in water pressure along the fault at larger depths. This means that the fault should be permeable. Often this is the case, since the rock material on both sides of the fault is often fractured because of the fault movement. In some cases however, the rock material within the fault zone consists of softer clay-like rocks, which causes smearing of the clay material along the fault. This results in an impermeable fault, since clay has a low permeability. In this case the water pressure at shallow depth is not directly translated to a higher pressure at larger depth or with a larger time delay.

Furthermore, the horizontal stresses are also based on a rough estimation. This estimation is based on theoretical assumptions and not on actual stress measurements at depth.

4.5 Influence of groundwater level rise

This approach explains how groundwater level increase leads to failure along a fault. The time-depth relation as presented in Fig. 30 does however not explain why the swarms of earthquakes happened at these specific periods. As mentioned in chap. 4.3, earthquakes swarms seem to be associated to a relatively rapid increase in groundwater level. This aspect of the velocity of groundwater increase is not incorporated into this approach.

4.6 Influence of fault orientation

In previous chapters it is explained how increasing water pressure leads to failure along a fault. It does however not explain why this occurs at the Kunrader fault and not (significantly) at other faults. A possible explanation lies in the orientation of the Kunrader fault, with respect to the regional stress regime.

As mentioned in chap. 4.2, general orientation of the RVRS faults is NW-SE, or in strike direction 315 degrees. The strike direction of the Kunrader fault is more NWW-SEE and deviates around 30 degrees from the general strike direction of RVRS faults. The strike direction of Kunrader fault is around 285 degrees. The fault dip is taken from (DOST & HAAK, 2007) and is assumed to be 80°. Since the Kunrader fault is not oriented in line with the regional stress regime, this fault has an apparent dip in the orientation of the regional stress regime. Fig. 32 shows how this apparent dip is determined in 4 steps for a fault with an 80° dip and an angle of 30° between strike directions.

When the fault dip is implemented in the Mohr-Coulomb analysis the stress state of the fault is found at the intersection of the Mohr circle and the line that is drawn from the minor principal stress upwards with the dip of the fault. When this point on the Mohr circle reaches the failure envelope, slip along the fault occurs. In Fig. 34 and Fig. 33 the dip (straight line) and apparent dip (dashed line) are drawn in the Mohr circle of Fig. 31. Looking at this graphical representation in detail, it can be seen that with the apparent dip the failure envelope is reached when adding less water pressure than for a fault with a corresponding actual dip with respect to the general stress field. In other words, the orientation of the Kunrader fault that deviates from the general orientation of faults in the area, gives the Kunrader fault an apparent dip (78,5 degrees) that makes it more prone to slip than the other faults in the area. To reach the failure

envelope, less water pressure (shorter red arrow in Fig. 33) is needed for the orientation of the Kunrader fault than for the other faults. This may be an explanation why earthquakes (movement along faults) are associated to this fault and not to other nearby faults, such as the Benzenrader fault.

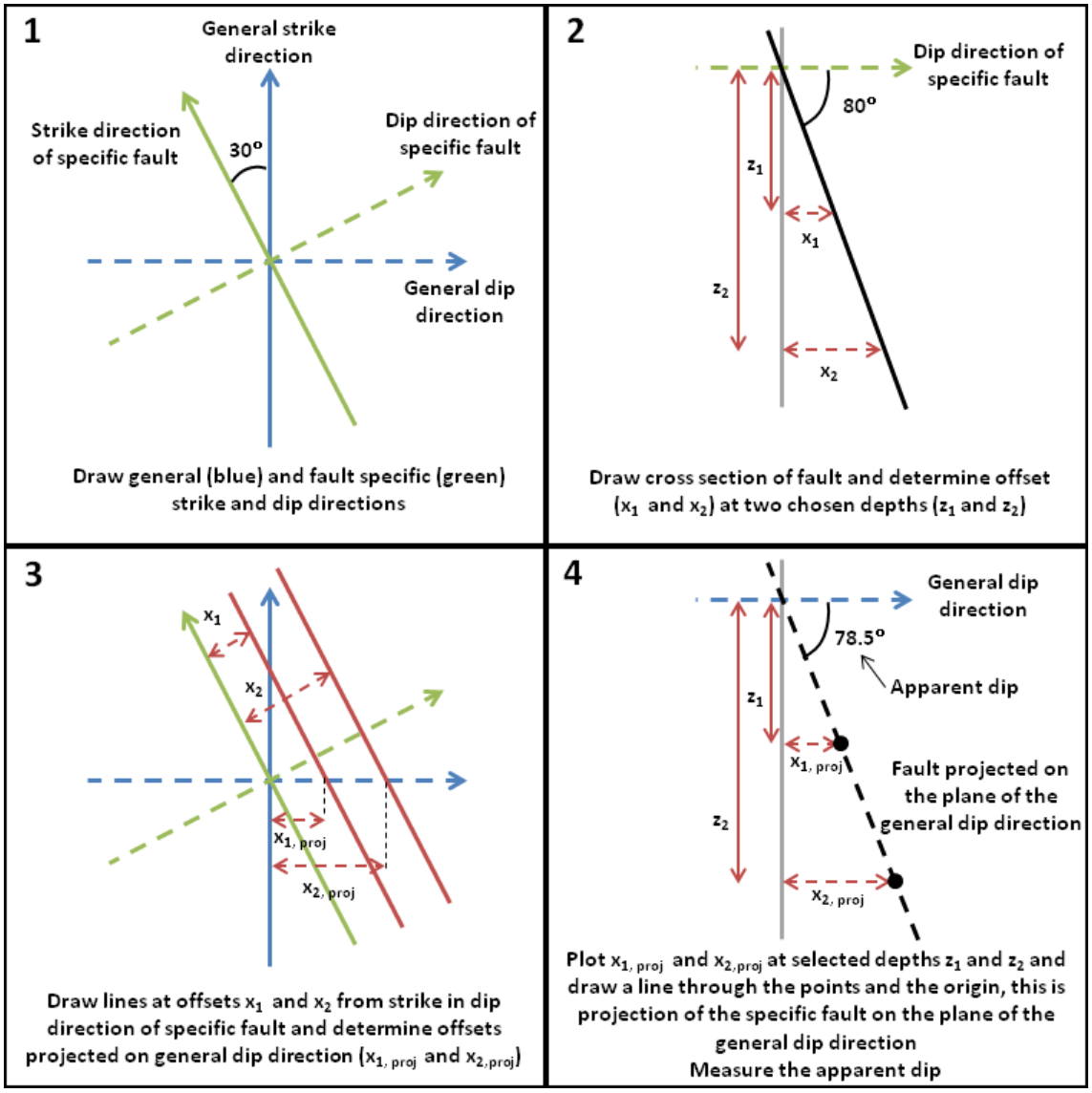

Fig. 33: Calculation of apparent dip

4.7 Findings

Based on the stress state analysis discussed in this chapter it is found that it is possible that the Kunrader fault is close to its critical state. This means that an increase in the groundwater level as experienced in the past could cause the fault to exceed its critical state and result in slip.

On the other hand, underground coal mining activities could similarly have resulted in measured seismic activity along the Kunrader fault. However, there are no records that seismic activity took place along the Kunrader fault during the mining period. It is also possible that the stresses induced by the mining activities brought the fault into a critical state and only required a trigger mechanism.

Mining could have also resulted in a more favourable stress condition (in terms of resistance to slip) due to the extraction of groundwater, which gives a higher effective stress along the fault.

It is also possible that seismic activity took place, but that is was not measured, felt or otherwise recorded. However, this is all speculative and nothing conclusive can be said about this.

Finally, normal tectonic movement could have also been the trigger mechanism for fault movement. According to current point of view of the KNMI, tectonic earthquakes occur at larger depths, larger than the depths at which the two swarms have occurred. It is therefore considered that the shallow earthquake swarms discussed here are more likely to be related to induced seismicity.

The analysis does also not provide an explanation for the time at which (swarms of) earthquakes occur. It does provide an explanation for the location of the swarms, since the Kunrader fault near Voerendaal has an apparent dip with

respect to the general stress field which makes it more prone to slip than the other faults in the area.

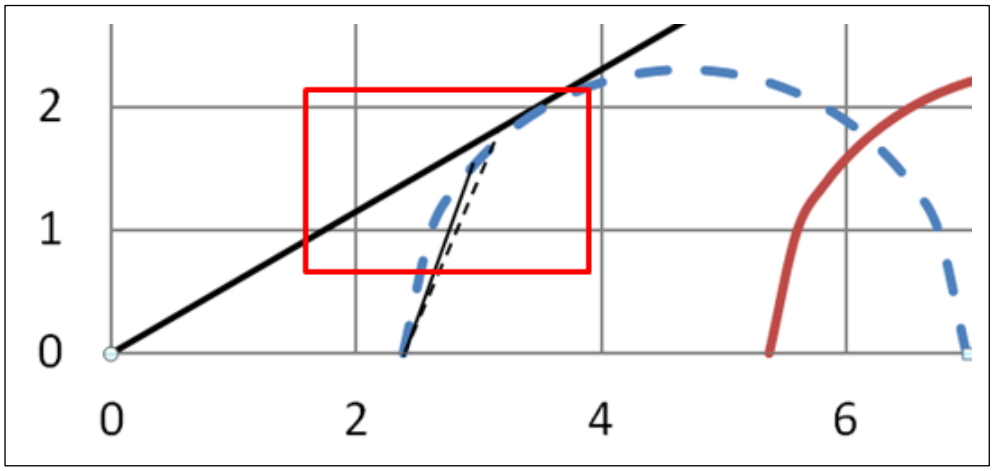

Fig. 34: Implementation of fault orientation in stress analysis. The red square is enlarged in Fig. 33

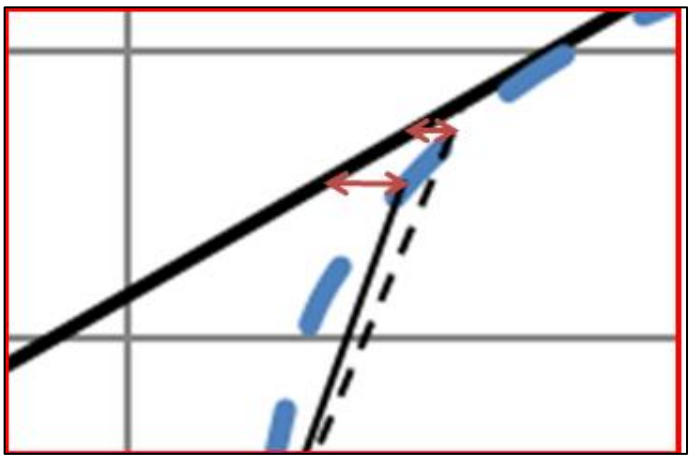

Fig. 35: Enlargement of red square in Fig. 34

5 Relation of seismic energy with groundwater rise

5.1 Introduction

The second approach to explain the earthquake mechanism is to see the rising groundwater level as a supply of energy to the system. (KLOSE, 2013) has related earthquake magnitudes to different tectonic regimes and geomechanical operations (mining, reservoir extraction/injection etc.). Fig. 35 illustrates that a (human-made) mass shift causes a change of energy in the subsurface that is released by an earthquake of which the magnitude can be measured.

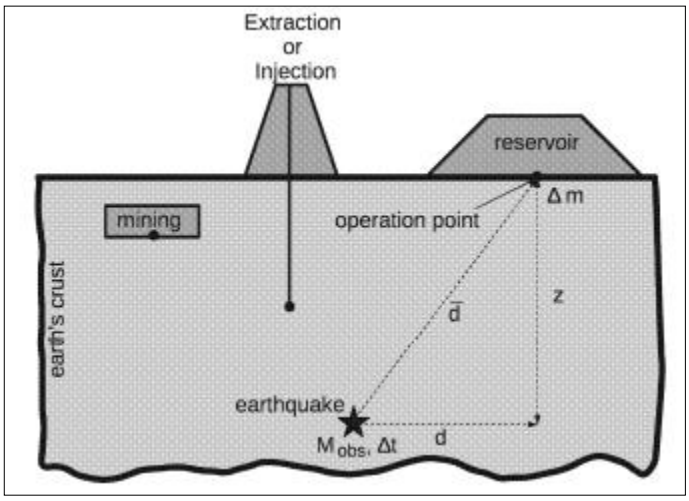

Fig. 36: Illustration of mass shift concept (KLOSE, 2013)

Based on a catalogue of 92 earthquakes, KLOSE (2013) has established empirical relations between induced and triggered earthquake magnitudes and the mass shift that caused it. An important limitation for the applicability of these relations is that they are valid for magnitudes larger than 3,0. For the Voerendaal swarms the majority of the shocks have magnitudes smaller than 3,0. However the concept remains valid. In order to compare the event from Voerendaal with the triggered and induced events analysed by KLOSE (2013), the equivalent increase

in mass due to groundwater rise until the largest event of the two swarms are plotted against the respective (moment) magnitudes of these events. This plot is shown in Fig. 36 together with the points and regression curves from KLOSE (2013).

It can be observed that the data points from the two swarms fall within the range of data points found by KLOSE (2013) for normal faults. The data points from the two swarms fall below the found regression curve (N) that KLOSE (2013) finds for normal faults. This means that the maximum magnitudes from the two swarms are lower than generally observed by KLOSE (2013) for induced and triggered seismicity. The reason could be that the events from the database compiled by KLOSE (2013) are mostly single events and not necessarily seismic swarms. The total energy released by the swarms together is thus larger than the single events (M_L 3,0 for the 1st swarm and M_L 3,9 for the 2nd swarm) used to compare with the data from KLOSE (2013). It should be noted that for induced seismicity in the Netherlands the moment magnitudes (M_W) are assumed to be the same to local magnitudes (M_L) for small events ($3 < M < 5$) (HANKS & BOORE, 1984; DEICHMANN, 2006).

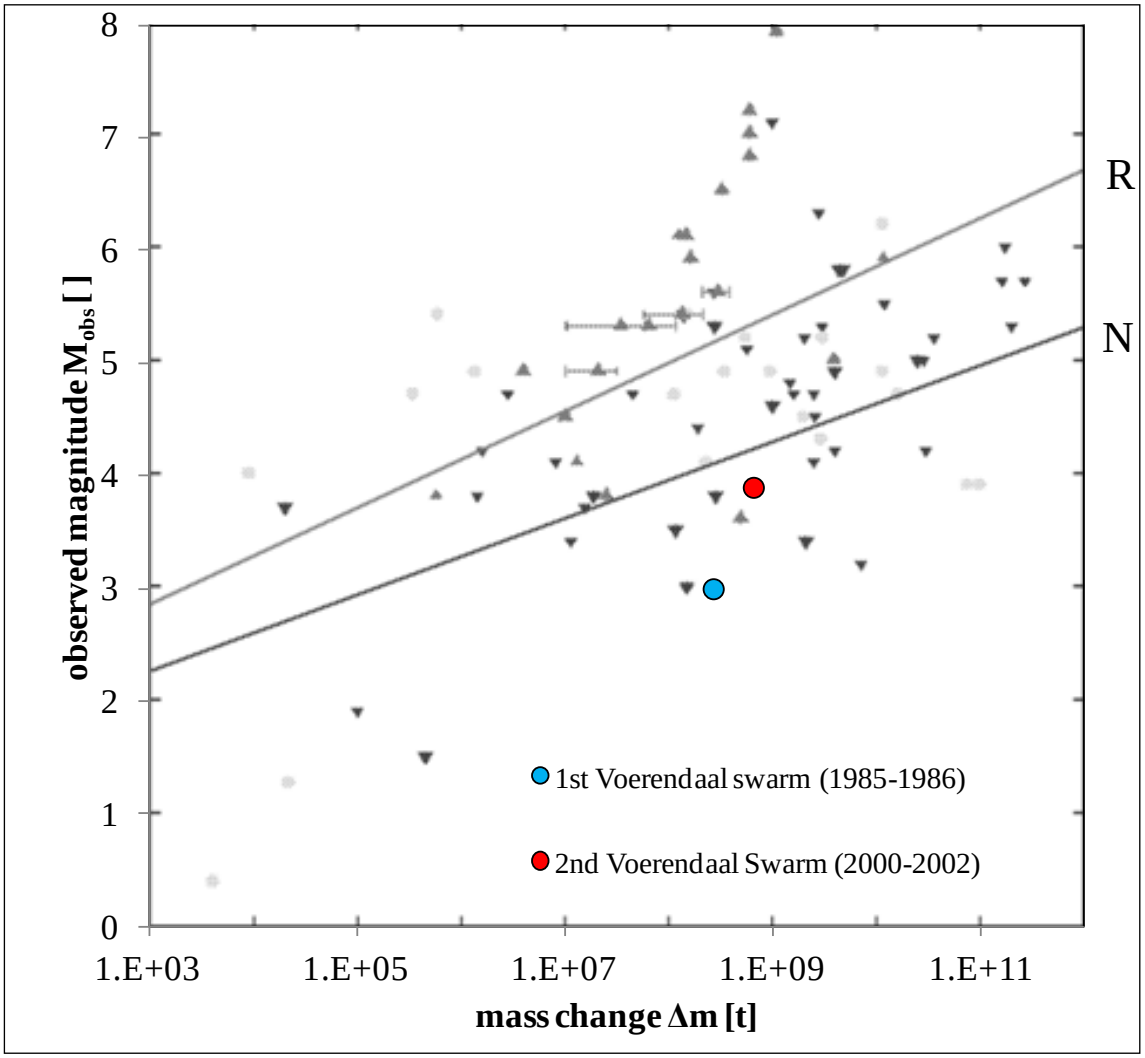

Fig. 37: Comparison of the mass change and observed (moment) magnitudes (M_W) of the two Voerendaal Swarms with data from induced and triggered earthquakes after KLOSE (2013). The data points with symbol ▼ are related to normal faults. The data points with symbol ▲ are related to reverse faults. The data points with symbol ● are related to strike-slip faults. Regression lines are provided for statistically strong and significant correlations, i.e. Normal fault regimes (N) and Reverse fault regimes (R) (KLOSE, 2013)

The addition of water to the system causes an energy build-up that is partly released as earthquakes, and partly by ground ground heave. To elaborate this approach for the Voerendaal swarms, three aspects need to be calculated and compared:

- The supply of energy over time since the start of water level rise;
- The energy that is absorbed by ground ground heave;
- The release of seismic energy over time.

In the next chapters these aspects are covered. This chapter is concluded with an outlook on the effect of future groundwater levels.

5.2 Increase of potential energy due to weight of groundwater mass

The rising water level represents a supply of potential energy to the system.

$$\Delta E = \Delta m \cdot g \cdot \Delta h_c$$

Where:

- ΔE is the change of potential energy in J
- Δm is the change of mass in kg
- g is the gravitational acceleration of 9,81 m/s^2
- Δh_c is the increase in height of the centre of the mass

Fig. 37 illustrates that with rising water level the mass of water (Δm) increases and the height of the centre of the mass also increases (Δh_c).

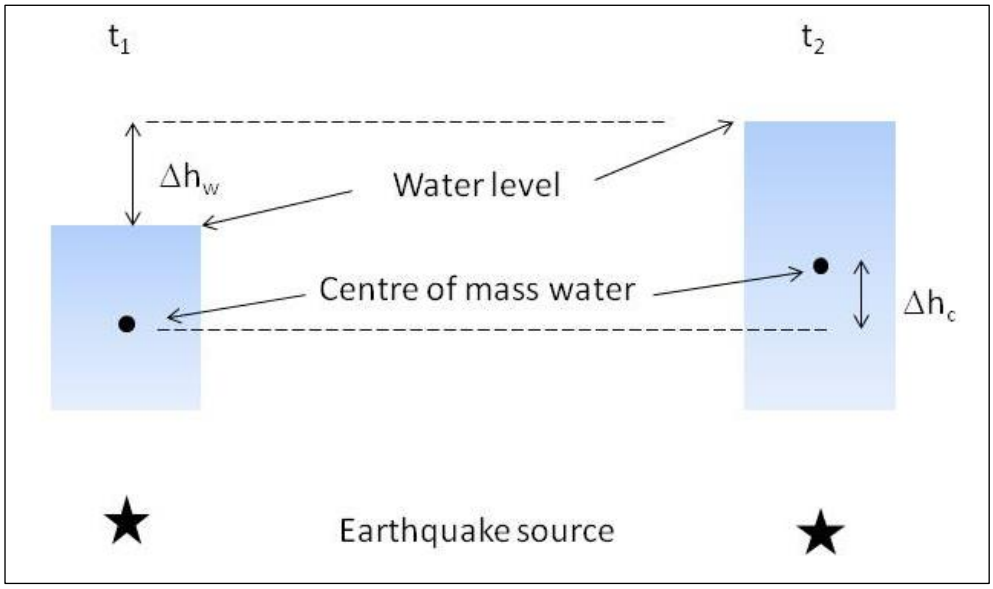

Fig. 38: Potential energy and water level rise

From Fig. 37 it can be concluded that $\Delta h_c = 0{,}5\Delta h_w$ and this is independent of the depth of the earthquake source.

Taking a porosity of 0,2 % for the Carboniferous (ROSNER, 2011) and 20 % (assumption) for the overburden, the supply of energy can be calculated per metre water level increase. In Carboniferous this is

$\Delta E = (1.000 \cdot 0{,}002) \cdot 9{,}81 \cdot 0{,}5 = 9{,}81$ J/m

and in overburden this is

$\Delta E = (1.000 \cdot 0{,}20) \cdot 9{,}81 \cdot 0{,}5 = 981$ J/m.

These values are valid for a column of 1 x 1 m and can be multiplied by the area of the Emma South basin (7.068.113 m^2) to convert it to basin-scale. The top of Carboniferous is taken at -100 mNAP, which corresponds to the borelog of VRD-01.

The accumulated potential energy due to rise of groundwater level is plotted in Fig. 38. The water level in shaft II of Oranje Nassau I mine was used as input and is plotted as well. Note that the largest water level increase in the mid-1970s does not coincide with a large increase in potential energy. Due to the low porosity in the Carboniferous (0,2 %) the increase in mass of the water is limited. The water table remains in Carboniferous until 1984, after which accumulated energy increases at a higher rate, because the water starts to collect in the overburden layers with higher porosity than the Carboniferous rock.

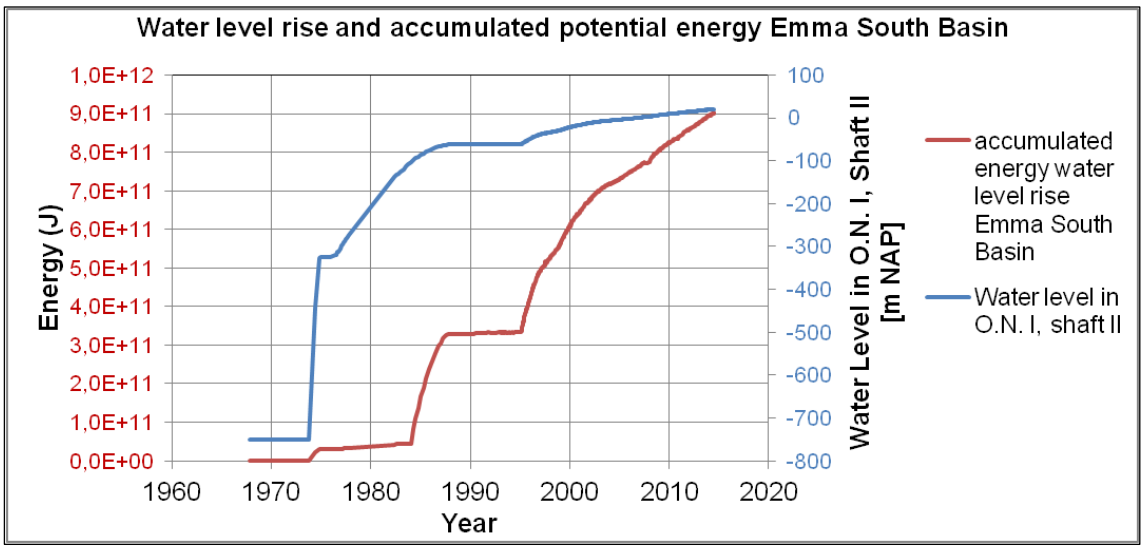

Fig. 39: Water level rise and accumulated potential energy Emma South basin

5.3 Decrease of potential energy due to ground ground heave

Part of the potential energy supplied by the water level rise is absorbed by ground ground heave. This energy is calculated in a similar way as explained above for a water level rise. For the (unit) weight of the ground heaveed ground

material 18 kN/m^3 [1]is assumed, with an effective (unit) weight of 8 kN/m^3 (unit weight ground material - unit weight of water, which is 10 kN/m^3) Fig. 39 shows ground ground heave curves based on levelling data for measurement locations in the Emma South basin. The data series of measurement location 060D0070 was chosen to calculate the potential energy associated with ground ground heave. This location was chosen since it provides an upper boundary of ground ground heave for this basin and measurements have been carried out since 1974. Fig. 39 shows the curve of the levelling data for 060D0070 and the accumulated potential energy that is related to the measured ground ground heave (which is an

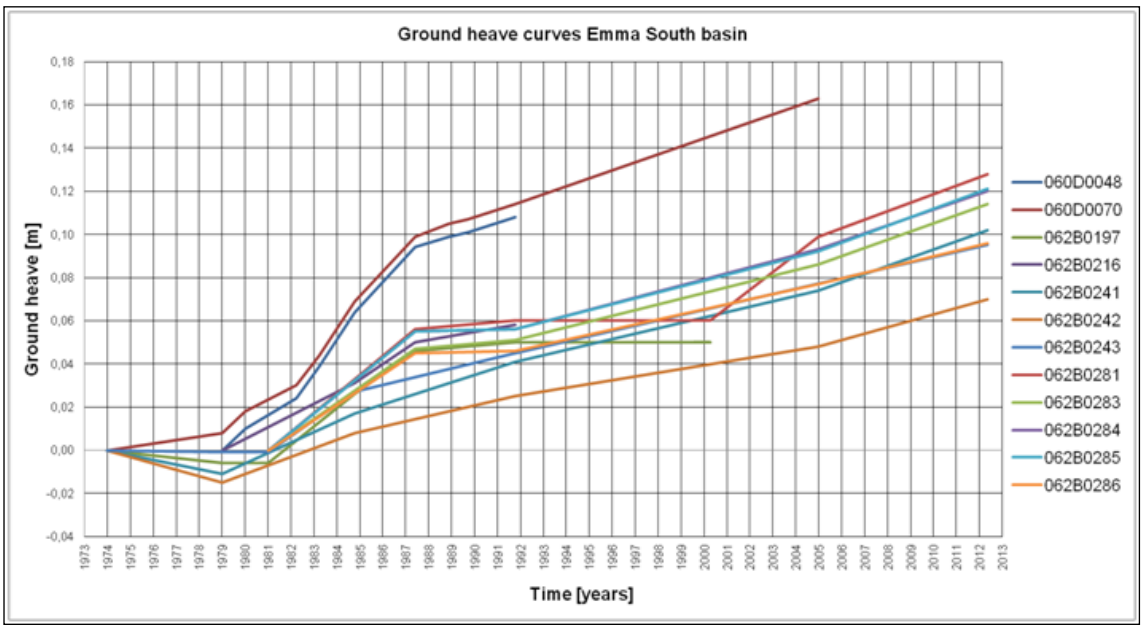

Fig. 40: Ground uplift curves Emma South basin

energy loss for the system).

It can be seen in Fig. 40 that release of potential energy due to ground ground heave is very minimal compared to the energy that is supplied over the years by

[1] The unit weight of ground material ranges generally between 15 (for soft clay) and 21 kN/m^3 (for dense rock). An average density for generic ground material of 18 kN/m^3 appears thus a safe assumption.

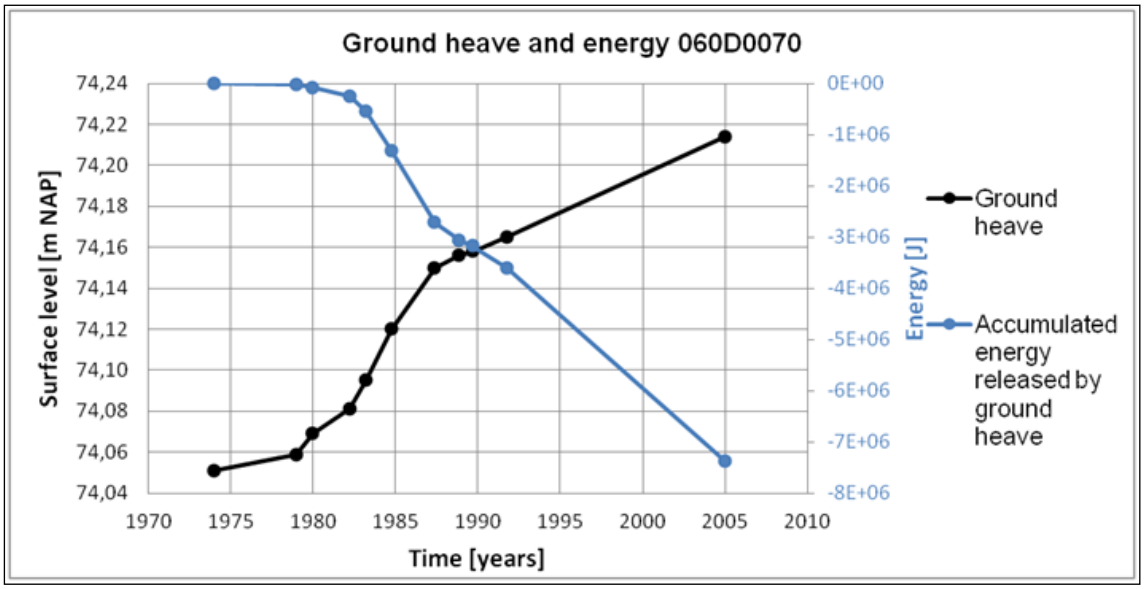

Fig. 41: Levelling data and accumulated energy released by ground uplift

the water level rise (5 orders of magnitude higher). Therefore it is concluded that the effect of ground heave on the energy balance is negligible.

5.4 Release of seismic energy over time

The released seismic energy can be calculated by converting the magnitude of each earthquake to the amount of energy. The equation given in chap. 3.3 is used for the conversion.

Earthquake magnitudes were taken from KNMI seismic catalogue and the energy from all events were summed resulting in:

- $E_s = 3{,}3 \cdot 10^9$ J for all events of the 1985 - 1986 swarm
- $E_s = 7{,}1 \cdot 10^{10}$ J for all events from the 2000 - 2002 swarm.

SPOTTISWOODE et al. (1975) explained that only a part of the total energy that is involved in an earthquake is radiated and therefore indirectly measured as a

magnitude. This is called the partitioning effect. From a number of case studies a maximum of 3 % was found as percentage of total energy that is radiated as seismic energy. This means that 97 % of the energy that is released during an earthquake is not measured, since it is not radiated. For every 3 J that are radiated, 97 J are released that remain unrecorded. This value was found for fluid injection in a well. The information regarding the percentage that should be applied to account for the partitioning effect is very limited. A well-founded choice for a certain value that is to be applied for the case of the rising mine water in the Limburg coal mines can therefore not be made. For this reason it was chosen to leave the partitioning effect out of this analysis.

In Fig. 41 the accumulated seismic energy that has been released during the two Voerendaal swarms is presented.

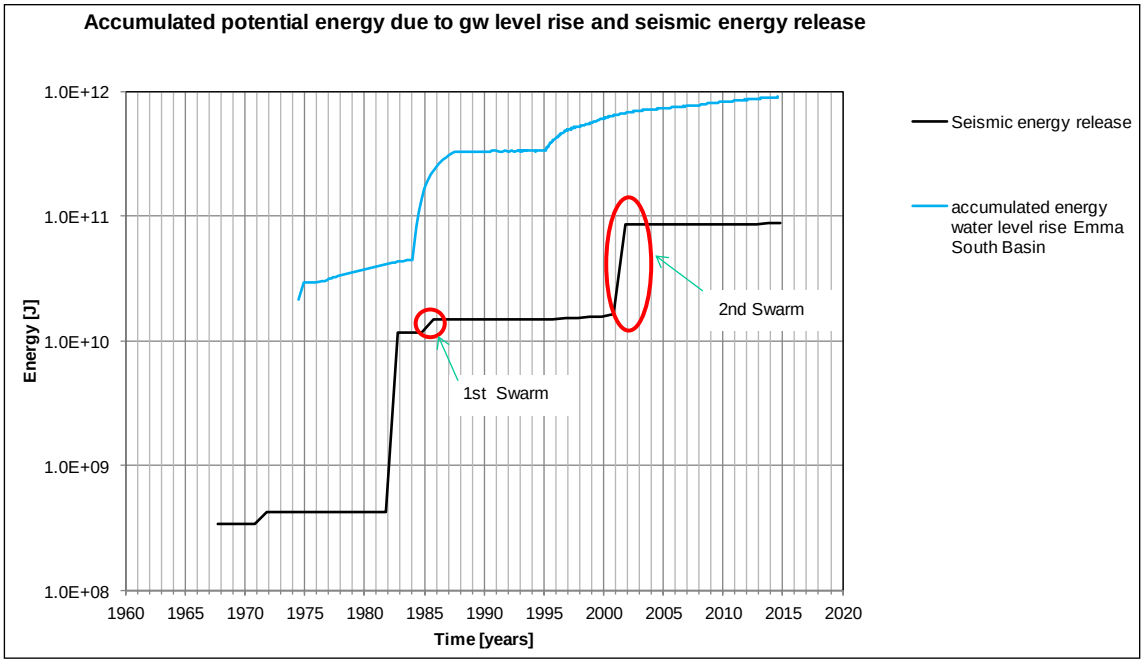

Fig. 42: Accumulated seismic energy released by the two Voerendaal swarms (black curve) vs. the accumulated energy due to groundwater level rise within the Emma South Basin

Because there is a much uncertainty regarding the percentage of the partitioning effect, it is not possible to make a fair comparison between the energy that is supplied to the system by water level rise and the energy release by earthquakes (energy release by ground ground heave is neglected here). Therefore it is also not possible to define an energy level at which the system has reached the point at which it will release seismic energy.

The swarm in 1985 - 1986 occurs after relatively low increase in potential energy. Until the end of the 1980s potential energy increases much more, but new swarms did not occur. Since 1984 the potential energy increases at a higher rate since the overburden with a higher porosity is reached, which means that per metre of water level increase, the additional mass of water is much higher than before. The swarm of 1985 - 1986 may be a response to this transition.

The explanation of the 2001 swarm may lie in the transition from a constant water level (until 1995) to a relatively fast water level increase afterwards. There is however a 5 - 6 year delay. GOLDBACH (2009) mentions that delays between start of flooding and the occurrence of seismicity have also been measured in other cases like the flooding of a South African gold mine and fluid injection in a well in Denver.

5.5 Future development of groundwater levels

From groundwater modelling it was found that the maximum water level in Emma-South basin in the future will be around +119,8 mNAP in the south east corner of the basin. In the northwest corner of the basin this will be +64,9 mNAP. This means an increase of 45 to 100 m with respect to the current situation in shaft II of Oranje Nassau I mine. When these water levels are reached, the system is in equilibrium. It is however unknown how much time it

will take before equilibrium is reached. For this reason only the maximum amount of energy that can be added to the system in the future can be calculated. With the current groundwater model it is not possible to show how the water level will develop over time. The average height of the water column that will be added with respect to the current situation is 72,5 m. Continuing with the calculation in chap. 5.2 with 20 % porosity this leads to an additional energy supply of 981 joules per metre of water level increase per m^2 of basin area. This results in $5{,}03 \cdot 10^{11}$ J of future energy supply for an average water level rise of 72,5 m over the entire Emma-South basin. As presented in chap. 5.2, until now around $9 \cdot 10^{11}$ J of energy has been added, so around half of this amount is still to be added in the future. It is unknown what the length of the period is during which this energy will be supplied and also what the rate of energy supply will be.

5.6 Findings

The energy balance analysis that has been discussed in this chapter does not provide an explanation for the location at which (swarms of) earthquakes occur. But it does suggest that (swarms) of earthquakes occur after an increase in the rate at which energy is supplied to the system by water level rise. After an increase in this rate, earthquakes seem to occur (with a delay).

It was found that the energy released by ground ground heave is very minimal compared to energy supplied by water level increase and release of seismic energy. Since groundwater modelling has indicated that final groundwater level will be 45 to 100 m higher than currently in the Oranje Nassau I mine about half of the amount of energy that has already been supplied by water level rise will still be added in the future.

A summary of the energy values are given in Tab. 3. Here a distinction is made between the total energy built up due to the groundwater rise since 1974 and the relative building up since the two swarms. Also the amount of energy release by the two swarms is given to provide some perspective on the relative amounts of energy. Tentatively, the proportions between the energy built up by the water level rise and the seismic energy release is also provided in terms of percentage. The first swarm released about 2 % of energy compared to the energy build up by the groundwater level rise, while the second swarm released about 11 % of energy compared to the total energy build up by the groundwater or about 15 % of energy compared to the energy built up since the previous swarm of 1985 - 1986.

There is still a substantial energy built up to be expected in the future, in the same order as the energy built up until the second swarm. Theoretically, the same amount or higher of seismic energy release could be expected from this potential energy increase as has been released by the previous two swarms together. However, the rate of increase is likely to be much less than was experienced in the past (the energy build up is thus more gradual). A fast rate in groundwater level increase could have been the triggering factor for the occurrence of the two swarms.

Tab. 3: Overview of amount of energy released by earthquakes and energy built up by groundwater level rise

	from 1974 - 1985 (1st Swarm)	from 1974 - 2000 (2nd Swarm)	from 1974 to stabilisation of groundwater level
Potential energy build-up by water level rise [J]	$1{,}67 \cdot 10^{11}$	$6{,}38 \cdot 10^{11}$ increase (from 1985 - 2000): $4{,}71 \cdot 10^{11}$	$14{,}05 \cdot 10^{11}$ increase (from 2000 to stabilisation): $7{,}67 \cdot 10^{11}$
Energy released by earthquakes [J]	$3{,}30 \cdot 10^{9}$ (1,9 %)	$7{,}43 \cdot 10^{10}$ (11,1%) increase: from 1985 - 2000): $7{,}10 \cdot 10^{10}$ (15,1%)	unknown
Energy released by ground ground heave [J]	$1{,}32 \cdot 10^{6}$	~$6{,}0 \cdot 10^{6}$ (interpolation)	unknown

6 Conclusions

This study has done a temporal and spatial analysis on groundwater level development, seismic data, ground heave and fault data to determine a possible relation between the occurrence of two earthquakes swarms around Voerendaal and the mine water level increase. The study looked at two possible mechanisms that could have triggered the earthquake swarms: (1) exceedance of the critical state of the active faults and (2) the increase and shift in mass due to groundwater level rise as a driving (energy) source.

In general, the South Limburg mining district is affected by natural seismicity. It is situated at the southern part of the Roer Valley Graben structure. There are some important active faults in the area. Two earthquake swarms have occurred in the past, one smaller swarm around 1985 - 1986 and a larger swarm around 2000 - 2002, known as the Voerendaal swarms. These swarms appear to be correlated to the Kunrader fault. The largest earthquake of the second swarm (M_L 3,9, 23.06.2001) has resulted in damage to houses and buildings, but there were no casualties.

The seismicity registered by the KNMI was compared to the variation in groundwater level over time, as well as to the ground deformations. Spatially, the seismicity was plotted in maps with the ground deformations. Temporally, the first Voerendaal swarm (1985 - 1986) appears about 11 to 12 years after the main groundwater increase of 1974 - 1975. The second Voerendaal swarm (2000 - 2002) appears about 5 to 6 years after the main groundwater rise of 1995.

The stress analysis shows that the Kunrader fault is close to its critical state. This means that an increase in groundwater level as experienced in the past could cause the fault to exceed its critical state and result in movement. However, the analysis does not provide an explanation for the time at which (swarms of)

earthquakes occur. It does provide an explanation for the location of the swarms, since the Kunrader fault near Voerendaal has an apparent dip with respect to the general stress field which makes it more prone to slip than the other faults in the area. The analysis is based on many assumptions, since not much is known about the exact characteristics of the Kunrader fault or other active faults in the area. The analysis is for instance very sensitive to the friction angle of the fault. An important assumption is also that the groundwater increase in the shallow subsurface results in water pressure increase along the fault at deeper levels where the earthquakes occur.

The mass shift caused by the increase in groundwater level on the north side of the Kunrader fault has been compared with other data from induced seismicity (KLOSE, 2013). Data from the two Voerendaal swarms appear to be related to data from induced events from normal stress fields. Tentatively, the Voerendaal events could thus also be classified as “induced events”.

The energy balance analysis does not provide an explanation for the location at which (swarms of) earthquakes occur. However, it does suggest that (swarms) of earthquakes occur after an increase in the rate at which energy is supplied to the system by water level rise. After an increase in this rate, earthquakes seem to occur with a delay. There appears to be a strong relation between the timing of the first swarm (1985 - 1986) with the moment that the groundwater has reached the upper part of the Carboniferous (1984) and started to saturate the overburden, which has a higher porosity and thus generated larger mass and energy.

The total amount of potential energy put into the system due to the increase in groundwater level is many times larger than the amount of energy released by seismicity. The first swarm released about 2 % of energy compared to the energy build up by the groundwater level rise, while the second swarm released about 11 % of energy compared to the total energy built up by the groundwater or

about 15 % of energy compared to the energy built up since the previous swarm of 1985 - 1986.

The two mechanisms investigated in this study (fault movement due to a decrease in shear resistance in faults and increase in mass due to a rise in the level of the mine water) can theoretically explain the occurrence of the two earthquake swarms around Voerendaal. There is still a substantial energy building up to be expected in the future, in the same order as the energy built up until the second swarm. Theoretically, the same amount or higher of seismic energy release could be expected from this potential energy increase as has been released by the previous two swarms together. However, the rate of increase (expected to be about 2 m per year) is less than was experienced in the past (the energy build up is thus more gradual). A fast rate in groundwater level increase could have been the triggering factor for the occurrence of the two swarms in the past.

Theoretically it is possible that another swarm of the same size as 2000 - 2002 can occur in the future, based on the increase in groundwater level alone. However, the amount of seismic energy that could be released and the expected magnitudes are not expected to increase the existing (natural) seismic hazard that is present in the area and therefore the existing seismic hazard map does not need to be adapted.

7 Bow-Tie-Analysis

A general overview about the systematic of the Bow-Tie-Analysis is given in chap. 1.6. With the results of the investigations in hand one Top Event has been identified regarding the hazard “small earthquakes”:

- triggered earthquakes (see Appendix 4)

In the following the relevant factors of the Bow-Tie are discussed. In the Bow-Tie systematics approach a distinction is made between prevention control measures and recovery control measures. “Prevention control measures” are measures implemented to reduce the probability of occurrence of the so-called “Threats”. “Recovery control measures” are measures that are implemented when the Top Event (e.g. change of deep groundwater quality) occurs, and that are designed to reduce the “Consequences” of such an occurrence or mitigate them altogether.

7.1 Introduction

In order to recommend mitigating measures one should look at the event that causes damage. In this case the event can be defined as “hazard for induced small earthquakes due to groundwater level rise”. However, it was concluded (see chap. 6) that induced seismicity due to groundwater rise is not likely to occur in the future and even if it will occur, it will not affect the existing seismic hazard in the area.

Mitigating measures should thus be taken in line with the existing seismic hazard. The cause for the induced seismicity is elaborated in this report and can tentatively be attributed to rapid groundwater rise (the “hazard”). The

consequence of seismicity is damage to buildings, similar to what has been experienced in Voerendaal during the M_L=3,9 earthquake of 23.06.2001.

7.2 Prevention control measures

It is not possible to prevent natural earthquakes. In the South Limburg area one has to accept this natural hazard. Induced seismicity is in theory possible (see chap. 6), but if the groundwater level increase is maintained at a gradual rate, the likelihood of occurrence is considered small.

However, it will remain important to carefully monitor the groundwater level development, especially near the Kunrader fault. Possible important future scenarios, such as the impact of closing the brown coal mining across the border in Germany and the associated impact on groundwater rise should be considered. Also the sudden discontinuation of industrial groundwater extractions in the area could have an impact.

Seismic monitoring to assess microseismicity could be an option to prevent induced seismicity. This is used on occasion in the geothermal industry and for the extraction of shale gas where water is injected near (active) faults. This is also referred to as the "traffic-light principle". If microseismicity is detected water injection is stopped or the injection pressure decreased until the seismicity is decreased. In this case, where it is difficult to control the (regional) groundwater level instantly and where it cannot be proven that groundwater is the main trigger for induced seismicity, seismic monitoring is not considered a useful mitigating measure.

From a scientific and seismological point of view, it is, however, recommended to obtain a better understanding of the Kunrader fault. This can be done through

the execution of a geophysical (seismic) survey across the Kunrader fault near Voerendaal. With an improved understanding of the fault system, a better analysis can be carried out with regard to the possible mechanisms leading to (induced) seismicity along this fault.

7.3 Recovery control measures

To mitigate the consequences of earthquakes one need to consider the existing seismic hazard in the area. As stated before, possible induced seismic events do not change the existing natural seismic hazard. The challenge here is that, to date, there are no guidelines for seismic-resistant design in force in the Netherlands. In the past, seismicity in the Netherlands was not considered high enough to require being taken into account in building norms or codes. Currently, a Dutch National Annex to Eurocode 8[1] is being formulated, but the status of this Annex is not clear. An initial step towards this national Annex has been made for the induced seismicity of the Groningen area in the form of the NPR. However, it is recommended that such an Annex should cover the whole of the Netherlands, especially the area with natural seismicity, i.e. the South Limburg area.

The consequence of having no official norm or code in place is that it is for authorities, such as building inspection from municipalities and provinces, difficult to enforce mitigating repair measures to obvious vulnerable (parts) of building, houses or structures. For instance during the $M_L = 3,9$ earthquake of 23.06.2001 several chimneys were damaged or fell to the ground. This is a potential hazard to persons that are standing or walking underneath. The repair of chimneys is a relatively simple measure, but difficult to enforce to the owner

[1] Eurocode 8 is the European norm for the earthquake-resistant design of buildings, bridges and other infrastructure (NEN-EN 1998-1:2005 EN).

without an earthquake norm in place. Other examples that can pose a risk to persons are large (glass) ornamental features attached to the front edifice of shops or office buildings, which are known to be vulnerable to seismic action.

Finally, it is advised to improve the public awareness on the subject of natural seismic risk and the likelihood of induced seismicity. It is important to create an open, clear and transparent communication towards the local population on these issues. This will aid individuals to take measures or ask help from the local authorities to advise them on how to improve the seismic resistance of their houses and structure. This will also help to prevent social unrest. All the mitigating measures in relation to the risk are presented in a Bow-Tie-diagram in Appendix 4.

Amsterdam, 31.08.2016

Witteveen + Bos

Dr. Ir. S. Slob Ceng Dr. C Sigaran-Loria

Ir. E. Weijermans Ir. S. Carelsen

References

BEKENDAM, R.F. (1998): Pillar stability and large-scale collapse of abandoned room and pillar limestone mines in South-Limburg, The Netherlands.-Ph.D. Dissertation TU Delft, 361 p.

BGR, SDAC (2014): Website: http://www.seismologie.bgr.de/sdac/erdbeben/ger_db.htm. Last accessed: 30.08.2016.

BISCHOFF, M., MEIER, T., BECKER, D. AND CETE, A. (2005): Mining induced seismicity in Hamm and Ibbenbüren (Germany).- Geophysical Research Abstracts, Vol. 7, 09971, EGU.

BISCHOFF, M., FISCHER, L., WEHLING-BENATELLI, S., FRITSCHEN, R., MEIER, T., FRIEDERICH, W. (2010): Spatio-temporal characteristics of mining induced seismicity in the eastern Ruhr-area.- Proceedings of the Workshop Induced seismicity: November 15 - 17, 2010, Luxembourg, (Cahiers du Centre Européen de Géodynamique et de Séismologie 30), Centre Européen de Géodynamique et de Séismologie, p. 6-7.

BNS (2016): Erdbebenstation Bensberg, Universität Zu Köln. Website: BNS: http://www.seismo.uni-koeln.de/.Last accessed: January, 2016.

CAMELBEECK, T. (1994): Mécanisme au foyer des tremblements de terre et contraintes tectoniques: le cas de la zone intraplaque belge.- Ph.D. Thesis, University of Louvain: 344 pp.

CARO CUENCA, M. AND HANSSEN, R. (2011). Radar time series analysis applied to study surface motion in the abandoned coal mines of Wassenberg. In GeoMonitoring11.

CARO CUENCA, M. (2012): Improving radar interferometry for monitoring fault-related surface deformation: Applications for the Roer Valley Graben and coal mine induced displacements in the southern Netherlands.- PhD Thesis, Department of Geoscience and Remote Sensing, TU Delft, 142 pp.

CSEM-EMSC (2014): Website: http://www.emsc-csem.org/Earthquake/for_seismologist.php . Last accessed: 30.08.2016.

DAHM, T., BECKER, D., BISCHOFF, M., CESCA, S., DOST, B., FRITSCHEN, R., HAINZL, S., KLOSE, C.D., KÜHN, D., LASOCKI, S., MEIER, TH., OHRNBERGER, M., RIVALTA, E., WEGLER, U., HUSEN, S. (2013): Recommendation for the discrimination of human-related to natural seismicity. Journal of Seismology, 17: p. 197 - 202.

DAHM, T., HAINZL, S., BECKER, D., BISSCHOFF, M., CESCA, S., DOST, B., FRITSCHEN, R., KUHN, D., LASOCKI, S., KLOSE, C. D., MEIER, T., OHRNBERGER, M., RIVALTA, E., SHAPIRO, S., WEGLER, U. (2010): How to discriminate induced, triggered and natural seismicity.- Proceedings of the Workshop Induced seismicity : November 15 - 17, 2010, Hotel Hilton, Luxembourg, Grand-Duchy of Luxembourg, (Cahiers du Centre Européen de Géodynamique et de Séismologie 30), Centre Européen de Géodynamique et de Séismologie, p. 69 - 76.

DEICHMANN, N. (2006): Local magnitude, a moment revisited.- Bulletin of the Seismological Society of America, 96: p. 1267 - 1277.

DE CROOK, TH. (1996): A seismic zoning map conforming to Eurocode 8, and practical earthquake parameter relations for The Netherlands.- Geologie en Mijnbouw, 75, p. 11 - 18.

DE VENT, I., ROEST, H. (2013): Lagging mining damage in the Netherlands? Recent signs of soil movement in the Zuid-Limburg coal district. Proceedings of the XV International ISM Congress 2013, Aachen (Germany), p. 27-41.

DE VOS, D. (2010): Probabilistic seismic hazard assessment for the Southern part of the Netherlands.- MSc Thesis, University of Utrecht, 58 pp.

DOST, B., HAAK, H.W. (2007): Natural and induced seismicity.- In: Geology of the Netherlands, Th.E. WONG, D.A.J. BATJES, J. de JAGER (Eds.), Royal Netherlands Academy of Arts and Sciences, p. 223 - 239.

DOST, B. (2015): personal communication (meeting) on 16.03.2015.

DUIN, E.J.T., DOORNENBAL, J.C., RIJKERS, R.H.B., VERBEEK, J.W., WONG, TH.E. (2006): Subsurface structure of the Netherlands – results of recent onshore and offshore mapping.- Netherlands Journal of Geoscience – Geologie en Mijnbouw, 85(4): 245 - 276.

EFEHR (2014): European Facility for Earthquake Hazard & Risk.- Website: http://www.efehr.org:8080/jetspeed/portal/hazard.psml. Last accessed: 30.08.2016.

FRITSCHEN, R. (2015): personal communication (e-mail) on 21.05.2015.

GELUK, M.C., DUIN, E.J.TH., DUSAR, M., RIJKERS, R.H.B., VAN DEN BERG, M.W. & VAN ROOIJEN, P. (1994): Stratigraphy and tectonics of the Roer Valley Graben.- Geologie en Mijnbouw 73, p. 129 - 141.

G.F.Z. (2013): Mining induced stress changes in a South African gold mine. Helmholtz Centre Potsdam, website: http://www.gfz-potsdam.de/en/section/seismic-hazard-and-stress-

field/projects/mining-induced-stress-change-modelling. Last accessed: 30.08.2016.

G.F.Z. (2016): Helmoltz-Zentrum Postdam. Website: http://www.gfz-potsdam.de/startseite. Last accessed: January 2016.

GDNRW (2016): Geological Survey NRW, Krefeld. Erdbebendienst. Website: http://www.gd.nrw.de. Last accessed: January 2016.

GIARDINI, D., WOESSNER, J., DANCIU, L., CROWLEY, H., COTTON, F., GRÜNTHAL, G., PINHO, R., VALENSISE, L. AND THE SHARE CONSORTIUM (2013): European Seismic Hazard Map. Map from SHARE consortium.- doi: 10.2777/30345, ISBN-13, 978-92-79-25148-1.

GOLDBACH, O. (2010): What is the seismic risk of mine flooding?- Proceedings from Science real and relevant conference 2010. Proceedings from CSIR 3rd Biennial Conference 2010. Science Real and Relevant, CSIR International Convention Centre, Pretoria 30 August – 01 September 2010, South Africa, 20 p.

GOLDBACH, O. D. (2009): Flooding-induced seismicity in mines, 11th SAGA Biennial Technical Meeting and Exhibition Swaziland, 16-18 September 2009, p. 391-401.

GONZÁLEZ, P.J., TIAMPO, K.F., PALANO, M., CANNAVÓ, F., FERNÁNDEZ, J. (2012): The 2011 Lorca earthquake slip distribution controlled by groundwater crustal unloading.- Nature Geoscience, 5, November 2012, p. 821 - 825.

GRÜNTHAL, G. (2004): Erdbeben und Erdbebengefährdung in Deutschland sowie im europäischen Kontext. Geographie und Schule, 151, 14-23.

GRÜNTHAL, G., WAHLSTRÖM, R., STROMEYER, D. (2009). The unified catalogue of earthquakes in central, northern, and northwestern Europe (CENEC) - updated and expanded to the last millennium.- Journal of Seismology 13(4), p. 517 - 541.

GUHA, S.K. (2000). Mining induced seismicity.- In: Induced Earthquakes, Springer, p. 159 - 215.

HANKS, T. C. AND D. M. BOORE (1984): Moment-magnitude relations in theory and practice.- Journal of Geophysical Research, 89, p. 6229 - 6235.

ISC (2014): International Seismological Centre. Website: http://www.isc.ac.uk. Last accessed: 30.08.2016.

KLOSE, C.D. (2013): Mechanical and statistical evidence of the causality of human-made mass shifts on the Earth's upper crust and the occurrence of earthquakes.- J. Seismology, vol. 13, no. 1, p. 109 - 135.

KNMI (2012): Monitoring induced seismicity in the North of the Netherlands: status report 2010.- Scientific report WR 2012-03, 39 pp.

KNMI (2013): Aardbevingen in Nederland 1904-2004. Website: http://www.sciamachy-validation.org/seismologie/kaart.html Last accessed: 30.08.2016.

KNMI (2014a): Seismologie, Aardbevingen in Nederland. Website: http://www.knmi.nl/seismologie/aardbevingen-nederland.html. Last accessed: 30.08.2016.

KNMI (2014b): Aardbevingen bij Voerendaal en Kunrade. Nieuws 31 Augustus 2002. Website: http://www.knmi.nl/cms/content/15063/ aardbevingen_bij_voerendaal_en_kunrade. Last accessed: 28.05.2015.

KNMI (2015): Natural seismicity. Data acquisition and processing. Website: http://www.sciamachy-validation.org/research/seismology/nat_seism_network.html. Last accessed: 30.08.2016.

KUBACKI, T.M., MCCARTER, M.K., PANKOW, K.L. (2010): Post-collapse seismicity of the Crandall Canyon Mine using double difference relocations. Proceedings from 31st International Conference on Ground Control Mining, 4 p.

MATRULLO, E., I CONTRUCCI, P. DOMINIQUE, M. BENNANI, H. AOCHI, J. KINSHER, P. BERNARD AND P. BIGARRÉ (2015): Analysis and interpretation of induced micro-seismicity by flooding of the Gardanne Coal basin (Provence - Southern France).- 77th EAGE Conference & Exhibition 2015, Madrid.

MCGARR, A. (1976): Seismic moments and volume changes.- J. Geophys. Res., vol. 81, no. 10, p. 1487 - 1494.

MCGARR, A., FLETCHER, J.B. (2005): Development of ground-motion prediction equations relevant to shallow mining-induced seismicity in the Trail Mountain Area, Emery County, Utah.- Bull. of the Seismol. Soc. of Am., 95(1), p. 31 - 47.

MENA, B., WIEMER, S.,BACHMANN, C. (2013): Building robust models to forecast the induced seismicity related to geothermal reservoir enhancement.- Bull. of the Seismol. Soc. of America, 103(1), p. 383 - 393.

NAS (2012): Induced seismicity potential in Energy Technologies. Washington, D.C., The National Academy of Sciences, 225 p.

NEN-EN 1998-1:2005 EN. Eurocode 8 - Ontwerp en berekening van aardbevingsbestendige constucties - Deel 1: Algemene regels, seismische belastingen en regels voor gebouwen.

NLOG (2016). Website: http://www.nlog.nl/boringen. Last accessed: 30.08.2016

ORB (2014): Royal Observatory of Belgium. Website: http://www.astro.oma.be/en/scientific-research/seismology. Last accessed: 28.05.2015.

QUINN, C.D., GLEN R.A., DIESSEL, C.F.K. (2007): Discussion of "Geomechanical modeling of the nucleation process of Australia's 1989 M5.6 Newcastle earthquake" by C.D. KLOSE. Earth Planet. Sci. Lett. 256 (2007) pp. 547–553.

REAMER, S.K., HINZEN, K.G. (2004): An earthquake catalog for the Northern Rhine Area, Central Europe (1975-2002).- Seismol. Res. Lett. 75, p. 713 - 725.

ROSNER, P. (2011): Der Grubenwasseranstieg im Aachener und Südlimburger Steinkohlenrevier - eine hydrogeologisch-bergbauliche Analyse der Wirkungszusammenhänge.- Rheinisch-Westfälischen Technischen Hochschule Aachen, PhD Thesis.

ROSNER, P. (2015): personal communication (conversation) on 29.05.2015.

SAARLAND (2014): Erderschütterungen, Website: http://www.saarland.de/119496.htm. Last accessed: 30.08.2016.

SPOTTISWOODE, S.M. AND A. MCGARR. (1975): Source parameters of tremors in a deep-level gold mine.- Bull. Seismol. Soc. Amer. 65, p. 897-899.

STAATSTOEZICHT OP DE MIJNEN (2014a): Na-ijlende gevolgen steenkolenwinning Zuid-Limburg (inventarisatie). Website: http://www.sodm.nl/sites/default/files/redactie/inventarisatie%20na-ijlende%20gevolgen%20steenkolenwinning.pdf. Last accessed: 28.05.2015.

STAATSTOEZICHT OP DE MIJNEN (2014b): Na-ijlende gevolgen steenkolenwinning Zuid-Limburg (onderzoeksplan). April 2014.

VANNESTE, K., CAMELBEECK, T., VERBEECK, K. (2013): A model of composite seismic sources for the Lower Rhine Graben, Northwest Europe.- Bull. of the Seismol. Soc. of Am., 103(2A), p. 984-1007.

WORUM, G., VAN WEES, J.-D., G. BADA, R.T. VAN BALEN, S. CLOETINGH, AND H. PAGNIER (2004): Slip tendency analysis as a tool to constrain fault reactivation: A numerical approach applied to three-dimensional fault models in the Roer Valley Rift system (southeast Netherlands).- J. Geophys. Res., 109, B02401, doi: 10.1029/2003JB002586.

Appendix 1

Na-ijlende gevolgen steenkolenwinning Zuid-Limburg

Final report of the working group
5.2.7 - small earthquakes

Seismic events of the Voerendaal Swarms

by

Projectgroup
"Na-ijlende gevolgen van de steenkolenwinning in Zuid-Limburg"
(projectgroup GS-ZL)

on behalf of
Ministerie van Economische Zaken - The Netherlands

Amsterdam, 31.08.2016

Appendix 1: Seismic events of the Voerendaal Swarms

Seismic events from the 1985-1986 Voerendaal swarm (the first swarm). Source: earthquake catalogue KNMI (2014a)

YYMMDD	TIME	LOCATION	LAT	LON	INT	MAG	DEPTH
19851207	231719.5	Kunrade	50.884	5.938	I	1.40	5.10
19851207	213217.6	Kunrade	50.885	5.932	1	1.50	5.40
19851207	212709.3	Kunrade	50.885	5.933	1	1.60	5.60
19851207	224721.7	Kunrade	50.884	5.933		2.30	5.60
19851207	224702.5	Kunrade	50.881	5.947	II	2.70	5.00
19851207	**230925.7**	**Kunrade,Hoofdschok**	**50.879**	**5.942**	**IV**	**3.00**	**5.00**
19851209	105924.2	Kunrade	50.907	5.968		1.50	3.60
19851209	105648.5	Kunrade	50.883	5.932	I	2.20	8.10
19860106	54215.42	Kunrade	50.883	5.928	I	2.40	2.30

Seismic events from the 2000-2002 Voerendaal swarm (the second swarm). Source: earthquake catalogue KNMI (2014a)

YYMMDD	TIME	LOCATION	LAT	LON	INT	MAG	DEPTH
20001220	65912.42	Voerendaal	50.870	5.937	3	2.30	5.70
20001220	70025.72	Voerendaal	50.873	5.938	4	2.50	3.80
20001220	232245.1	Voerendaal	50.875	5.942		1.00	4.00
20001220	71350.55	Voerendaal	50.875	5.942		1.10	4.60
20001221	1854.86	Voerendaal	50.874	5.935	2	1.50	4.60
20001223	5555.75	Voerendaal	50.860	5.933	2	1.70	1.10
20001231	12108.88	Voerendaal	50.881	5.935		0.40	8.80
20010102	154355.4	Voerendaal	50.879	5.937		0.70	5.00
20010105	115307.2	Voerendaal	50.872	5.958		1.10	3.00
20010109	15323.4	Voerendaal	50.881	5.938	2	1.00	5.00
20010115	33753.13	Voerendaal	50.873	5.938		0.90	4.00
20010130	230223.4	Voerendaal	50.846	5.927		0.30	2.00
20010130	224324.4	Voerendaal	50.878	5.932		1.10	3.00
20010130	224327.2	Voerendaal	50.877	5.932		1.70	3.00
20010130	23318.77	Voerendaal	50.870	5.932		0.70	3.00
20010130	212704.1	Voerendaal	50.868	5.932		0.60	3.00
20010202	140326.9	Voerendaal	50.946	5.932		0.60	3.00
20010202	122229.6	Voerendaal	50.913	5.932		0.40	3.00
20010203	172221.4	Voerendaal	50.877	5.927		1.70	2.90
20010207	140429.9	Voerendaal	50.903	5.960		1.00	3.00
20010306	34912.06	Voerendaal	50.877	5.930		0.80	6.90
20010307	213144.6	Voerendaal	50.876	5.930	2	1.40	3.50
20010307	94040.71	Voerendaal	50.889	5.932		0.70	5.00
20010307	93643.87	Voerendaal	50.869	5.932		0.40	5.00

YYMMDD	TIME	LOCATION	LAT	LON	INT	MAG	DEPTH
20010307	164609.1	Voerendaal	50.867	5.932		0.80	5.00
20010307	100534.6	Voerendaal	50.867	5.932		1.30	5.90
20010307	92002.64	Voerendaal	50.864	5.933		1.00	5.00
20010307	101941.9	Voerendaal	50.899	5.935		0.90	5.00
20010307	120249.1	Voerendaal	50.876	5.937		0.70	5.00
20010307	91758.91	Voerendaal	50.869	5.937	4.5	3.10	0.00
20010307	214726.6	Voerendaal	50.874	5.940		1.10	6.00
20010307	102912.9	Voerendaal	50.871	5.947	4.5	3.00	4.00
20010307	110359.5	Voerendaal	50.869	5.947	4.5	3.10	3.90
20010308	11151.9	Voerendaal	50.875	5.930		0.00	5.00
20010308	195157.8	Voerendaal	50.890	5.932		0.70	8.30
20010308	225321.5	Voerendaal	50.877	5.932		0.00	6.30
20010308	31241.28	Voerendaal	50.871	5.932		0.60	7.70
20010308	225327.5	Voerendaal	50.878	5.935		0.30	5.00
20010308	14217.81	Voerendaal	50.865	5.937		0.60	5.00
20010310	164746.6	Voerendaal	50.874	5.932	3	2.30	3.90
20010310	44825.82	Voerendaal	50.903	6.025		0.30	6.00
20010312	175445.7	Voerendaal	50.890	5.932		0.70	5.00
20010312	35219.35	Voerendaal	50.883	5.932		0.10	9.10
20010322	164530.3	Voerendaal	50.873	5.925		1.10	6.10
20010322	164526.1	Voerendaal	50.872	5.925		0.80	5.50
20010325	142308.1	Voerendaal	50.867	5.877		1.20	7.50
20010409	170538.9	Voerendaal	50.884	5.930		0.80	3.00
20010511	205119.6	Voerendaal	50.872	5.927		0.90	5.50
20010609	32318.45	Voerendaal	50.885	5.955		0.70	6.40
20010616	165313.6	Voerendaal	50.868	5.918		1.10	3.90
20010616	52935.84	Voerendaal	50.887	5.922		1.40	9.10
20010616	52437.79	Voerendaal	50.870	5.925		2.80	4.30
20010617	232338.9	Voerendaal	50.872	5.932		0.40	5.00
20010617	215546.7	Voerendaal	50.877	5.933		1.00	5.00
20010620	71942.34	Ransdaal	50.863	5.918		2.00	4.90
20010620	72258.54	Voerendaal	50.869	5.932		0.90	3.00
20010621	42836.94	Voerendaal	50.871	5.920		1.70	1.40
20010621	43837.97	Voerendaal	50.887	5.937		0.90	3.60
20010623	140405.9	Voerendaal	50.883	5.867		1.00	5.00
20010623	23540.7	Voerendaal	50.871	5.902		1.50	4.00
20010623	15345.17	Ransdaal	50.870	5.910		3.50	4.00
20010623	20153.64	Voerendaal	50.877	5.920		1.10	7.90
20010623	20231.32	Ransdaal	50.870	5.920		3.20	3.30
20010623	20022.98	Voerendaal	50.879	5.925		-0.10	5.00
20010623	20023.01	Voerendaal	50.879	5.925		-0.10	5.00
20010623	15856.16	Voerendaal	50.879	5.925		0.00	5.00
20010623	20133.19	Voerendaal	50.879	5.925		0.10	5.00
20010623	15003.91	Voerendaal	50.879	5.925		0.30	5.00
20010623	20049.35	Voerendaal	50.879	5.925		0.30	5.00
20010623	14759.94	Voerendaal	50.879	5.925		0.50	5.00

YYMMDD	TIME	LOCATION	LAT	LON	INT	MAG	DEPTH
20010623	20638.39	Voerendaal	50.879	5.925		0.50	5.00
20010623	25521.09	Voerendaal	50.879	5.925		0.50	5.00
20010623	40325.77	Voerendaal	50.879	5.925		0.50	5.00
20010623	45401.06	Voerendaal	50.879	5.925		0.50	5.00
20010623	143308.4	Voerendaal	50.879	5.925		0.50	5.00
20010623	15916.17	Voerendaal	50.879	5.925		0.60	5.00
20010623	33839.09	Voerendaal	50.879	5.925		0.60	5.00
20010623	41045.32	Voerendaal	50.879	5.925		0.60	5.00
20010623	144819.7	Voerendaal	50.879	5.925		0.70	5.00
20010623	233003.3	Voerendaal	50.879	5.925		0.70	5.00
20010623	20650.85	Voerendaal	50.879	5.925		0.80	5.00
20010623	21113.17	Voerendaal	50.879	5.925		0.80	5.00
20010623	21832.67	Voerendaal	50.879	5.925		0.80	5.00
20010623	20832.65	Voerendaal	50.879	5.925		0.90	5.00
20010623	102051.3	Voerendaal	50.879	5.925		0.90	5.00
20010623	15300.46	Voerendaal	50.886	5.927		1.40	4.20
20010623	104416.5	Voerendaal	50.876	5.927		1.00	8.70
20010623	90324.71	Voerendaal	50.893	5.928		1.00	8.20
20010623	22855.18	Voerendaal	50.868	5.928		1.10	10.40
20010623	41800.91	Voerendaal	50.880	5.930		1.40	4.10
20010623	24515.61	Voerendaal	50.874	5.930		2.20	6.20
20010623	14458.06	Voerendaal	50.882	5.932		0.50	5.00
20010623	22851.45	Voerendaal	50.877	5.932		0.50	8.00
20010623	**14003.39**	**Voerendaal**	**50.876**	**5.932**		**3.90**	**2.20**
20010623	154655.2	Voerendaal	50.865	5.933		1.50	2.00
20010624	35214.92	Voerendaal	50.874	5.902		1.30	2.00
20010624	14621.28	Voerendaal	50.864	5.903		1.40	4.00
20010624	24255.29	Voerendaal	50.866	5.905		0.70	3.00
20010624	50905.56	Voerendaal	50.867	5.935		0.90	3.50
20010625	4905.35	Voerendaal	50.876	5.933		0.90	6.60
20010625	154305.5	Voerendaal	50.869	5.933		0.70	3.00
20010626	194508	Voerendaal	50.888	5.935		1.00	5.00
20010627	90522.7	Voerendaal	50.776	5.780		0.90	5.00
20010701	94940.6	Voerendaal	50.885	5.918		0.80	5.00
20010703	163337.8	Voerendaal	50.888	5.932		1.00	5.00
20010704	211712.1	Voerendaal	50.886	5.932		0.60	4.00
20010704	123830.9	Voerendaal	50.884	5.932		0.20	5.00
20010704	124034.3	Voerendaal	50.879	5.932		0.30	5.00
20010704	184327.4	Voerendaal	50.854	5.995		0.60	5.00
20010704	123847	Voerendaal	50.842	6.008		0.20	5.00
20010707	133908.2	Voerendaal	50.874	5.930		2.40	2.00
20010707	134211.7	Voerendaal	50.870	5.930		0.20	3.00
20010707	125350.6	Voerendaal	50.872	5.932		0.60	3.00
20010707	171221.2	Voerendaal	50.821	5.932		0.60	5.00
20010708	84944.85	Voerendaal	50.892	5.932		0.40	3.00
20010708	85651.83	Voerendaal	50.877	5.932		0.10	3.00

YYMMDD	TIME	LOCATION	LAT	LON	INT	MAG	DEPTH
20010710	172411.2	Voerendaal	50.864	5.933		0.80	5.00
20010711	63939.37	Voerendaal	50.880	5.932		0.70	5.00
20010714	125250	Voerendaal	50.873	5.900		1.30	6.60
20010714	125002.7	Ransdaal	50.872	5.910	3	2.20	2.40
20010714	125213.6	Voerendaal	50.879	5.920		1.50	4.00
20010716	215147.4	Voerendaal	50.886	5.885		1.40	4.00
20010719	2415.88	Voerendaal	50.910	5.923		0.20	5.00
20010719	181949.9	Voerendaal	50.880	5.932		0.10	3.00
20010729	82426.66	Voerendaal	50.889	5.932		0.30	3.00
20010809	15058.81	Voerendaal	50.881	5.922		1.50	4.00
20010813	180047.5	Voerendaal	50.876	5.877		1.60	3.60
20010813	110506.9	Voerendaal	50.868	5.883		0.60	4.00
20010822	10142.29	Voerendaal	50.878	5.932		0.10	6.90
20010905	53637.99	Hoensbroek	50.918	5.927		0.30	5.00
20010906	131448.7	Voerendaal	50.887	5.932		1.10	5.00
20010913	222853.4	Voerendaal	50.887	5.932		0.30	3.00
20010926	232354.5	Voerendaal	50.873	5.935		0.10	3.00
20011030	191020.6	Voerendaal	50.892	5.932		0.60	5.00
20011101	34706.81	Voerendaal	50.885	5.932		0.70	5.50
20011124	15327.82	Voerendaal	50.866	5.960		1.30	7.50
20011208	181606.9	Voerendaal	50.871	5.910		0.90	1.00
20011211	41316.91	Voerendaal	50.862	5.932		0.30	5.00
20011212	122501.4	Voerendaal	50.873	5.932		0.20	5.00
20011227	212051.8	Voerendaal	50.870	5.933		0.40	7.20
20020117	185254	Voerendaal	50.871	5.900		0.80	8.20
20020315	32904.9	Voerendaal	50.916	5.913		0.80	5.00
20020831	212833.1	Voerendaal	50.874	5.938		2.60	5.00
20020831	225402.9	Voerendaal	50.875	5.942		0.90	8.40
20020831	73325.45	Voerendaal	50.875	5.947		0.90	8.00

Appendix 2

Na-ijlende gevolgen steenkolenwinning Zuid-Limburg

Final report of the working group
5.2.7 - small earthquakes

Deep borehole log used for the stress calculations (From: NLOG, 2016)

by

Projectgroup
"Na-ijlende gevolgen van de steenkolenwinning in Zuid-Limburg"
(projectgroup GS-ZL)

on behalf of
Ministerie van Economische Zaken - The Netherlands

Amsterdam, 31.08.2016

Appendix 2: Deep borehole log used for the stress calculations (From: NLOG, 2016)

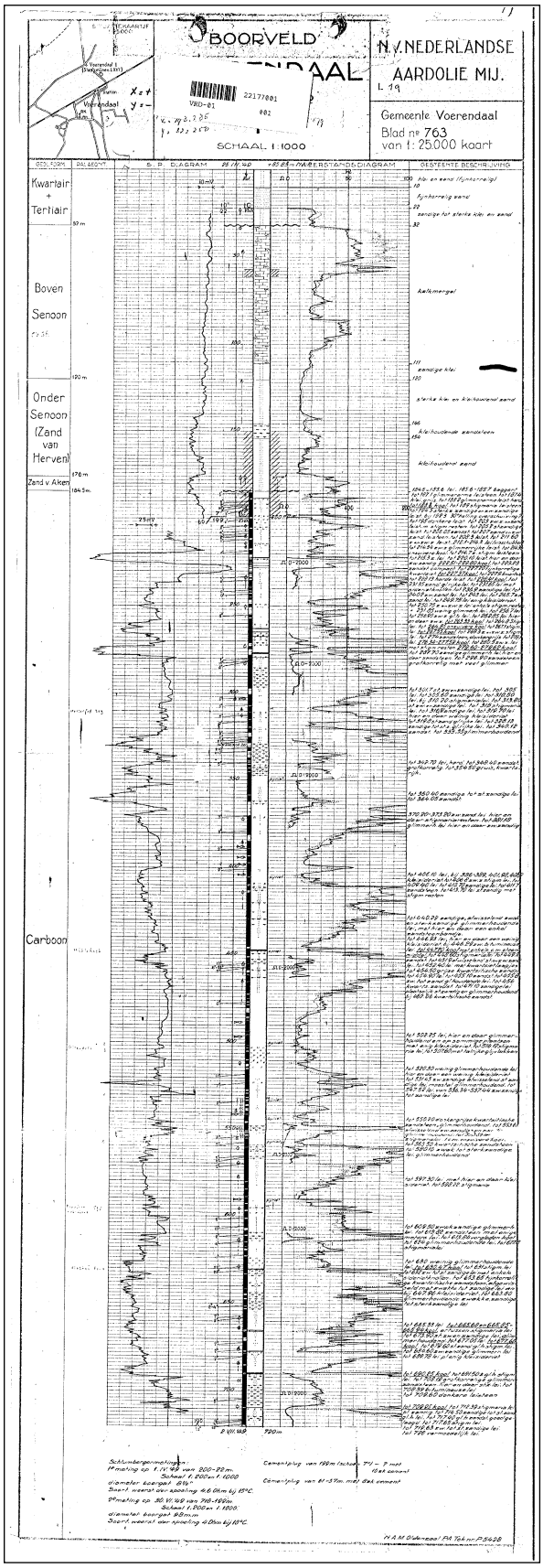

Appendix 3

Na-ijlende gevolgen steenkolenwinning Zuid-Limburg

Final report of the working group
5.2.7 - small earthquakes

Seismic hazard map of the Netherlands

by

Projectgroup
"Na-ijlende gevolgen van de steenkolenwinning in Zuid-Limburg"
(projectgroup GS-ZL)

on behalf of
Ministerie van Economische Zaken - The Netherlands

Amsterdam, 31.08.2016
(Rev. a: 02. December 2016)

Appendix 3: Seismic hazard map of the Netherlands

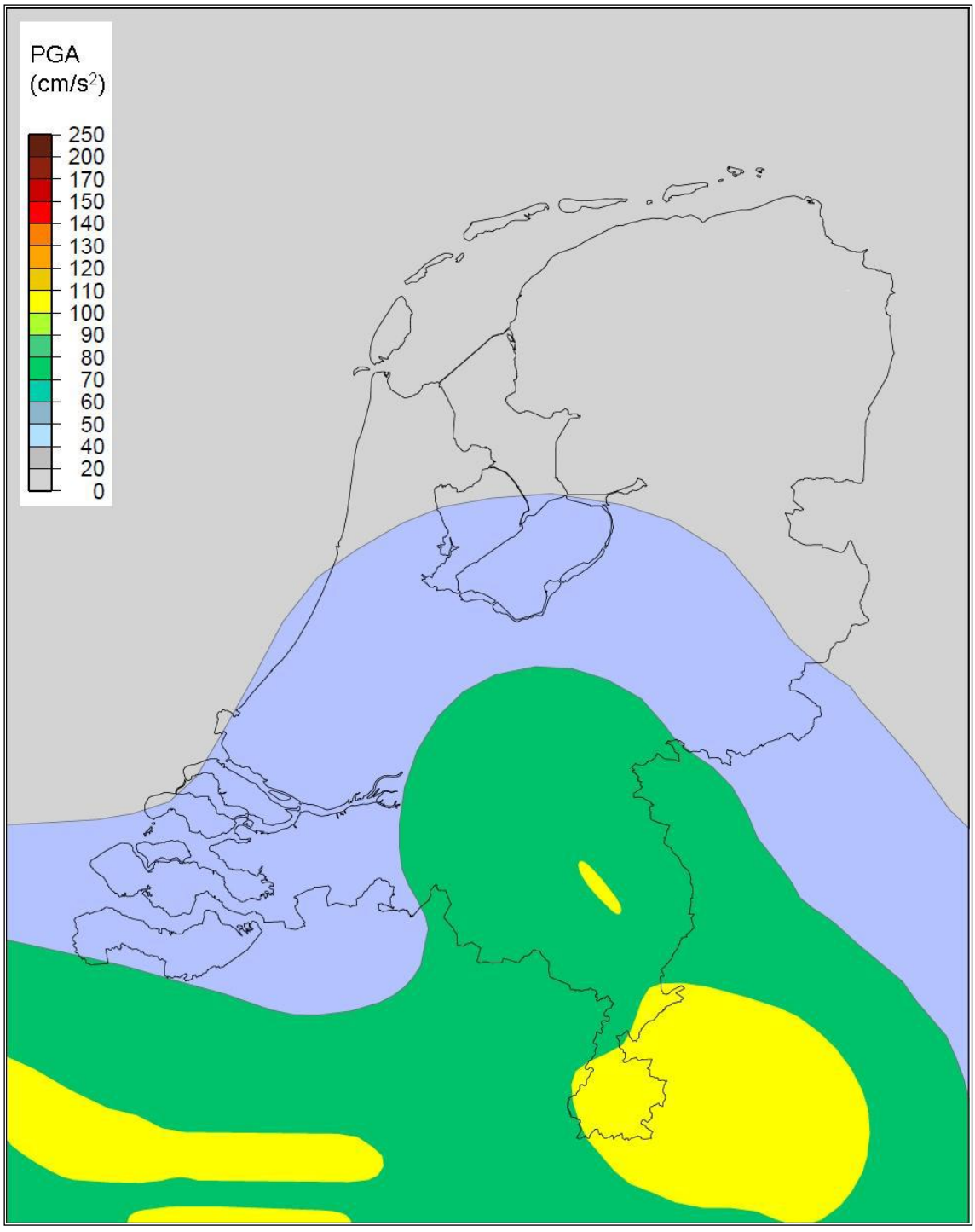

Peak Ground Acceleration with 10 % probability of exceedence during 50 years (475 year return period) for the Netherlands (DE CROOK, 1996).

Appendix 4

Na-ijlende gevolgen steenkolenwinning Zuid-Limburg

Final report of the working group
5.2.7 - small earthquakes

Bow-Tie-diagram

by

Projectgroup
"Na-ijlende gevolgen van de steenkolenwinning in Zuid-Limburg"
(projectgroup GS-ZL)

on behalf of
Ministerie van Economische Zaken - The Netherlands

Amsterdam, 31.08.2016
(Rev. a: 02. December 2016)

5.2.7 Small earthquakes

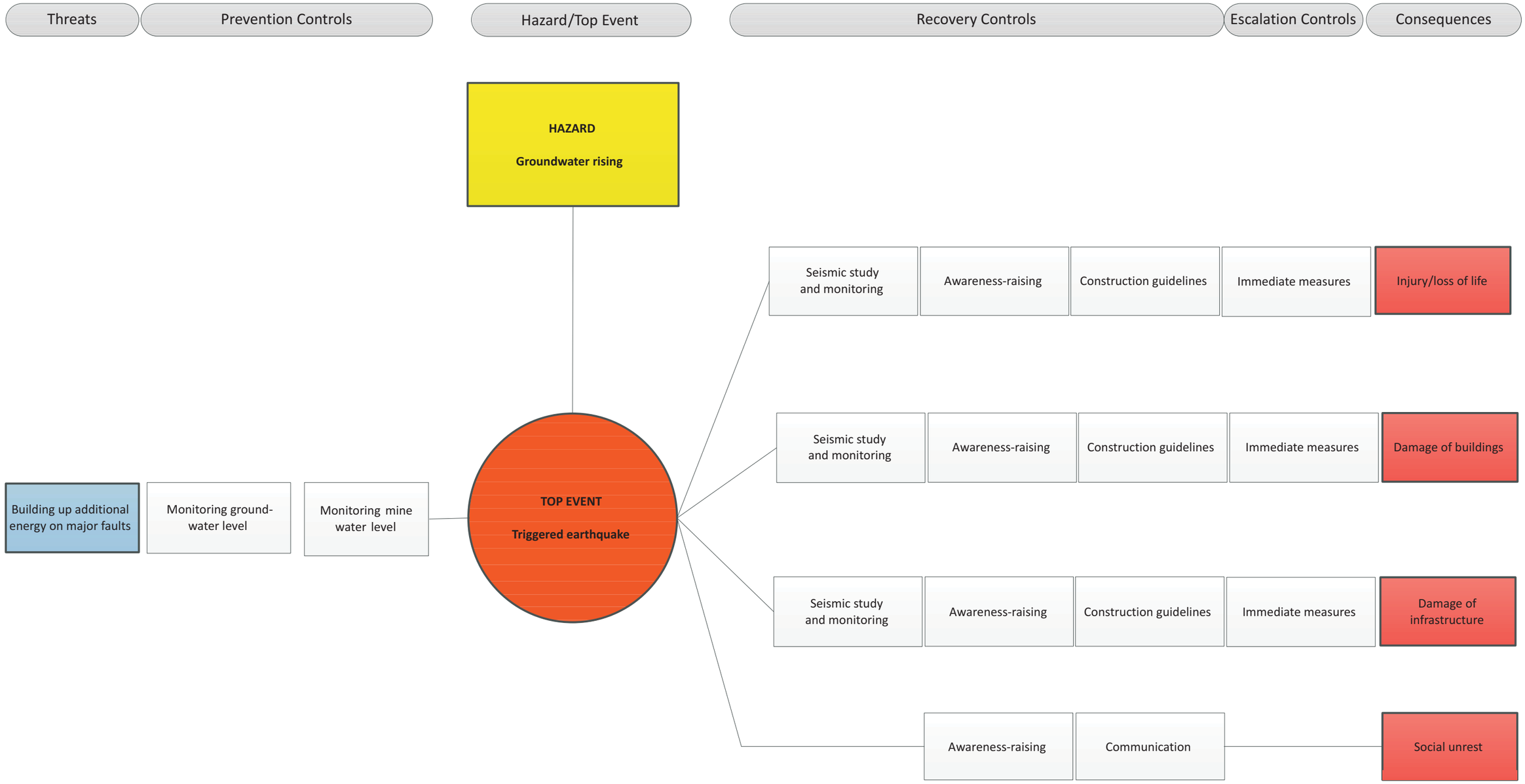

App. 4